A Study on Soil-Plant-Atmosphere Interaction for Green Infrastructure

Thesis
submitted in partial fulfillment of the requirements
of the degree of

DOCTOR OF PHILOSOPHY

by

Vinay Kumar Gadi

Roll No. 156104019

Department of Civil Engineering

Indian Institute of Technology Guwahati

Guwahati-781039, India

July, 2020

Dedicated to my parents, sister and uncle

CERTIFICATE

This is to certify that the thesis entitled **"A Study on Soil-Plant-Atmosphere Interaction for Green Infrastructure"** submitted by Vinay Kumar Gadi to the Indian Institute of Technology Guwahati, for the award of the degree of Doctor of Philosophy (PhD) in Civil Engineering is a record of bonafide research work carried out by him under our supervision and guidance. The thesis work, in our opinion, has reached the requisite standard fulfilling the requirement for the degree of Doctor of Philosophy.

The results contained in this thesis have not been submitted in part or full to any other University or Institute for award of any degree or diploma.

Prof. Sreedeep S
Department of Civil Engineering
Indian Institute of Technology Guwahati
Guwahati, 781039
Date:

Prof. Lingaraj Sahoo
Department of Biotechnology
Indian Institute of Technology Guwahati
Guwahati, 781039
Date:

STATEMENT

I do hereby declare that the matter embodied in this thesis is the result of investigations carried out by me in the Department of Civil Engineering, Indian Institute of Technology Guwahati, Guwahati, Assam, India.

In keeping with the general practice of reporting scientific observations, due acknowledgements have been made wherever the work described is based on the findings of other investigators.

(Vinay Kumar Gadi)

Guwahati, 781039

Date: 6th July, 2020

ACKNOWLEDGEMENTS

I express my humble gratitude towards my supervisors Prof. Sreedeep S, Prof. Sahoo L and Dr. Ankit Garg, for their guidance and motivation throughout this research work. I am always indebted to them for the freedom that they had given me to work at my schedule during this research work. I am thankful for the kind nature and all valuable time that they spent for me during my doctoral study. I am highly grateful to them for the precious guidance and valuable suggestions that will travel a long way in moulding my personality and career.

I am thankful to the members of doctoral committee Dr. Sreeja P, Dr. Ravi K and Dr. Prasenjit Khanikar for their constructive comments and valuable suggestions during my Doctoral program. I would also like to thank Dr. Christian Berretta (Academic research fellow, University of Leeds, UK), Dr. Hazra B (Associate Professor, Indian Institute of Technology Guwahati), Ms. Charu Monga (Assistant Professor, Indian Institute of Technology Guwahati), Prof. C.W.W. Ng (Hong Kong University of Science and Technology), Prof. Hong-Hu Zhu (Nanjing University, Nanjing, China), Dr. Lili Wei (Associate Professor, Chinese Academy of Sciences, China), Dr. Sanyogita Andriyas (Lecturer, Water Engineering, Asian Institute of Technology, Thailand), Dr. Hong Zhu (postdoctoral researcher, Hong Kong University of Science and Technology), Dr. J. J. Ni (postdoctoral researcher, Hong Kong University of Science and Technology), Prof. J. H. Li (Harbin Institute of Technology), Dr. J. Liu (Associate Professor, Qingdao University of Technology) and Prof. C. R. Patra (NIT Rourkela) for their timely inputs. The final shape of the thesis would not have been possible without their valuable feedback. I extend my thanks to the examiners of this thesis for their invaluable suggestions that helped in improving the thesis.

I highly appreciate Ministry of Human Resource Development (MHRD), India for providing me the fellowship. I thank Director of the Institute, Head of the Civil Engineering

Department, Dean Academics, and Dean R&D of IIT Guwahati for strengthening the research environment of the Institute to conduct my research. I am also thankful to Shantou University, China for the support in current research.

I would like to thank Dr. Sanandam, Mr. Rojimul, Mr. Shivam, Mr. Manish, Ms. Indu, Mr. Siraj, Dr. Sanjeev, Mr. Muthu, Mr. Prabin, Mr. Arka, Mr. Prakash, Mr. Bharat, Mr. Priyanshu, Mr. Rakesh, Mr. Shubham, Mr. Abhishek, Mr. Anjaneyulu, Ms. Richa, Mr. Janarul, Ms. Anangsha, Ms. Himashree, Dr. Sudheer, Mr. Atma, Mr. Gaurav and Mr. Patwa for the support in the experiments and valuable discussions in the laboratory. I also extend thanks to lab staff: Mr. Hariram Upadhyay and Mr. Asim.

I would like to thank my friends who made my time at IIT Guwahati enjoyable and helped me not to miss my home. My special thanks to Mr. Vinay, Mr. Suresh, Mr. Viswanth, Mr. Venkatesh, Mr. Mukhesh, Mr. Kranthi, Mr. Hanumath, Mr. Rajeev, Mr. Vimal, Mr. Tharun, Ms. Saswathi, Mr. Anant, Mr. Kiran, Mr. Bhanu for helping me at various points of time during my stay at IIT Guwahati.

I received incredible support and encouragement from my parents, uncle and sister. They kept me motivated and gave me a free hand without letting me know what all difficulties they were facing. Without their great support and unconditional love, this thesis would not have been possible. I thank all of them from the bottom of my heart.

I thank the Almighty God for showering the blessings upon me that I could reach up to here.

Vinay Kumar Gadi

156104019

CONTENTS

ABSTRACT

The presence of vegetation in the upper layer of vadose zone results in complex moisture dynamics (soil-plant-atmosphere interaction) due to the combined effects of transpiration and soil water evaporation. Unsaturated soil-root composite hydraulic properties, transpiration and soil water evaporation and effect of plant parameters (i.e., leaf area index (LAI), grass density, shoot length (SL) and stomatal conductance) on soil property are keys for understanding this complex moisture dynamics. Plant parameters and unsaturated soil properties were not considered holistically by previous researchers to understand soil-plant-atmosphere interaction. The main objective of this study is to explore the soil-plant-atmosphere interaction by considering the soil (cracks, suction and hydraulic conductivity) and plant parameters (vegetation density, LAI and stomatal conductance) together. Effect of crop and non-crop species growth on crack intensity factor (CIF) were investigated in the current study. In addition, effect of plant parameters on evapotranspiration induced suction was numerically analyzed. It is evident that large number of sensors are usually installed to monitor the suction in geotechnical infrastructure. Therefore, a non-intrusive and economical technique was developed to differentiate the 1) mix grass cover under tree shade (MUT); 2) mix grass cover under self-shade (MUS) and 3) mix grass cover without shade (MWS) in relatively large areas. Changes in stomatal conductance and surface area of vegetation at high suction ((high suction; > 100 kPa) were rarely investigated previously. Hence, effect of suction on stomatal conductance and surface area was investigated in this study. Furthermore, spatial and temporal heterogeneity of hydraulic conductivity in green space was rarely focused. Field monitoring was conducted in an urban green space to understand the spatial and temporal heterogeneity of surface hydraulic conductivity during the life period of mix grass. It is known that suction and surface hydraulic conductivity are interpreted from soil surface water content. Non-

invasive and cost effective technique is vital to interpret soil surface water content. Therefore, colour analysis technique was demonstrated to interpret soil surface water content. This study on soil-plant-atmosphere interaction helps to analyze the performance of green infrastructure accurately. Correlations were found between shoot parameters (SL, LAI, vegetation density) and CIF for the selected crop and non-crop species. Numerical analysis revealed that changes in shoot and root parameters could alter the suction by 11 % - 300 %. In addition, time required to attain wilting point was found to depend on plant parameters. Two new relationships i.e., Stomatal conductance characteristic curve (SCCC) and surface area characteristic curve (SACC) were found. The elementary hypothesis of spatial uniformity of surface hydraulic conductivity during life span of mix grass was not found to be true from the present study. The spatial and temporal heterogeneity of surface hydraulic conductivity was found mainly due to non-uniformity in grass growth and tree shade.

Keywords: soil-plant-atmosphere interaction, cracks, suction, hydraulic conductivity, vegetation density, leaf area index, stomatal conductance, green infrastructure

LIST OF FIGURES

LIST OF TABLES

NOMENCLATURE

θ	Volumetric water content (m^3/m^3)
t	Time (hours)
z	Vertical coordinate (m)
r	Radial coordinate (m)
K	Unsaturated hydraulic conductivity (m/ hour)
Ψ	Suction (kPa)
$\alpha(\psi, r, z)$	Transpiration reduction function (varies between 0 and 1)
S_p	Potential water uptake over root zone ($hour^{-1}$)
$[\alpha(\psi, r, z) S_p]$	Sink term
θ_s	Saturated volumetric water content
θ_r	Residual volumetric water content
α	Related to inverse of air entry value
m, n	Parameters related to pore size distribution

ABBREVIATION

LAI	Leaf area index
SL	Shoot length
CIF	Crack intensity factor
MUT	Mix grass cover under tree shade
MUS	Mix grass cover under self-shade
MWS	Mix grass cover without shade
SCCC	Stomatal conductance characteristic curve
SACC	Surface area characteristic curve
SWRC	Soil water retention curve
SRCWRC	Soil root composite water retention curve
R_{df}	Root distribution function
RAI	Root area index
SIZ	Suction influence zone
EDZ	Evaporation dominant zone
PAR	Photosynthetically active radiation
GGL	Green grass under light
GGS	Green grass under self-shade
CWG	Completely wilted grass
UAV	Unmanned air vehicle
DOS	Degree of saturation
A_c	Crack area
A_t	Total area

PET	Potential evapotranspiration
VWC	Volumetric water content

CHAPTER 1 INTRODUCTION

The use of vegetation is recognized as an eco-friendly solution for stabilizing slope, river bank, landfill covers and accelerate ground water recharge through urban areas (Stokes et al., 2009; Leung et al., 2015a; Liang et al., 2017). The implications of vegetation in geotechnical and ecological infrastructure (i.e., green infrastructure) are shown in Fig. 1.1. Bioengineered slope refers to the use of any form of vegetation, as an engineering material to reduce soil erosion, increase shear strength and enhance slope stability (Leung et al., 2015b). Urban green space (i.e., lawns and parks) promotes health, psychological activity and physical well-being of urban residents (Wolch et al., 2014). In addition, it features multiple benefits for infiltrating storm water and conveying it to a water course or reuse (Garg et al., 2015b, c). Extensive schemes were implemented to increase urban green space and has been acknowledged as eco system justice issue (Wolch et al., 2014; Villeneuve et al., 2012). The surface layer of landfill cover system is mostly covered with vegetation (Waugh et al., 1994), to minimize soil erosion.

The layer of soil above the ground water level, which is partially saturated or unsaturated, is termed as the vadose zone. The zone constituting the top portion of the vadose zone, where the roots of plant grow comprises root zone (Stephens, 1995). Within root zone, the complex moisture dynamics (soil-plant-atmosphere interaction) occur due to the combined effects of transpiration and soil water evaporation. The appraisal of soil-plant-atmosphere interaction requires interdisciplinary approach combining properties of unsaturated soil mechanics and plant parameters. In unsaturated soil mechanics, crack formation, suction and hydraulic conductivity are essential properties to understand water flow in soil. On the other hand, canopy parameters (i.e., vegetation density, leaf area index (LAI) and stomatal conductance) are vital parameters to analyze evap-otranspiration. These parameters from unsaturated soil mechanics and plant physiology are

interdependent and their correlation is essential for the understanding of soil-plant-atmosphere interaction.

Previous studies have not integrated the plant parameters and unsaturated soil properties to understand soil-plant-atmosphere interaction. In addition, vegetation growth was rarely considered to analyze the performance and stability of green infrastructure. Furthermore, effect of seasonal variation on vegetation growth was also not taken into account in previous studies. The understanding of relationship between soil and canopy parameters help to devise drainage schemes in urban green space and analyze the stability of geotechnical infrastructure accurately. This need for accurate understanding of soil-plant-atmosphere interaction has motivated this research work.

Surface area covered by vegetation varies spatially in green infrastructure (Casper and Jackson, 1997). Heterogeneity of surface area exposed to photosynthetically active radiation is commonly grouped into four categories. Those are green grass under light, green grass under self shade, green grass under tree shade and completely wilted grass (Boardman, 1977). Large number of high capacity tensiometers or water potential sensors and moisture content sensors are usually installed to monitor the spatial heterogeneity of suction in green infrastructure (Garg et al., 2015c). This may not be economical in relatively large areas. Hence, development of non- destructive, feasible and economical technique is essential to devise optimal instrumentation plan in relatively large areas. In addition, surface hydraulic conductivity and evapotranspiration induced suction in green infrastructure in large areas are interpreted from soil surface moisture content. However, large number of moisture content sensors could not be installed in relatively wide areas. Then, periodic maintenance of sensors would not be feasible during long-term monitoring (Bhatt et al., 2016). Therefore, development of non- destructive,

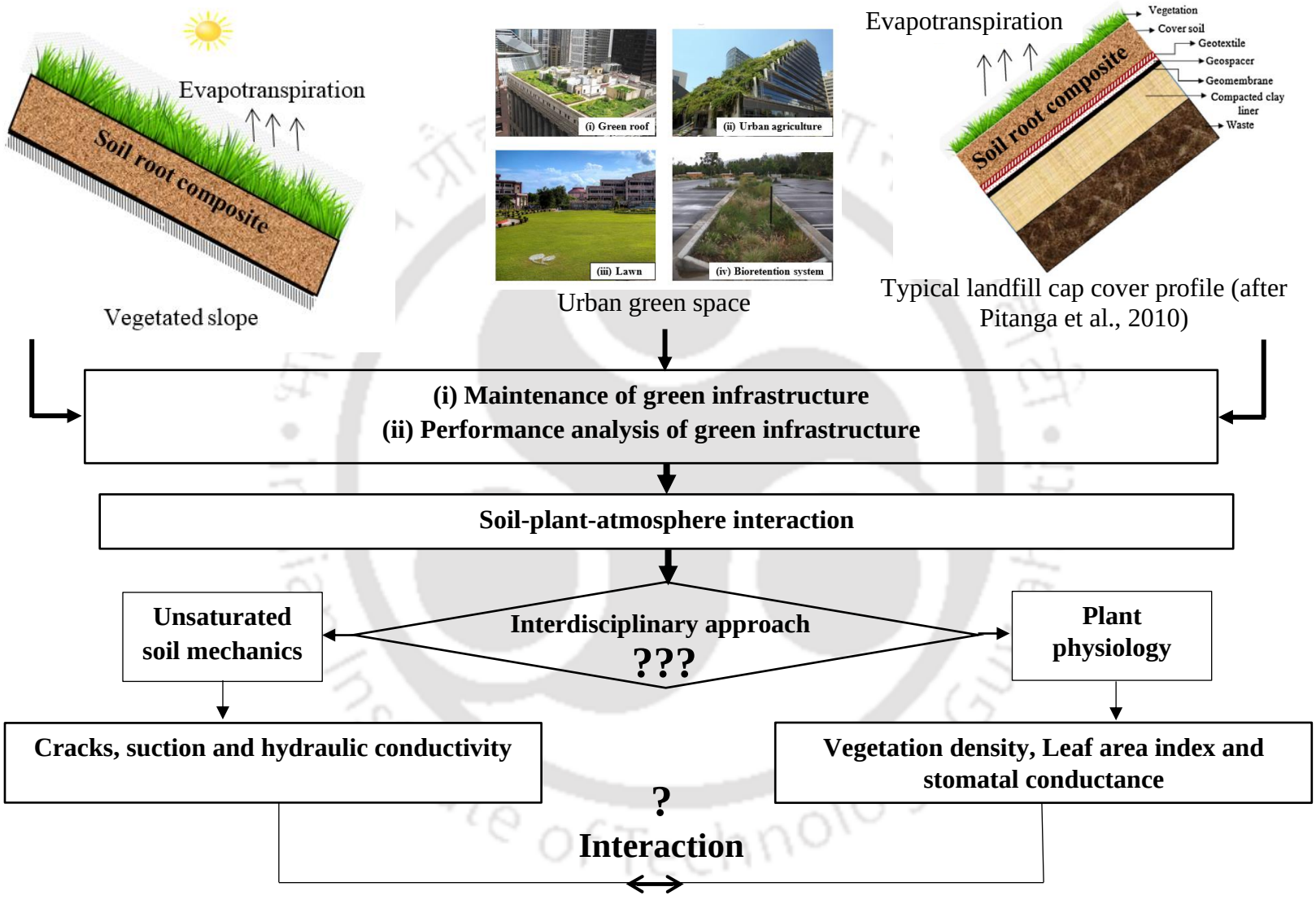

Fig. 1.1 Importance of understanding the soil-plant-atmosphere interaction

feasible and economical technique is essential to measure soil surface water content in green infrastructure.

Effect of vegetation (mix grass and cowpea) growth on crack formation was explored to understand the correlation between growth and cracking. Experimental test pots were used to observe crack formation on vegetated and bare soil. A systematic parametric study is conducted considering three different scenarios to explore simultaneous effects of soil hydraulic properties and plant root as well as shoot properties on suction induced in soil-root composite. This is conducted considering three different scenarios: effect of root properties during the absence of transpiration (Scenario 1); individual effect of only root properties (root distribution function (Rdf) and root area index (RAI); Scenario 2) in the presence of evapotranspiration; and combined effects of canopy (LAI) and root properties (Rdf and RAI) in the presence of evapotranspiration (Scenario 3). Colour analysis technique was demonstrated to differentiate (i) mix grass cover under tree shade (MUT); (ii) mix grass cover under self-shade (MUS); and (iii) mix grass cover without shade (MWS). Mix grass species in a compacted soil mass (important for bioengineering) subjected to drought stress (suction > 100 kPa) to investigate relationship among evapotranspiration induced suction, stomatal conductance and surface area. A new colour analysis technique was demonstrated to interpret soil surface water content. The brightness variation of soil samples was quantified using the change in mean gray value of the images. Field monitoring has been conducted for a year (life period of mix grass) in a green space to understand the spatial and temporal heterogeneity of surface hydraulic conductivity in mix vegetation.

CHAPTER 2 REVIEW OF LITERATURE

2.1 General

The understanding of soil-plant-atmosphere interaction needs interdisciplinary approach combining properties of unsaturated soil mechanics and plant parameters. Surface cracks, suction and infiltration are important properties of unsaturated soil. On the other hand, vegetation density, leaf area index and stomatal conductance are essential plant parameters. Previous studies related to crack formation, suction and hydraulic conductivity in vegetated soil were highlighted in this section. In addition, the gaps that need to be addressed between unsaturated soil mechanics and plant parameters were presented.

2.2 Crack formation in vegetated soil

Desiccation cracking is a common phenomenon in fine grained soil, and is observed in undisturbed soil on drying. A desiccation crack occurs when the drying induced surface tensile stress (suction) reaches the soil tensile strength (Corte and Higashi, 1960). These cracks on the surface expose the interior of the soil to climatic conditions (Yesiller et al., 2000). Cracks in soil have implication in agriculture engineering (Torres et al., 2004), landfill cover system (Costa et al., 2013;), road embankments and green infrastructure (Stovin et al., 2013; Berretta et al., 2014; Bordoloi et al. 2015; Bordoloi et al., 2017; Vardhan et al., 2017). Surface cracking has both positive and negative attributes in the field of agriculture. Improved drainage during harvest of crop (Bouma et al., 1979; Yoshida and Adachi, 2004), improved infiltration (Swartz, 1966) and solute-microorganism transport (Ringrose-Voase and Sanidad, 1996; Chertkov and Ravina, 1999) are such positive attributes of desiccation cracks in agricultural field. However, rapid transport of water and solute through soil cracks, leads to drought condition (Thomas and Phillips, 1979) and nutrient leaching (Coles and Trudgill, 1985) respectively. Moreover, such cracks are the precursor for the formation

of gullies, which ultimately leads to fertile soil loss due to erosion (Ollobarren et al., 2016). Cracks also facilitate excess soil water evaporation in agricultural fields by opening up secondary evaporation planes in its profile (Torres et al., 2004).

The effect of cracking on landfill cover has garnered considerable attention in the recent past. Landfill cover is susceptible to cracking during cycles of drying-wetting, which eventually is detrimental to the integrity of the liner (Andersland and Al-Moussawi, 1987; Albright et al., 2006; Li and Zhang, 2010; Costa et al., 2013). Surface cracks can have marked increase of water infiltration into the liner material and subsequently give rise to excess leachate generation (Snow, 1969; Yuen et al., 1998; Rayhani et al., 2008; Li et al., 2011; Bordoloi et al. 2017; Ni et al., 2020). The landfill cover material is mostly covered with vegetation (Waugh et al., 1994), to minimize soil erosion. The crack formation and intensity are influenced by the plant cover distribution (Johnston and Hill, 1944; Dasog et al., 1988) and type of crop (Fox, 1964, Mitchell and van Genuchten, 1992). Upon vegetation induced transpiration, soil moisture would be further reduced through root-water uptake, as compared to bare soil (Blight, 2003; Hemmati et al., 2012). Thus vegetation leads to transpiration induced suction in the soil. Li et al. (2016) recently have studied the effect of *Festuca arundinacea* grass on cracking on landfill cover. However, they have not considered the effect of shoot parameters on crack formation in the soil. Shoot parameters (LAI, SL and vegetation density) greatly affect transpiration induced suction, because of their influence on intercepted radiant energy (Leung et al., 2015a, b; Garg et al. 2015b). LAI is defined as the one-sided green leaf area per unit ground canopy area. Vegetation density is defined as the proportion of the surface area covered by the vegetation in the considered area. As far as authors are aware, rarely any studies have been done to correlate such shoot parameters with quantitative crack

parameter for repeated drying-wetting cycles as commonly encountered due to seasonal effect and rainfall.

Quantification of cracks in soil is important to model water retention, flow and balance at surface (Arnold et al. 2005, Baer et al. 2009) of any topography. Basic measurement of cracks has been reported in past studies. Manual measurement using a bilateral device consisting of a wire probe to measure crack width has been devised (El Abedine and Robinson, 1971). Soil crack distribution in situ has been measured using polythene sheets by Logsdon et al. (1990). Such conventional manual measurement techniques are difficult to measure the highly irregular crack network (Tang et al., 2012). Hence, digital image-processing approaches are attaining increased acceptance in the field of soil characterization due to its non-destructive analysis and accuracy (Macai et al., 1993; Yesiller et al., 2000). The widely accepted CIF approach using captured images (Yesiller et al., 2000; Li et al., 2016) has been used extensively to measure and quantify cracks. Ratio of crack area to the total area of soil surface is referred as CIF. The CIF approach has been used in many studies (Mi, 1995; Miller et al., 1998; Li et al., 2016; Chaduvula et al. 2017; Wang et al. 2017; Jayanthi et al. 2017) as a descriptor of the extent of surficial cracking.

2.3 Effect of plant parameters on suction induced in vegetated soil

Evapotranspiration is a process of the sum of evaporation from soil surface and transpiration through root water uptake. It is a process through which soil-root composite induces suction. Suction governs the shear strength of vegetated slope. The shear strength equation can be written as

$$\tau = c' + \sigma' \tan\phi' + (u_a - u_w) \tan \varphi^b \qquad (2.1)$$

where, c' is effective cohesion parameter, σ' is effective stress, $u_a - u_w$ is suction induced in rooted soil, $\phi'$is friction angle with respect to changes in σ' when $(u_a - u_w)$ is held constant, φ^b is friction angle with respect to changes in $(u_a - u_w)$ when σ' is held constant.

In addition, suction influences the hydraulic conductivity in urban green infrastructure (i.e., green roofs, biofilters, vegetated landfills, slopes, urban landscape (lawns). Hence, understanding suction induced in soil-root composite is important to assess the runoff, ground water recharge (Leung et al., 2015a), erosion and slope stability (Lee et al., 2005; Ng et al., 2015b; Liu et al., 2016; Feng et al., 2017).

It is evident that, plant canopy properties (LAI) and root properties (root distribution function (R_{df}) and root area index (RAI)) affect evapotranspiration induced suction (Ng et al., 2015b; Garg et al., 2015b; Liu et al., 2016; Feng et al., 2017). Definition of LAI was included in section 2.2. RAI is the ratio of root surface area to soil surface area surrounded by roots. Ratio of root area index of the considered plant to the maximum root area index is termed as normalized root area index. Ratio of root depth of the considered plant to the maximum root depth is referred as normalized root depth. Distribution of RAI in root zone is represented with $R_{df.}$ Roots may influence the suction induced in soil-root composite during the absence of transpiration also (Leung et al. 2015b). In addition to these, transpiration reduction function (α (ψ, r, z)) enable the researchers to understand the ratio of actual to potential transpiration rate with respect to the suction (Garg et al., 2015a). α (ψ, r, z) physically shows the plant's ability to adjust its capability of water uptake according to the suction induced in soil-root composite (Garg et al. 2015a). Feddes et al. (1978) formulated the α (ψ, r, z) by connecting anaerobiosis point (ψ_1), wilting point (ψ_3) and one empirical parameter (ψ_2), which indicates maximum water uptake (α (ψ, r, z) = 1). Garg et al. (2015a) shows that, ψ_1, ψ_2 and ψ_3 varies with change in species type.

Garg and Ng (2015) investigated the effect of soil density on transpiration induced suction. In their study, coupled effects of root distribution change and soil hydraulic properties change was investigated. Although coupled effects were considered, soil-root composite water retention curves (SRCWRCs) and hydraulic conductivity were not incorporated. Bare soil water retention curves (SWRCs) and their derived hydraulic conductivities were adopted, which are found to be dissimilar to SRCWRCs (Leung et al., 2015b). Differences between LAIs (i.e., canopy properties) and their effect on evapotranspiration induced soil suction was also not considered. In addition, transpiration reduction variation with type of species was not considered. In most of the geotechnical engineering studies (Eaton and Giles, 2009; Lin et al., 2010; Leung and Ng, 2013; Zhu and Zhang, 2015a; Kokutse et al., 2016) related to suction induced in soil-root composite, combined effects of R_{df} and LAI are rarely considered. In addition, wilting point attaining time for non-crop species was also very rarely investigated. Lower the time taken to reach wilting point, signifies shorter duration of vegetation effects on performance of green infrastructure. This has not yet been considered while designing or analyzing performance of engineered green infrastructures.

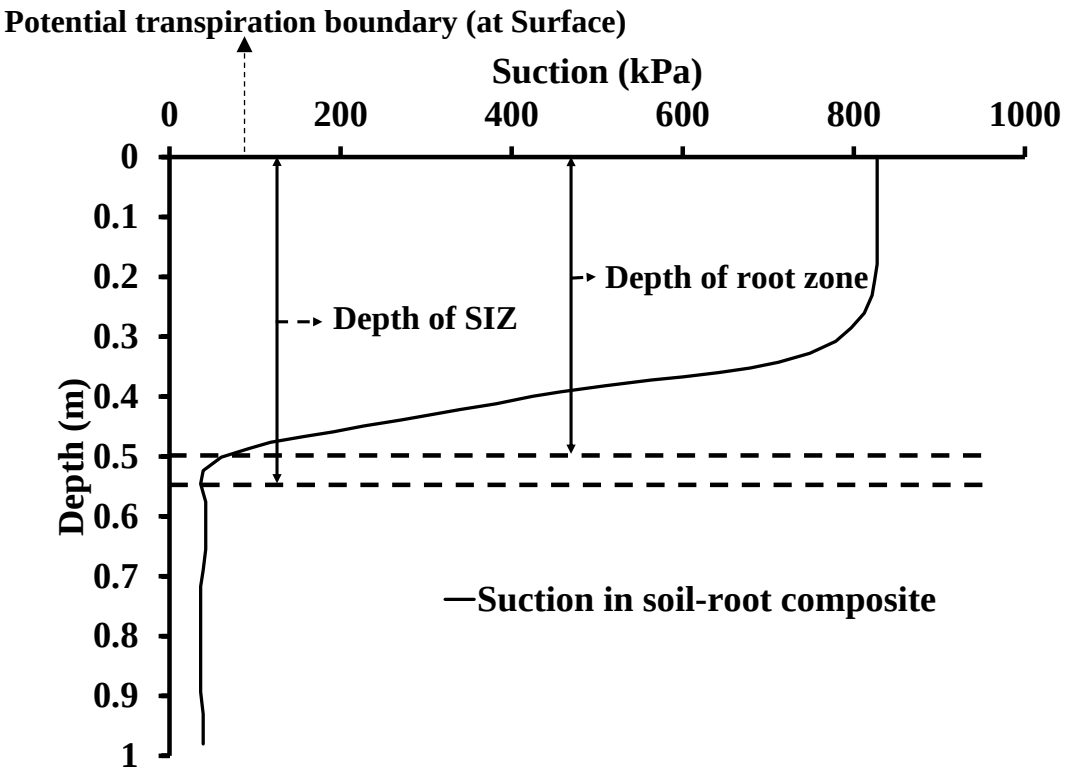

Fig. 2.1 Computed suction profile of soil-root composite subjected to transpiration (simulation ID: 85U30; after Garg and Ng (2015) and illustration of proposed SIZ index

Fig. 2.1 shows the computed suction profile of soil-root composite subjected to transpiration. SIZ can be seen at 0.55 m depth, which is 1.1 times of the root depth. SIZ implies the depth up to which, variation of suction with respect to initial condition is notable i.e., greater than 1 kPa due to evaporation or infiltration. It can also be observed that, potential transpiration was assigned at the surface. However, potential evapotranspiration boundary may be appropriate, which has been rarely assigned by previous researchers. In this study, potential evapotranspiration was assigned at the surface. In addition to SIZ, a new parameter (Evaporation dominant zone; EDZ) was defined in this study for improving quantification of suction profiles. Suction can reach very high value in the region near to the surface. It may be due to drying out of the superficial soil

where the hydraulic conductivity is too low. Soil moisture in deeper region could not seep upwards due to such low hydraulic conductivity. This signifies region in vegetated soil, dominated by relatively higher suctions induced due to evaporation. This region is indicated as EDZ. Depth of EDZ and SIZ may increase or decrease with time. As far as authors aware, rarely any study has investigated the temporal variation of suction profile, EDZ and SIZ. These parameters will help in analyzing green infrastructure performance and in decision making or instrumentation planning for monitoring of green infrastructures.

2.4 Design of instrumentation plan in vegetated soil

Recent studies (Panda et al., 2017a, b) state that, development of non-invasive and cost effective techniques is vital for present scenario of civil engineering. Such techniques reduce the complexities involved in development of sustainable technology. Colour is an optical perception characteristic of human being (Cook et al., 1985). Colour is described through various categories such as violet, indigo, blue, green, yellow, orange and red (Smith and Guild, 1993). These categories are related to wavelength of the light, which is reflected from the objects. Physical properties such as light absorption and emission spectra govern the reflection (Al-Azzawi, 2006a, b). Normally, mix grass under tree shade (MUT) appears dark green. Whereas, mix grass under self-shade (MUS) and mix grass without shade (MWS) appear medium green and light green respectively (Oren-Shamir et al., 2001). MUT, MUS and MWS have great implications in planning instrumentation for measuring suction in green infrastructure.

Suction is generally measured by installing the instrumentation in vegetated soil (Garg et al., 2015b). Previous researchers (Garg et al., 2015b; Leung and Ng, 2016; Leung et al., 2015; Leung and Ng, 2013; Gonzalez-Ollauri and Mickovski, 2015; Song et al., 2017) conducted field

monitoring to understand the suction variation in vegetated soil by installing instruments. However, tree shade or self-shade of vegetation rarely considered for instrumentation planning. In any vegetated soil, suction induced in root zone depends on various atmospheric parameters such as relative humidity (Ng et al., 2016), air temperature and intercepted radiant energy in form of photosynthetically active radiation (PAR; Leung et al., 2015b). However, PAR may not intercept vegetation cover of green infrastructures due to tree shade or self-shade (Boardman, 1977). In such case, suction induced due to evapotranspiration would be very low (Garg et al., 2015b; Poë et al., 2015). This low suction can further influence hydraulic conductivity (Garg et al., 2015b) i.e., water balance of green infrastructure.

Recent study (Leung et al., 2015a) shows that, spatial and temporal variation of mix grass growth would be highly heterogeneous in green infrastructure. Hydraulic conductivity was also found to vary spatially and temporally corresponding to vegetation growth. It was observed that, difference between hydraulic conductivity of mix grass cover under shade and not under shade can be up to 400 %. One of the reasons for this was reported to be suction difference between mix grass cover under shade and not under shade. This shows, a thorough understanding the spatial heterogeneity of mix grass cover under shade is essential to devise an instrumentation plan. Such instrumentation plan could capture the spatial heterogeneity of suction accurately. However, any technique to differentiate and quantify the mix grass under shade and without shade was not demonstrated previously. Furthermore, proportion of mix grass cover under shade could change with time in green infrastructure (Garg et al., 2015b). Additional instruments may need to be installed, according to change in proportion of mix grass under shade with time. Hence, it is vital to develop and demonstrate a non-invasive technique to differentiate grass under shade and without shade, which can be valid for season change also.

Colour analysis technique was previously used by hydrologists, agriculturalists and ecologists (Philipp and Rath, 2002; Congalton, 1991). It was found to be an efficient, low-cost and non-invasive image processing technique. Working principle of colour analysis involves differentiation or quantification of objects on the basis of their colour or spectral reflectance by processing the image (Guyer et al., 1986). Colour analysis was adopted by hydrologists to categorize buildings, water bodies, forests, agricultural lands and other types of land cover in satellite images. These are commonly categorized on the basis of spectral reflectance of land cover (Joseph, 2005). Commercially available remote sensing tools (ArcGIS, ERDAS IMAGINE, Geomatica etc.) were widely used for such categorization on the basis of spectral reflectance. However, most of them are large scale studies. Furthermore, satellite images mainly capture the canopy of trees and top view of land cover (Joseph, 2005). Hence, the area under the tree canopies in urban areas or forests could not be categorized using satellite images.

Colour analysis technique was used by agriculturalists and ecologists to differentiate plant/soil (Andreasen et al., 1997), crop/weed (Strothmann et al., 2017), living/dead plant (Meyer and Neto, 2008), diseased/healthy leaves (Johannes et al., 2017) and human/plant in field (Campos et al., 2016), and for automatic seedling transplantation system (Lin et al., 1994). Such differentiation was done based on hue variation, in majority of the agricultural and ecological studies. Hues refer to the pure colours of visible light in electromagnetic spectrum i.e., violet, indigo, blue, green, yellow, orange and red (Russ and Russ, 2007). As far as authors are aware, MUT, MUS and MWS were rarely differentiated in previous studies. Such differentiation requires categorization of brightness of hue (i.e., brightness of green colour for vegetation).

2.5 Effect of suction on plant parameters

Most of the previous researchers (Lehmann et al., 1998; Czarnes et al. 2000; Pollen-Bankhead and Simon 2010) used tensiometers to measure suction in vegetated soil. The restricted suction measurement range of tensiometer (1-100 kPa) is not suitable for soils having relatively high silt or clay content (Gallage and Uchimura, 2010; Abhijit et al., 2013). This translates to the fact that low range of suction measurement may not be helpful to study the suction developed in the root zone for drought condition. It is worth noting that the green infrastructure is subjected to intense and frequent droughts (Garg et al., 2015a). As a result of water deficit, relatively high suction (> 1500 kPa) occurs in the root zone (Garg et al., 2015a). Therefore, measurement of higher range of suction than what can be recorded using tensiometer is a pressing need for studying green infrastructure. A few researchers have measured suction induced in root zone under drought conditions (Garg et al., 2015a) for studying the response close to the wilting point (in general = 1500 kPa; Feddes, 1982; Garg et al., 2015a). However, there are not many studies that integrate the evapotranspiration induced suction response in root zone with plant parameters, which is invariably necessary to understand the abiotic stress response of plants in green infrastructure.

Stomatal conductance is one of the crucial plant parameters, which governs the evapotranspiration through vegetation in green infrastructure (Wong et al., 1979). Penman-Monteith equation was proposed by Monteith (1965) to show the relation between evapotranspiration and stomatal conductance. Stomatal conductance is the measure of rate of carbon dioxide uptake or water loss through stomata of leaf. This can be demonstrated using mechanism of opening and closing of stomata (plural form of stoma). Transpiration occurs as long as stoma open and it stops when stoma is closed (Tipple and Pagani 2007). Light and health conditions of mix grass exist in green infrastructure were found to be highly heterogeneous

spatially. This spatial heterogeneity is usually grouped into three categories of mix grass. Those three categories are green grass under sun light (GGL), green grass under self-shade (GGS) and completely wilted grass (CWG), respectively.

It is evident that partial or complete closure of stomata occurs in mix grass due to water stress (high suction; Tobin and Kulmatiski, 2018). As a result of stomatal closure, stomatal conductance of the leaf varies (Tipple and Pagani 2007; Jarvis and Mansfield 1981) and would also depend on parts of the day (i.e., morning, afternoon and evening; Lo Gullo et al., 2005; Beadle et al., 1985). There are not many studies that deals with the variation of stomatal conductance with evapotranspiration induced suction (specifically range of suction > 100 kPa). Surface area of vegetation is another key parameter to estimate suction induced due to evapotranspiration in green infrastructure (Garg et al., 2015b, c; Ng et al., 2016). It is well known that surface area of mix grass decreases with time due to shrinkage of grass during drying period (Anjum et al., 2011). The surface area variation with increase in suction was rarely quantified previously. A recent study (Garg and Ng, 2015) shows that suction induced due to relatively large vegetation surface area could be 10 times higher than that of small surface area of vegetation cover. Hence, incorporation of stomatal conductance and surface area of vegetation is deemed necessary for analyzing evapotranspiration induced suction in green infrastructure projects.

2.6 Interpretation of soil surface water content

Soil surface water content affects the interaction between earth surface and atmosphere significantly. Interaction between earth surface and atmosphere includes exchange of mass and energy between surface of the earth and atmosphere (Deardorff, 1977). Surface water content

influences the partition of net radiation into latent heat and sensible heat (Famiglietti et al., 1998). This partition is the primary factor for cloud formation (Kuo, 1965). Models developed for numerical analysis of cloud formation consist of surface water content (Chen and Avissar, 1994). In addition, surface water content governs the evaporation. A large number of models were developed to estimate the evaporation using surface moisture content (Chanzy and Bruckler, 1993; Camillo and Schmugge, 1984; Bernard et al., 1986; Choudhury and Monteith, 1988). Furthermore, such evaporation induces suction near to the surface (Gasmo et al., 1999). This suction affects the infiltration and runoff that occur due to precipitation (Hino et al., 1988). Hence, accurate measurement of surface water content is important to understand soil-plant-atmosphere interaction.

A significant number of reliable approaches were developed to measure surface water content by previous researchers. Those were mainly remote sensing (Jackson, 1993; Engman and Chauhan, 1995; Kumar et al., 2018; van der Schalie et al., 2018) and ground based methods (Schmugge et al., 1980). In addition, satellite-based unmanned air vehicle (UAV) was developed by Van de Vyvere and Desenfans (2016) to measure surface water content of soil. Although remote sensing is a non-intrusive technique, resolution of observations is relatively high (Büyüksalih and Jacobsen, 2006; Habib et al., 2007). Therefore, accuracy of the obtained observations would be relatively low. Furthermore, remote sensing could not capture the ground information in highly urbanized zones (Kumar et al., 2018). Ground-based methods include gravimetry, neutron scattering, gamma attenuation and composite dielectric approach (Reynolds, 1970; Zreda et al., 2008; Reginato and Van Bavel, 1964; Roth et al., 1990). However, ground-based methods are economically infeasible to measure surface water content in very large areas. This is because ground-based methods require large number of instruments and labor force. These shortcomings

in previously developed approaches show the importance of a non-intrusive, feasible and cost effective approach to measure surface water content. It has to be noted that the reflection phenomenon was widely used by the previous researchers to categorize rocks and minerals (McCord et al., 1970; McCord et al., 1974; Clark, 1999; Tilley, 2010; Lau et al., 2017). Spectral reflectometry is the commonly adopted method to understand the reflectance of various minerals (Clark, 1999).

Few studies (Gómez-Robledo et al., 2013; Min and Huy, 2008; Yoshimoto et al., 2011; Peters et al., 2011; Sills et al., 2017) demonstrated non-intrusive colour analysis techniques to identify the surface water content on the basis of the reflection phenomenon in dry and wet soil. Fig. 2.2a and b shows the typical illustration of the reflection phenomenon in dry and wet medium (i.e., soil in this study). Light enters from one medium to another at air-water interface. As light rays incident on air-water interface, they undergo both reflection and refraction. Light rays cannot enter the soil particle, which is an opaque medium. Therefore, it is important to note that no refraction occurs at the soil particle and air interface. Hence, a major proportion of the incident light is reflected from the dry soil (see Fig. 2.2a; Al-Azzawi, 2006).

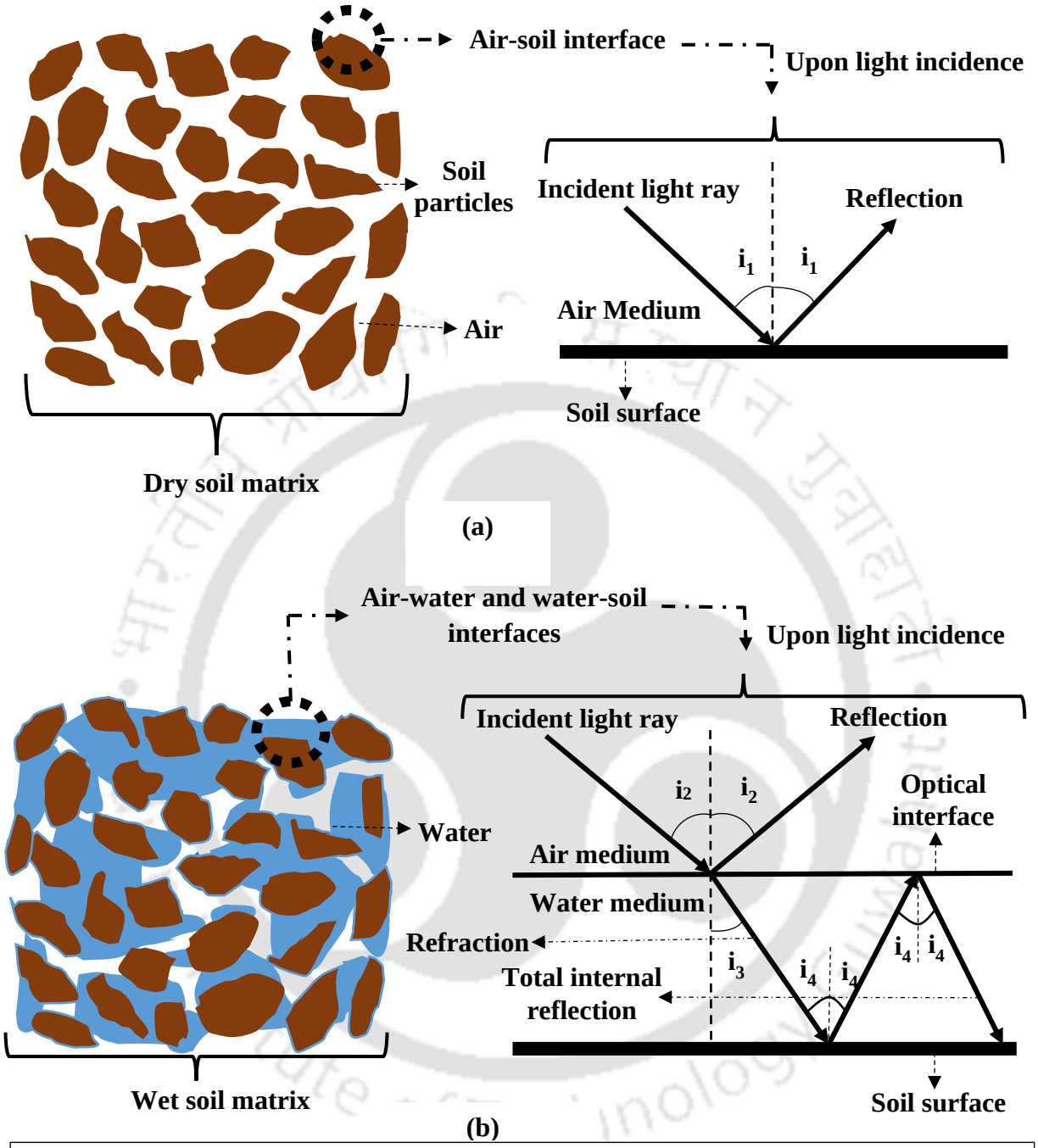

* Dry soil appears relatively bright due to the majority of incidental rays reflection

Wet soil appears relatively dark due to the occurrence of refraction and total internal reflection, which decreases light reflection

This difference in brightness can be identified on a scale, which shows dissimilarity between weakest intensity of light and strongest intensity of light (gray scale; Russ and Russ, 2007)

Fig. 2.2 Reflection phenomenon in (a) Dry soil and (b) Wet soil

Dry soil appears relatively bright due to this phenomenon. In case of the wet soil, light rays enter from air to water and refraction can be observed at the air-water interface (Fig. 2.2b). This refracted light incidents on water-soil interface and gets reflected. Similarly, several reflections may occur and the reflected light rays may reach the water-air interface. At this interface, light enters from a denser medium to a rarer medium. Due to this, light may reflect back to water medium depending on the angle of incidence. Such phenomenon is known as total internal reflection (see Fig. 2.2b; Al-Azzawi, 2006). Fewer light rays are reflected from the surface of wet soil because of the existence of reflection, refraction and total internal reflection, thereby making it appear relatively darker. This difference in brightness between dry soil and wet soil is the basis of a non-intrusive colour analysis technique.

Majority of the soil colour analysis approaches suggested by previous researchers are valid for controlled light conditions in laboratories (Gómez-Robledo et al., 2013; Min and Huy, 2008; Yoshimoto et al., 2011). Controlled light conditions refer to the presence of uniform light intensity over the entire selected soil domain. Incandescent lamps were used in previous studies to ensure controlled light conditions. However, light conditions could not be controlled manually in relatively large areas. It is evident that colour contrast occurs within the selected soil domain under uncontrolled light conditions. This is due to spatial heterogeneity of light intensity in the soil domain (Al-Azzawi, 2006). In addition, light intensity varies with time during the period of day light (Baker and Steemers, 2014). Hence, previous colour analysis approaches may not be applicable for monitoring surface water content in relatively large areas under natural light conditions. Recent studies (Peters et al., 2011; Sills et al., 2017) have demonstrated the colour analysis approach to differentiate the degree of saturation (DOS; i.e., from 5 % to 100 %) of transparent porous media (quartz and oil mixture) under uncontrolled light conditions. However,

soil is an opaque medium. As a result, correlation developed by Sills et al. (2017) would not be applicable to differentiate the surface water content of partially transparent or opaque moist soil. In addition, colour was analyzed at only one DOS between 40 % and 85 % in case of coarse quartz and oil mixture in their approach. Furthermore, DOS below 40 % was not considered for colour analysis of fine quartz and oil mixture. These shortcomings in previous studies show that novel, cost effective and feasible colour analysis approach needs to be developed to differentiate the soil surface water content under uncontrolled light conditions.

2.7 Spatial and temporal heterogeneity of surface hydraulic conductivity in urban space vegetated with deciduous species

Surface hydraulic conductivity of vegetated soil governs the ground water recharge, moisture content in vadose zone and stability of green infrastructure (Garg et al., 2018; Garg et al., 2019). In addition, surface hydraulic conductivity influences long term performance of green infrastructure (Garg et al., 2015 a, b, c). Surface hydraulic conductivity in vegetated soil was studied extensively by previous researchers (Mitchell et al., 1995; Huat et al., 2006; Leung et al., 2015). Few researchers show that surface hydraulic conductivity may increase due to presence of roots (Van Noordwijk et al., 1991). Whereas, decrease in hydraulic conductivity was found in some other studies (Gish and Jury, 1983). Although effect of roots was explored, variation of surface hydraulic conductivity in mix vegetation has been rarely studied. In addition, change in hydraulic conductivity with growth of vegetation was also rarely explored. Mix grass growth is usually expressed in terms of vegetation density. Various atmospheric parameters such as, rain fall, temperature and relative humidity influence the vegetation growth (Boisvenue and Running, 2006). In addition, growth response of deciduous species and evergreen species would be dissimilar (Smith et al., 2001). Generally, deciduous species are widely used in green

infrastructure. The effect of growth dynamics of grass on surface hydraulic conductivity was rarely studied by previous researchers. Spatial heterogeneity of hydraulic conductivity in mixed vegetation was investigated by a recent study. However, the surface hydraulic conductivity variation during entire life period of the selected species was not explored previously. It is known that growth rate varies with change in distance from trunk of the tree. Any effect of this dissimilarity on surface hydraulic conductivity was also not studied previously. Furthermore, long term field monitoring was rarely conducted to consider the seasonal effect on vegetation. Most of the numerical modelers (De Silva et al., 2008; Deb et al., 2013; Zhu and Zhang, 2015a, b; Garg and Ng, 2015) presume that hydraulic conductivity around trunk of the tree is axi-symmetric. However, validity of this assumption during entire life period of deciduous species was rarely investigated.

2.8 Summary and critical appraisal of literature review

The reviewed literature indicates that there are not many studies exploring the crack formation, suction and hydraulic conductivity in vegetated soil. In addition, cracks induced in vegetated soil were rarely related with canopy parameters such as LAI and vegetation density. This relationship is vital to analyze the water use efficiency and model the water balance at surface for vegetated soil. Commercially available sensors are usually installed to interpret suction in vegetated soil. However, non-intrusive and economical technique to devise instrumentation plan was not developed previously. Suction induced in vegetated soil was studied extensively by previous researchers. Nevertheless, relationship between suction and canopy parameters were rarely studied. This relationship is vital for numerical modelers and scientists to analyze the performance of green infrastructure accurately. It is evident that presence of roots may increase or decrease the

hydraulic conductivity. Although hydraulic conductivity was studied by previous researchers, spatial and temporal heterogeneity of vegetation growth in green space was rarely considered in previous studies. In addition, effect of spatial and temporal variation of vegetation growth on hydraulic conductivity was also rarely explored previously. Spatial and temporal variation of hydraulic conductivity is vital to devise drainage schemes in the green infrastructure. Furthermore, remote sensing is mainly used non-intrusive method to interpret soil surface water content. However, the resolution of satellite images used to interpret soil surface water content would be relatively low. Hence, such interpretation may not be accurate.

2.9 Objective and scope of the study

The main objective of this research work is to explore the soil-plant-atmosphere interaction by laboratory, field and numerical studies considering plant parameters and unsaturated soil parameters together. The following are various scopes of this study to achieve the objective:

1. Quantification of cracks induced in vegetated soil.

2. Numerical analysis of effect of plant parameters on evapotranspiration induced suction.

3. Demonstration and validation of non-intrusive colour analysis technique to quantify the spatial heterogeneity in mix grass cover.

4. Investigate the effect of evapotranspiration induced suction on plant parameters.

5. Demonstration and validation of non-intrusive colour analysis technique to interpret soil surface water content.

6. Investigation of spatial and temporal heterogeneity of surface hydraulic conductivity in urban space vegetated with mix grass.

2.10 Organization of the thesis

This thesis consists of eleven chapters. Chapter 1 deals with the introduction of the problem and motivation behind this research work. Chapter 2 describes the previous literature related to the soil-plant-atmosphere interaction and the background information of soil and plant parameters leading to the scope of the attempted research. In chapter 3 and 4, crack formation in soil vegetated with crop and non-crop species are presented. Effect of plant parameters on suction induced in vegetated soil was analyzed numerically and shown in chapter 5. Demonstration and validation of a novel colour analysis technique to devise instrumentation plan in vegetated soil is presented in Chapter 6. Chapter 7 explains the influence of suction on canopy parameters. Chapter 8 demonstrates the colour analysis technique to interpret soil surface water content. Chapter 9 details the spatial and temporal heterogeneity of surface hydraulic conductivity in a green space. Chapter 10 summarizes the conclusions, limitations and future scope of the present study.

CHAPTER 3 CRACK FORMATION IN SOIL VEGETATED WITH CROP SPECIES

3.1 General

This chapter presents the effect of vegetation (*cowpea*) growth on crack formation for exploring correlation between plant growth and cracking. Growth of vegetation was expressed in terms of shoot parameters (shoot length (SL) and leaf area index (LAI)). Crack formation was expressed in form of crack intensity factor (CIF). Experimental test pots were used to observe crack formation on vegetated and bare soil in greenhouse. Ratio of crack area to the total area of soil surface is referred as CIF. The one-sided green leaf area per unit ground canopy area is referred as LAI.

3.2 Material and methods

3.2.1 Soil property

Red soil is selected for investigation, which is commonly found in subtropical regions (Narayana and Babu, 1983; Wang et al., 2004; Huang et al., 2010). Soil was collected from a hill site in north east region in India. The soil is classified as ML, according to unified soil classification system (USCS; ASTM D2487-11). Grain size distribution of the soil reveal that the soil constituted mainly of silt (50 %) and clay (25 %), followed by fine sand (19 %) and medium sand (6 %). Liquid limit, plastic limit and shrinkage limit are 41 %, 25 % and 13 % respectively. Basic physical and engineering properties of the soil are summarized in **Table 3.1**. These properties were determined by following the provisions stated in ASTM codes (ASTM D854-06; ASTM D2487-10; ASTM D698-07 and ASTM D4318-93).

Table 3.1 Engineering properties of red soil

Sl. No	Soil property	Value
1	Specific gravity	2.55
2	Grain Size Distribution	
	Coarse Sand (4.75mm-2mm)	0 (%)
	Medium Sand (2mm-0.425mm)	6 (%)
	Fine Sand (0.425mm-0.075mm)	19 (%)
	Silt (0.075mm-0.002mm)	50 (%)
	Clay (<0.002mm)	25 (%)
3	Consistency Limits	
	Liquid Limit	41 (%)
	Plastic Limit	25 (%)
	Shrinkage Index	12 (%)
	Plasticity Index	16 (%)
4	Compaction Characteristics	
	Optimum Moisture Content	17 (%)
	Maximum Dry Density	1.70 (g/cc)

3.2.2 Plant species and germination condition

The vegetation type selected is a crop species, Cowpea (*Vigna unguiculata*). Cowpea is an important crop widely cultivated by farmers in Sub Saharan countries and Asia, Africa and America (Singh et al., 2003). Cowpea is well known for its adaptation to nutrient poor soils (Solleti et al., 2008). The growth stage of cowpea is generally classified into three stages, namely vegetative growth stage (first 30-40 days), reproductive growth stage (next 20 days) and physiological maturity stage (last 15 days) (Mass and Poss 1988, Agyeman et al. 2014). However, the maturity time (63 -80 days) is reported to vary due to different local climatic conditions and species (Agyeman et al. 2014). The matured seeds of cowpea cultivar, Pusa Komal were procured from Seed Corporation of India, New Delhi. The seeds were germinated on cotton moistened with tap water, in petri dishes for three days in dark, at 25 ^{0}C under florescent light (140 μE $m^{-2}s^{-1}$). The germinated seedlings were transferred to the pots for conducting experiments.

3.2.3 Test plan

A test plan is designed to quantify and compare CIF between bare and vegetated soil in controlled irrigation for a period of 70 days until the plant completes reproductive growth stage. Apart from irrigation, plant parameters were subjected to natural environmental conditions. All the experiments were conducted in a greenhouse (Fig. 3.1). In total, 10 pots (5 vegetated pots, 5 bare pots) were monitored in the test duration. The seedlings of the plant species were germinated and transplanted to the 5 pots. All the 10 pots were irrigated at a regular interval. The evaporation/evapotranspiration rate was measured regularly and reported in later section. The SL

was measured manually and the crack surface and LAI were measured using image analysis as discussed in later section.

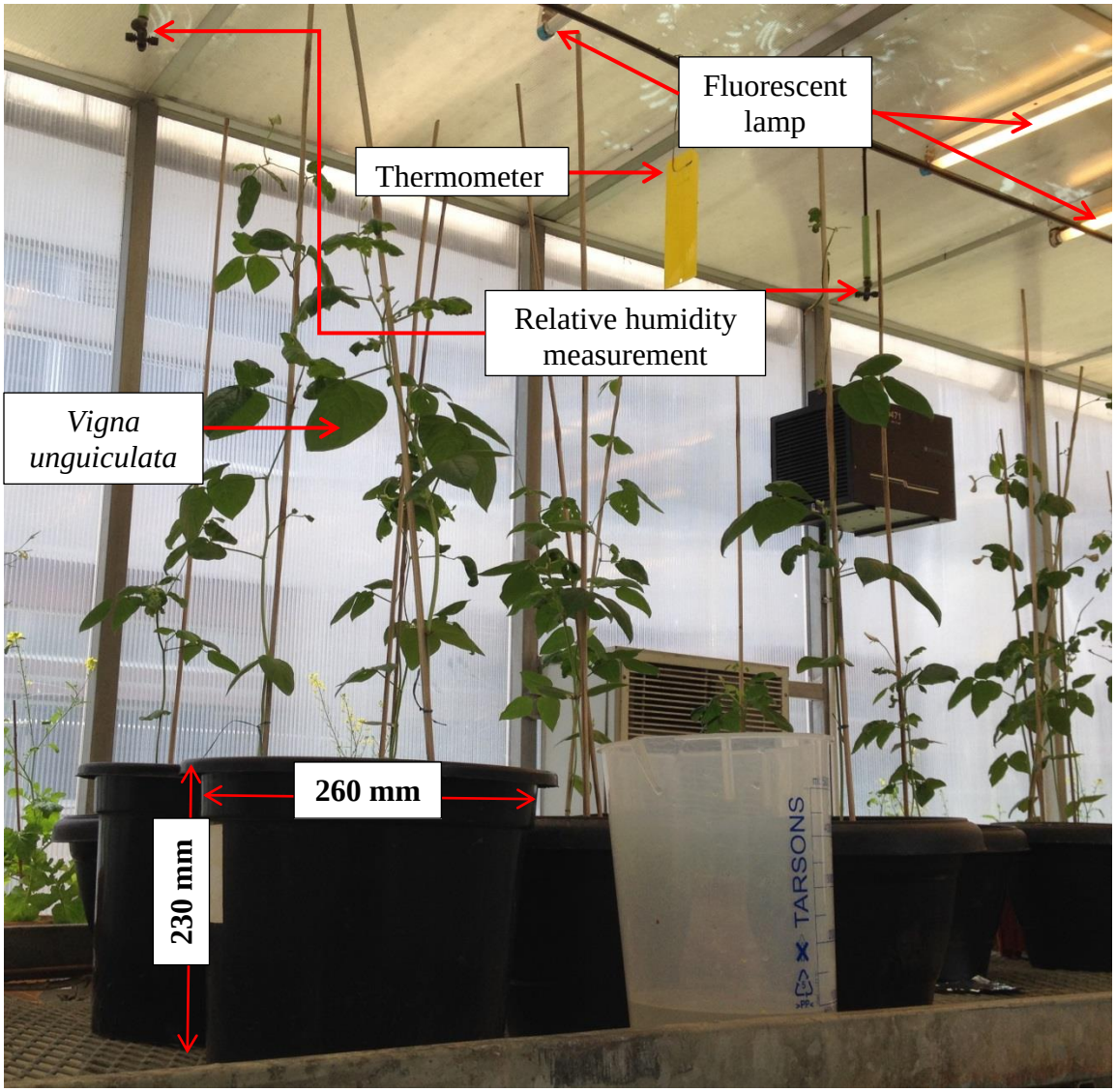

Fig. 3.1 Overview of experimental setup placed in greenhouse

3.2.4 Experimental setup

The relative humidity and temperature were observed at 52 ±8 % and 26 ±4 ^{0}C, respectively. To provide radiant energy to the legume seedlings, a provision of white fluorescent lamps capable of emitting light with photosynthetic photon flux density of 50 µmol m^{-2} s^{-1} was mounted on top (2.5 m from floor base). The cylindrical pots used to conduct experiment were made from PVC plastic in house. Its dimensions were 260 mm diameter and 230 mm depth with perforated base to allow water drainage from the bottom. The soil was compacted in three equal layers to maintain a uniform density of 1.3 g/cc (equivalent to 0.77 maximum dry density of soil) up to 185 mm from bottom. All the 10 pots were irrigated (400 mL per pot using a watering can) regularly after 3 days of interval as shown in Fig. 3.2 after transplantation. Evapotranspiration and evaporation rate of 5 vegetated and 5 bare pots were measured by observing change in weight. Fig. 3.2 shows the mean and standard deviation of evaporation/evapotranspiration rate after transplantation (3 day interval). It is to be noted that the evapotranspiration and evaporation rate noted in the study was calculated for all 10 different pots individually. SL for all the vegetated pots has been measured using a metric scale at the same 3 day interval after transplantation. The surface crack formation and leaf area photos were captured regularly after 9 days interval starting from 15th day after transplantation. Canon EOS 600D with lens range (18-55 mm), horizontal/vertical resolution of 72 dpi was used to capture images under early morning ambient light. The exposure time, focal length and ISO speed was maintained at 1/30 sec, 23 mm and ISO-640, respectively for crack analysis. Photographs were captured carefully from the same angle (45^0) and height (0.75m from floor base) using a frame with adjustable height (Fig. 3.3), to minimize any observational error for CIF analysis. In case of LAI analysis, the exposure time, focal length and ISO speed was maintained

at 1/60 sec, 30 mm and ISO-400 respectively and the photographs were captured from a fixed position (1.5m above and parallel to the floor base).

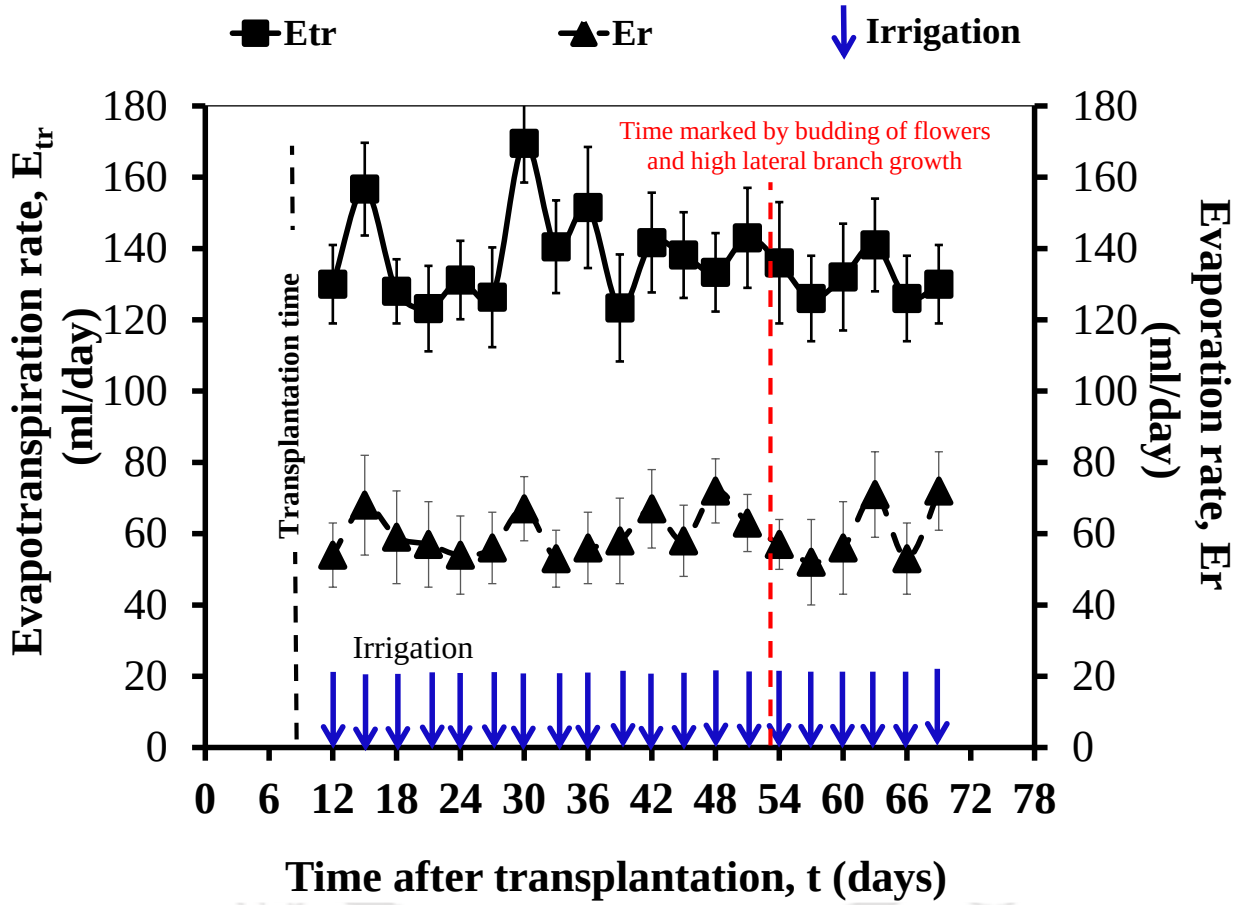

Fig. 3.2 Measured evapotranspiration and evaporation rate of soil along with irrigation schedule during testing period

3.2.5 Procedure for analysis of CIF and LAI

In this study, the image-processing software ImageJ (Rasband, 2011), has been used to analyze the surface crack and leaf area. The surface crack has been analyzed using the CIF parameter which is the ratio of crack area (A_c) to the total area of soil considered (A_t). The 'A_c' and 'A_t' of drying

soil mass were determined using photographs of desiccating soil at regular interval of time (15, 24, 33, 42, 51, 60 and 69 days; at various ages of plants) after transplantation. Cracks appear darker than remaining uncracked soil in photographs of a drying soil (Yesiller et al., 2000). This colour contrast between cracked and uncracked soil for the same photographic condition is used to analyze CIF. For CIF analysis, the captured image is imported into ImageJ, and the digitized image is cropped to only account for the soil surface as shown in Fig. 3.3. The image was cropped such that any boundary shrinkage was excluded and only surface cracks were taken for further analysis. In order to calculate the areas, the cropped image was transformed into binary image as shown in Fig. 3.3**.** The pixels that are occupied by the cracks (white portion) and by the total soil surface (both white and black) is calculated to obtain CIF of soil. To ensure equal soil surface area analyzed for all pots, each pot was calibrated to account for equal number of pixel area. This was done by maintaining same height and angle of captured image and it was cross checked by observing the pixel area (accuracy of ±2 %) for the soil pot. For example in Fig. 3.3, 560 cm^2 soil area of pot (diameter = 26 cm) was calibrated to 7719028 pixels.

The LAI of the vegetated soil is obtained using colour threshold technique using ImageJ. As in the case of CIF calculation, the captured image is imported into ImageJ, and the digitized image is cropped to only account for the plant canopy as shown in Fig. 3.3. To calculate the leaf area, the cropped image was adjusted (for hue, saturation and brightness) using (Threshold Colour) option in the software (refer Fig. 3.3). Under this option, only those pixels are selected that fall under the leaf colour (white portion in Fig. 3.3). These pixels are calculated and taken into account as leaf area. The ratio of the leaf area and total plant canopy area is used to calculate LAI. Any noise (unwanted area) was subtracted in both measurements (CIF and LAI).

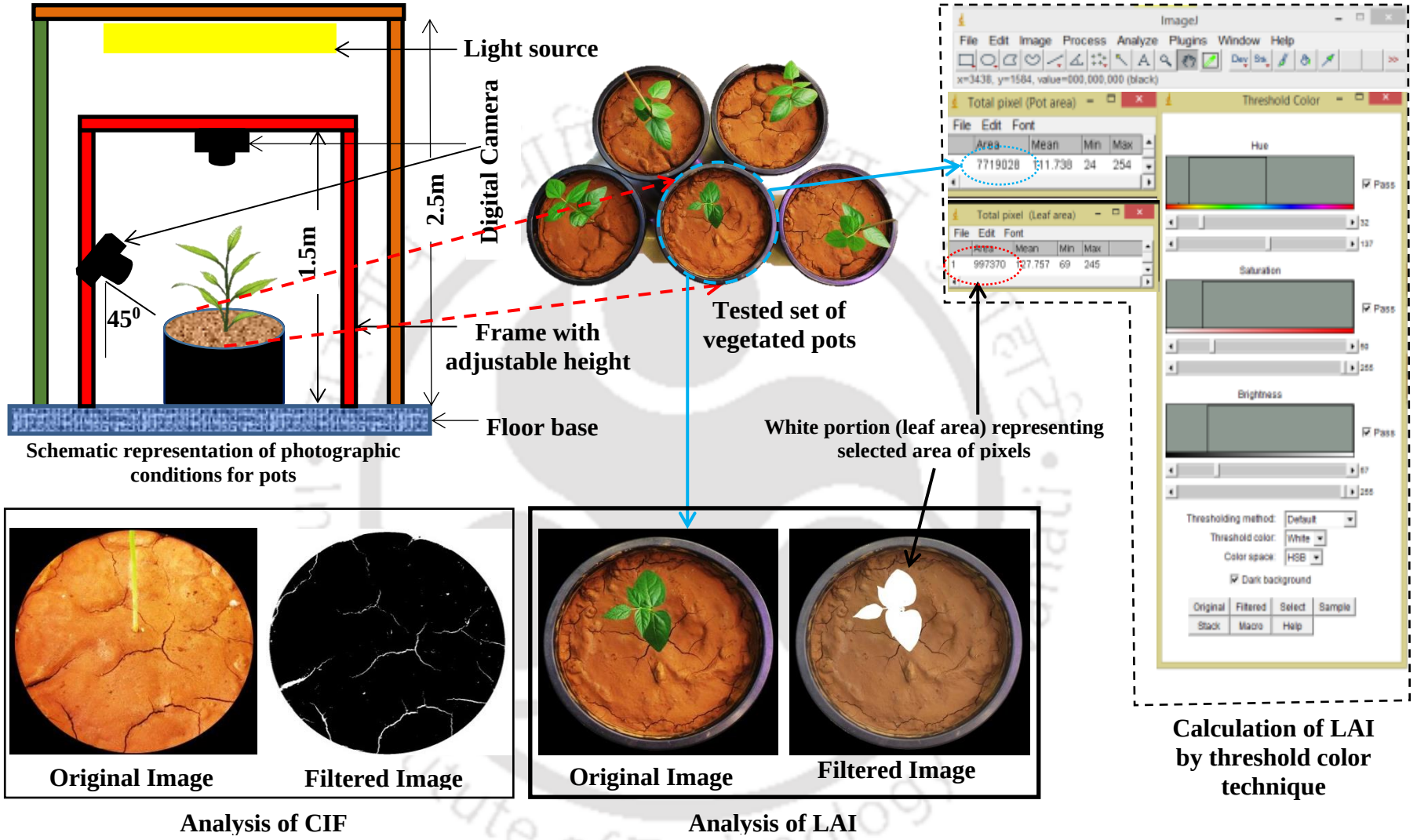

Fig. 3.3 Determination of LAI and CIF respectively by image analysis using threshold colour technique

3.3. Results and discussion

3.3.1 Variation of CIF with time for both bare and vegetated soil

As shown in Fig. 3.4(a), the mean CIF value for bare soil increased from 0.93 to 3.22 up to 51 days. From 51 to 70 days, the CIF value is seen to be relatively constant. This trend has been observed in previous literature (Tang et al., 2012; Li et al., 2016; Wang et al. 2017). The CIF variation for bare soil has been fitted and represented by Eq. 3.1 with an R^2 value of 0.97. The analyzed time-lapse binary image of cracked soil for a particular bare pot has been shown in Fig. 3.4(b).

$$CIF_{bare} = -0.0004t^2 + 0.0772t + 0.1752 \qquad (\text{where } 15 \leq t\ (\text{days}) \leq 70) \qquad (3.1)$$

This increase in CIF can be attributed to repeated drying-wetting cycles as reported in similar studies with clay (Yesiller et al., 2000; Tang et al., 2012; Li et al., 2016; Wang et al. 2017). During the drying cycle, the soil possesses relatively high soil strength which resists cracking (tensile) forces related to high suction. The drying spell is accompanied by shrinkage of soil which further causes structural rearrangement of soil particles and potential breaking of bonds (Tang et al., 2012). The subsequent wetting cycle causes decrease in soil strength. This in turn, increases tendency of cracking in next drying cycle (Yesiller et al., 2000).

A similar trend has been observed in variation of CIF for the first 33 days in all 3 vegetated pots. The mean CIF increase from 0.93 to 5 for the initial 33 days and the CIF remained relatively constant thereafter up to 70 days. The CIF values for vegetated soil were observed to be greater than bare soil as shown in Fig. 3.4(a). This relative increase of CIF values for vegetated soil can be attributed to transpiration induced suction. As observed in Fig. 3.2, the evapotranspiration rate of vegetated soil is much higher than the evaporation rate of bare soil.

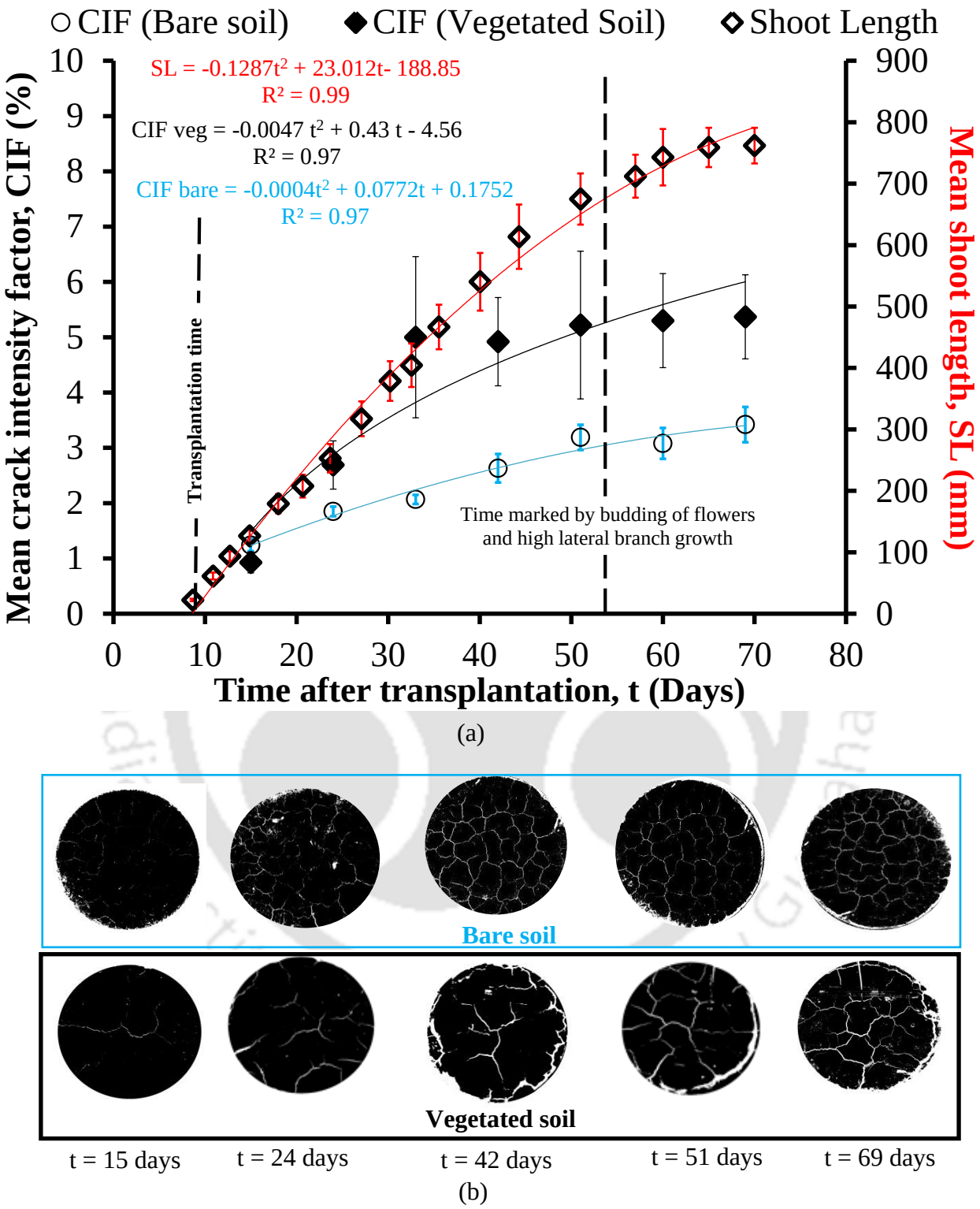

Fig. 3.4 Variation of (a) CIF (bare and vegetated soil) and SL of plant with time (b) Binary image representation of cracks (white section) with time for a single pot (bare and vegetated soil)

This results in relatively higher suction (transpiration induced) in vegetated soil and correspondingly induces more cracks as compared to bare soil (Garg et al., 2015a, b, c; Leung et al., 2015b). The CIF variation for vegetated soil has been fitted using a polynomial equation and represented in Eq. 3.2. The R^2 value of Eq. 3.2 is 0.97.

$$CIF_{veg} = -0.0047\ t^2 + 0.423\ t - 4.56 \qquad (\text{where } 15 \leq t\ (\text{days}) \leq 70) \qquad (3.2)$$

The time lapse crack variation for the test period in a single vegetated pot has been shown in Fig. 3.4(b)**.** The binary image representation of cracks in the pot shows that there has been an increase in cracks till 33 days after transplantation. Thereafter the crack portions are relatively same. This is due to CIF attaining its maximum potential earlier than that of bare soil due to transpiration after which there is no further increase in crack surface.

3.3.2 Relationship between shoot parameters and CIF for vegetated soil

The SL variation throughout the experiment has been monitored for all the five vegetated pots up to 70 days. A linear increase in mean SL has been observed initially up to 50 days at the vegetation stage of the plant as shown in Fig. 3.4. The SL growth rate decreases after 50 days. This slowing down of SL is due to energy of the plant being expended for flower growth. This has been fitted as a second degree polynomial equation (Eq. 3.3). The R^2 value of the equation is 0.99.

$$SL = -0.1287t^2 + 23.012t - 188.85 \qquad (\text{where } 9 \leq t\ (\text{days}) \leq 70) \qquad (3.3)$$

The effect of SL on crack formation is proportional up to 33 days. With increase in SL there is a visible increase in CIF as shown in Fig. 3.4. This is due to increase in transpiration due

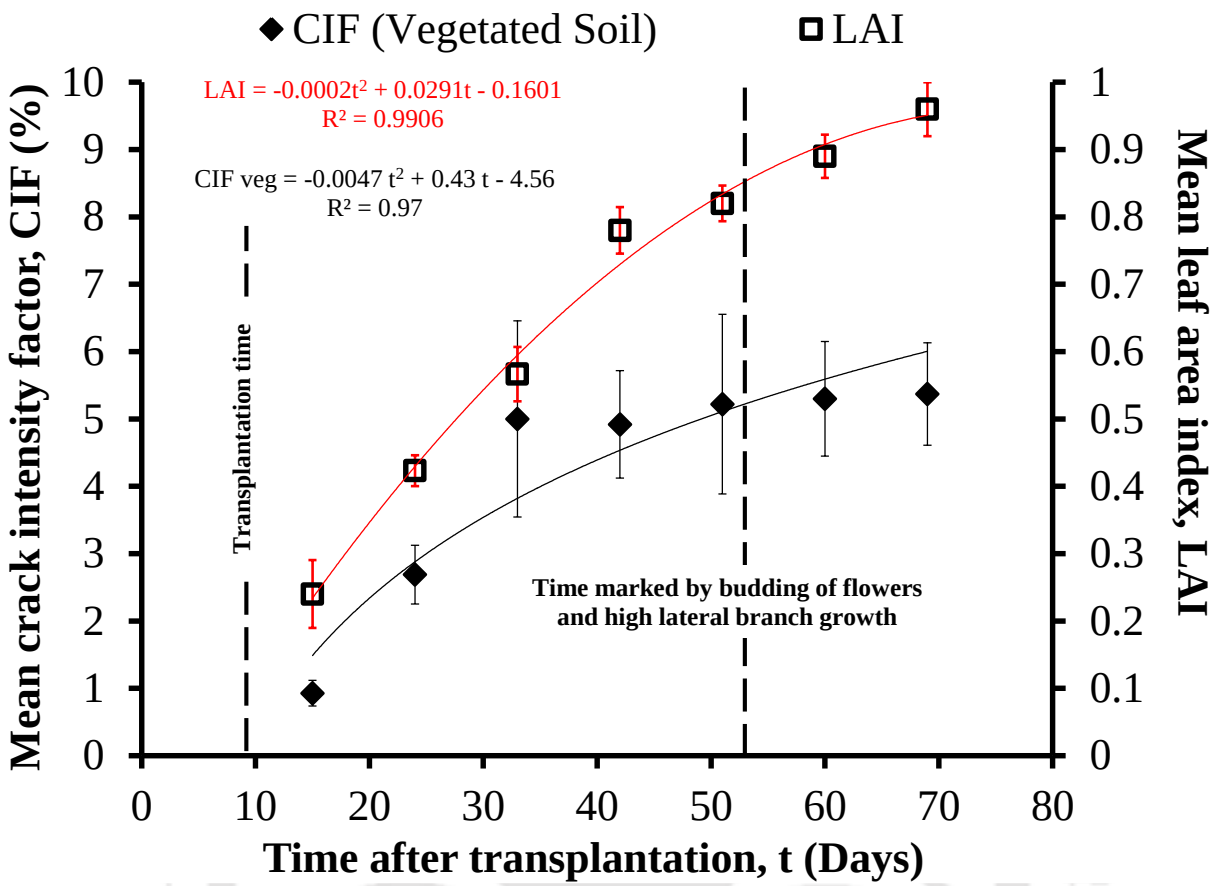

(a)

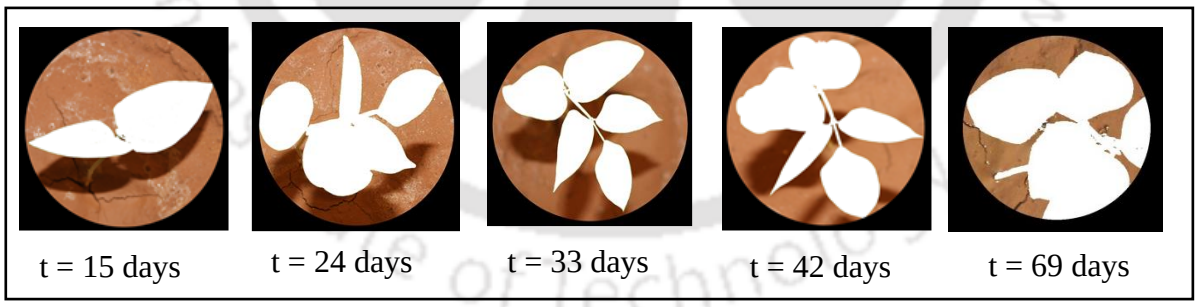

(b)

Fig. 3.5 Variation of (a) CIF (vegetated soil) and its corresponding LAI with time (b) threshold image representation of leaf area (white portion) with time for a single pot

to plant growth throughout this period. This period of plant growth is marked by preliminary growth of lateral branches (with leaves), which contributes to enhanced transpiration. After 33 days of shoot growth (i.e. SL = 400 mm), the CIF values showed no visible increase but remained constant thereafter. The relationship between SL and CIF for the plant species has been fitted to give a third degree polynomial equation and represented by Eq. 3.4. The R^2 value in Eq. 3.4 is 0.97.

$$CIF_{veg} = 2E\text{-}08SL^3 - 5E\text{-}05SL^2 + 0.034SL - 2.79 \quad (\text{where } 127 \leq SL\ (mm) \leq 762) \qquad (3.4)$$

The LAI variation for the entire testing period has been measured using colour threshold analysis using ImageJ. As shown in Fig. 3.5(a), LAI increased from 0.24 to 0.96 with increase in time. This LAI variation with time is given by Eq. 3.5. The R^2 value is 0.99 for Eq. 3.5.

$$LAI = -0.0002t^2 + 0.0291t - 0.1601 \quad (\text{where } 15 \leq t\ (\text{days}) \leq 70) \qquad (3.5)$$

As in the case of SL, the effect of LAI on crack formation is proportional up to 33 days after which the CIF remains relatively constant. The LAI corresponding to 33 days after transplantation was 0.56. The relationship with LAI and CIF for the entire testing period was represented by a second degree polynomial equation (eq. 3.6). The R^2 value of equation 3.6 is 0.96.

$$CIF_{veg} = -11.75\ LAI^2 + 20.15\ LAI - 3.29 \quad (\text{where } 0.24 \leq LAI \leq 0.96) \qquad (3.6)$$

In this study, LAI values are found to be low for the cowpea plants (less than 1). However, grass species may exhibit relatively higher LAI values (Garg et al., 2015b) and the equation may not be valid for such species with higher LAI. Further studies are needed for other type of species with higher LAI. The LAI variation for a single pot has been shown in Fig. 3.5(b). It is evident that there is a gradual increase in LAI with time.

3.4. Summary and conclusion

The present study investigates the effect of a plant species (*cowpea)* growth, on the cracking of soil for repeated drying-wetting cycles. The tests were done to explore any correlations between shoot parameters and its corresponding CIF. Based on the results and discussion, the following conclusions have been drawn and discussed. The CIF values for vegetated soil were relatively higher than bare soil throughout the test period. This increase in crack was attributed to transpiration induced suction in case of vegetated soil. CIF increases linearly with SL up to a threshold value of 400 mm, marked by initiation of leaf growth in lateral branches. After attaining SL equal to 400 mm, there was no visible increase in CIF corresponding to further growth (up to 762 mm) of plants. The CIF increases with LAI for the selected species up to LAI equaling 0.56. The CIF value remained relatively constant thereafter with further increase in LAI. Correlations were developed to relate the CIF with SL and LAI. The obtained correlations can be adopted while designing drainage, analyzing water use efficiency and modeling water balance at surface for soil vegetated with cowpea.

CHAPTER 4 CRACK FORMATION IN SOIL VEGETATED WITH NON-CROP SPECIES

4.1 General

This chapter presents effect of mix grass (non-crop species; *Axonopus Compressus* and *Cynadon Dactylon*) growth on crack formation. Growth of mix grass was expressed in terms of vegetation density. The vegetation density (VD) is defined as the ratio of the two dimensional vegetation area to the two-dimensional total area in consideration. Crack formation was expressed in form of crack intensity factor (CIF). Experimental test pots were used to observe crack formation on vegetated and bare soil.

4.2 Material and methods

4.2.1 Test plan, setup and instrumentation

The engineering properties of the selected soil are discussed in section 3.2.1. Two test series were conducted in compacted soil with and without vegetation; plant characteristics (vegetation density) and soil properties (suction, CIF) were determined. Mix grass, which is a combination of two grass species namely, *Axonopus Compressus* and *Cynadon Dactylon* were selected for the study. The selection was based on its (i) wide spread existence in subtropical regions (Sun and Liddle 1993; Avilés-Nova et al., 2008), (ii) drought tolerance ability, which is suitable for low maintenance and erosion control (Eusebius et al., 2002) and (iii) the recognition of its significant ornamental and eco-friendly values for land and slope rehabilitation and reforestation (Singh et al., 2013). It should be noted that the selected species are non-crop species and supplementary nutrients are not needed for growth. Rhizomes of both species were collected from nearby green space.

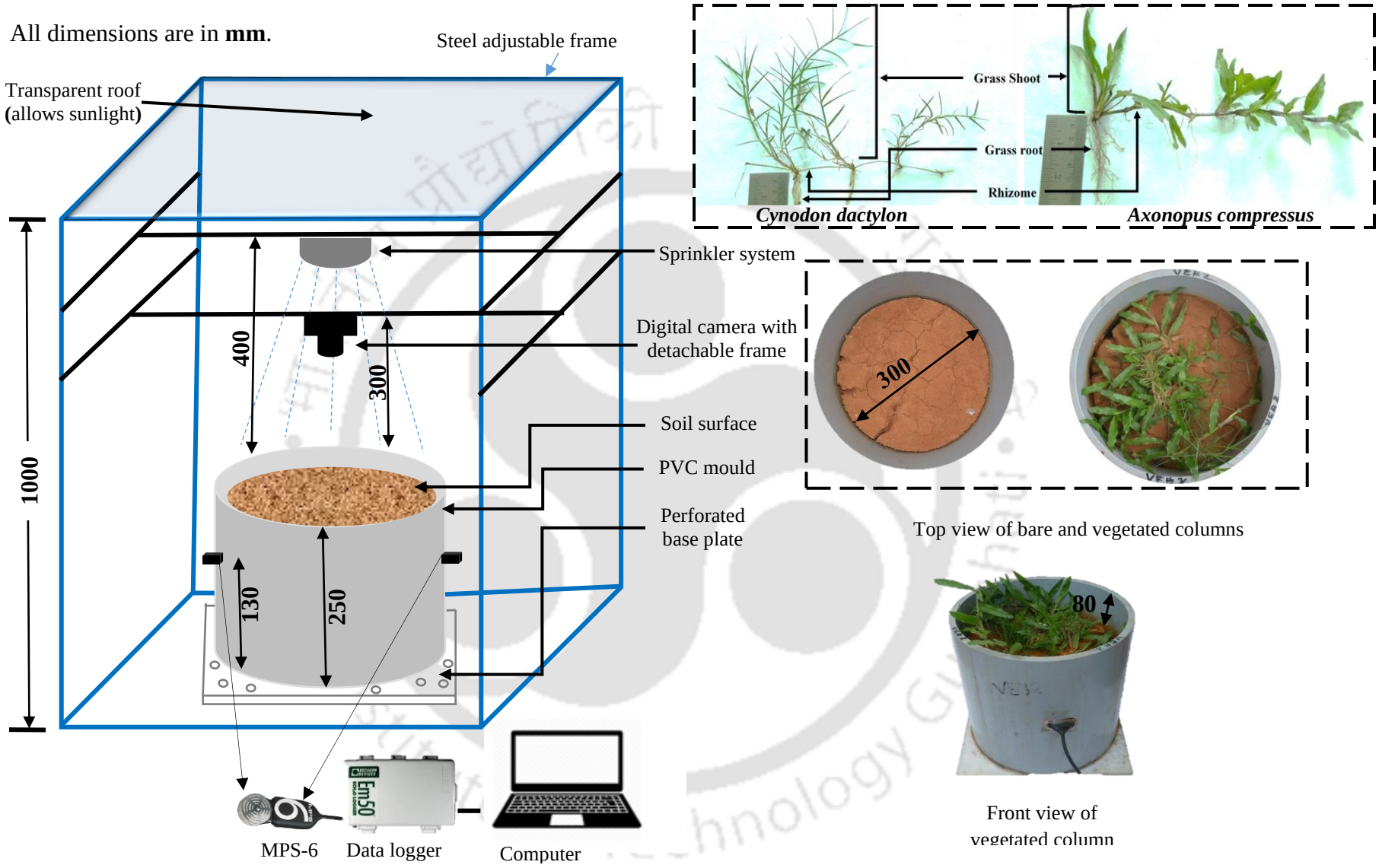

Fig. 4.1 Schematic representation of experimental setup used to measure CIF and vegetation density

Fig. 4.1 shows the schematic setup of the vegetated soil column along with a control bare column. 27 columns (24 and 3 with and without vegetation respectively with diameter 300mm adhering to minimum representative elementary volume requirements for desiccation; (Li and Zhang, 2010) and height 250mm) were fabricated in-house. The MPS-6 sensors (Meter, 2016a) were installed to measure suction as shown in Fig. 4.1. Dummy tubes were placed during compaction at the locations of suction sensors. The diameter of these tubes is relatively less as compared to sensors, to ensure the tight contact between soil and instruments after installation.

Soil sample was compacted statically to a targeted dry density of 1.56 g/c.c (i.e., equivalent to relative compaction of 90 %). Relative compaction refers to the percentage ratio of the adopted dry density for sample preparation to the maximum dry density determined by the standard Proctor compaction test. The selected relative compaction is commonly adopted for embankment construction (Li et al., 2016). A vertical force of 60 kN was applied to statically compact the soil (Reddy and Jagadish, 1993). The final height of the sample is 170mm from base. A perforated PVC base plate was attached to the mould to allow drainage. A filter paper was placed on base plate to prevent loss of soil particles from mould. In addition, the inner surface of the mould was coated with lubricant to reduce interface friction between soil and PVC. The soil was compacted in three different layers of equal thickness.

Three rhizomes of both species were collected from nearby grassland and transplanted to central portion of soil column (20 mm depth) for enabling equal probability for growth. The compacted soil columns for both series were then exposed to environmental conditions within a steel frame with a transparent roof. The transparent roof protected the columns from natural rainfall, while allowing daily sunlight and wind. The meteorological parameters were measured by a micro-climate monitoring system (MCMS, METER Group, USA) which was placed adjacent

to the columns with a radial distance of 1.2 m. The steel frame is equipped with an adjustable sprinkler and digital camera mount system. The camera was used to monitor the CIF and vegetation density evolution with time. The measured meteorological parameters were also used to estimate potential evaporation and evapotranspiration rate (Penman, 1948; Monteith, 1965).

4.2.2 Test procedure

Monitoring of the aforementioned parameters for both test series was done for a period of 73 days from transplantation. Initially, all columns were daily irrigated (500 ml) for allowing vegetation growth until the 18th day when rhizome developed into grass leaves (3-4 in number for each species). Further on, the plants were water stressed and irrigation was done at an interval of 7 days by providing 1000 ml of tap water. The sensors were placed at 4-cm depth to capture the near surface suction as well as suction induced by root water uptake as previously stated in the literature (Ng et al., 2014) for grass species. Drying of soil in the 7-day interval naturally results in desiccation cracks in both bare and vegetated soil. The maximum crack in each drying cycle and corresponding vegetation growth was quantified by CIF and vegetation density respectively by the colour threshold technique. The approach for obtaining CIF and vegetation density is depicted schematically in Fig. 3.3. To obtain clear CIF data for the vegetated columns, the vegetation shoot was cut off entirely from 3 vegetated columns at the end of each drying cycle.

4.3 Results and discussion

Fig. 4.2a shows the evolution of desiccation cracks with time and vegetation density (at 32, 46, 60, 67 and 73 days) in the form of CIF for both bare and vegetated soil. All the parameters in this study are measured at the end of each drying cycle and reported with their mean and standard-error of the mean. It is seen that up-to 3rd cycle the cracks in both bare and vegetated soil are seen to be of similar magnitude where vegetation density growth is relatively less (12.23 ±1.3 %) (Fig. 4.2b). Thereafter, the crack magnitude increases for the bare soil in comparison to vegetated soil. There is considerable variation in the CIF values at the end of 4th cycle where CIF exhibited by bare soil is considerably higher than vegetated soil. Bare soil CIF increases up-to 2.65±0.56 at the end of the 6th cycle (60 days) and becomes constant thereafter. A CIF potential for the same soil and irrigation patterns have reported (in chapter 3) a maximum CIF of 3.15 for a compaction condition of 0.8 MDD. However, in the case of vegetated soil, there is barely any increase in CIF after vegetation density of 40 % and 6th drying cycle (DC). This is contrary to the case of the same vegetated soil where crop species *Vigna unguiculata* was grown. It was reported that maximum CIF is almost double than that for bare soil (see chapter 3) due to the species' high transpiration rate. However, for another grass species *Festuca arundinacea*, CIF of vegetated soil was found to be lower (0.36 %) than that of bare soil (1.03 %) (Li et al., 2016). Additionally, Fig. 4.2c showcases the effect of vegetation density on CIF for the current vegetation type and it is seen that an average vegetation density of 40 % for the current species restricts the CIF up-to 2.1 ± 0.03. Fibrous root growth beneath the soil surface restricts and reinforces the propagation of crack planes in soil by the "bridge effect" similar to the case of fiber reinforced soil (Zhou et al., 2009; Loades et al. 2010; Tang et al. 2007). Thus, during later DCs where roots start to propagate throughout the soil it is expected that root propagation potentially restricts the CIF value. However, *Vigna unguiculata*

consists tap root system (Kang et al., 1985; Kahn and Stoffella, 1991; Burridge et al., 2016). Unlike fibrous root system, tap roots would not be propagated horizontally. Hence, soil vegetated with *Vigna unguiculata* induces higher CIF than bare soil.

It is contentious in literature whether grass species restrict desiccation by root bridge-effect (Zhou et al., 2009) or promote cracks by restricting self-healing and high transpiration induced suction (Ng and Leung, 2012, Sinnathamby et al., 2014). To study this, it is important to know the suction variation in both bare and vegetated soil as well as understand the transpiration rate of the plant-species itself. At first, the matric suction monitored at 40 mm depth from the surface for both vegetated and bare soil is shown in Fig. 4.3. It is seen that for the first 5 cycles, the suction exhibited by vegetated soil is relatively more than bare soil. However, in the last 3 cycles of monitoring the suction exhibited by both bare and vegetated soil is seen to be relatively same. This is probably explained by the growing grass canopy that is intercepting the radiant energy of sun from reaching the soil surface and consequently decreases surface evaporation (Garg et al., 2015c). In general, vegetated columns experienced more if not less range of suction throughout the monitoring period and still showcased less CIF as compared to bare soil. Hence, for this mixed grass species and allied conditions, the role of transpiration induced suction in promoting cracks is probably not significant.

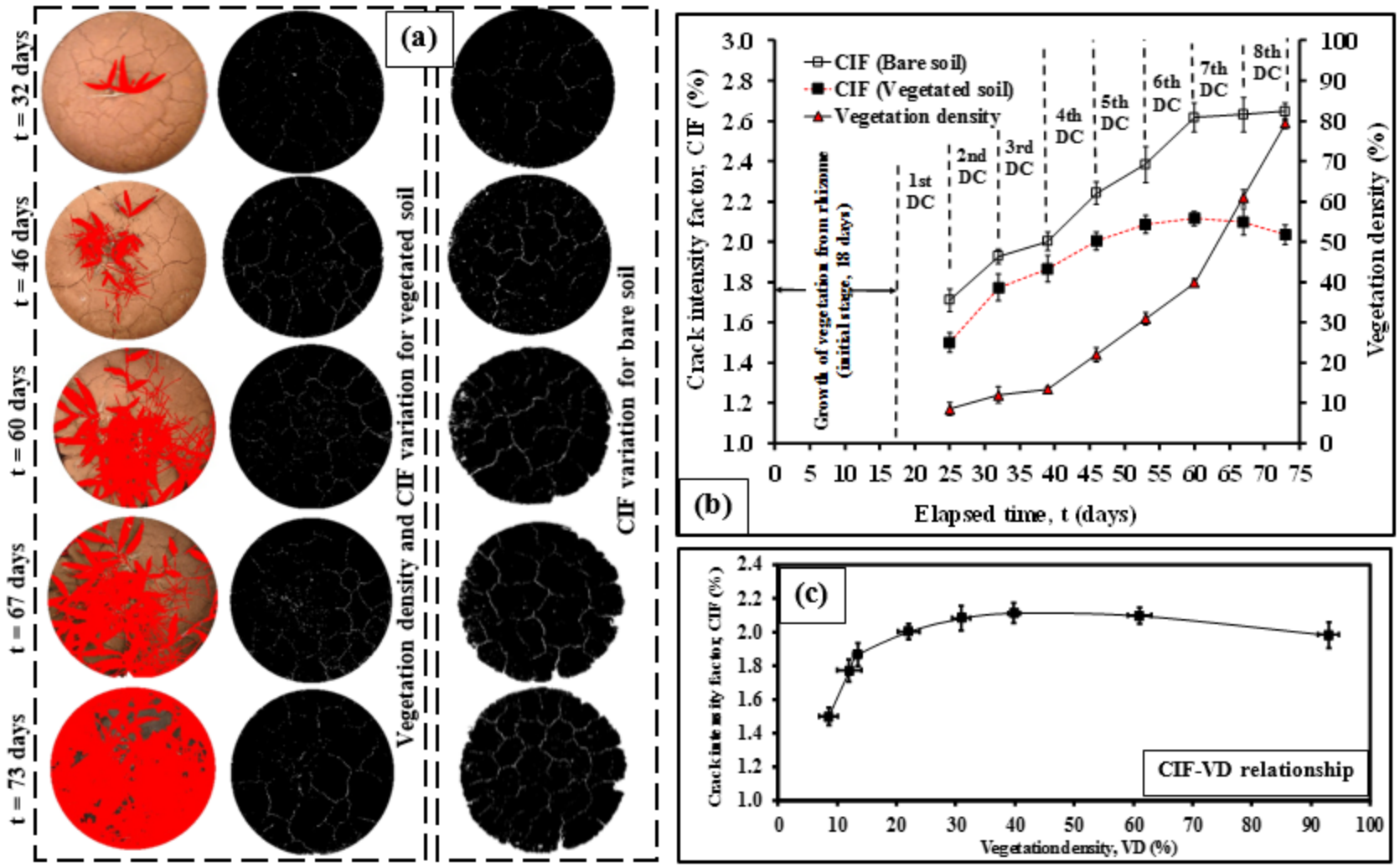

Fig. 4.2 Variation of (a-b) CIF (both bare and vegetated soil) and vegetationd density during the monitoring period; and corresponding (c) CIF-vegetation density relationship

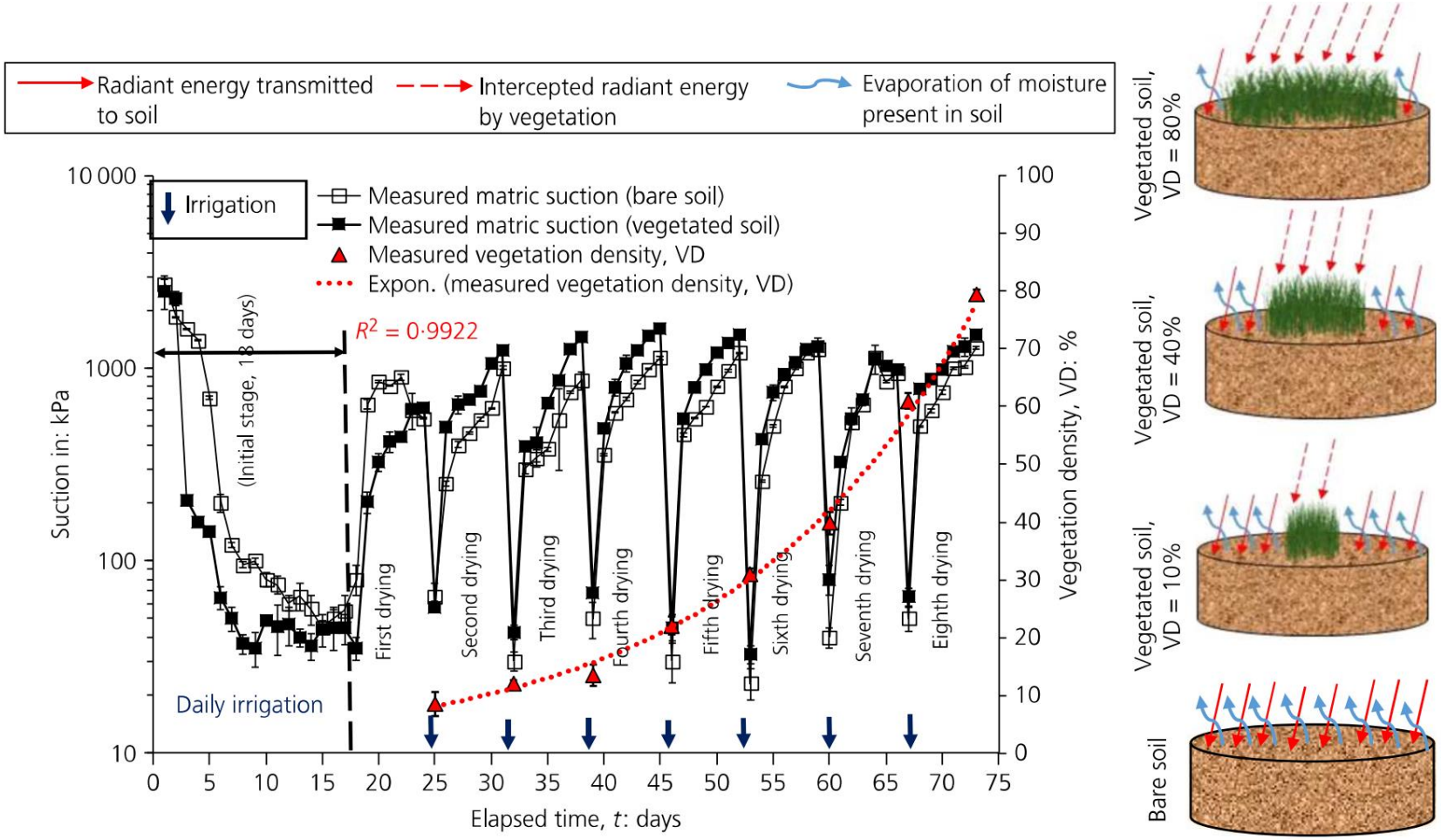

Fig. 4.3 Suction response for bare and vegetated soil during the study with schematic representation of intercepted radiant energy by vegetation density increase

4.4 Summary and conclusion

This study monitors and explores the effect of vegetation growth of two native grass-species on soil desiccation parameters (CIF, matric-suction). The desiccation parameters of vegetated soil were compared with that of bare soil for an early plant establishment period of 73 days. It is seen that the grass species helped reducing (≈ 20 %) the maximum CIF of the bare soil. This was attributed to bridge effect caused by root growth. A threshold vegetation density growth of 40 % restricts further increase in CIF for the native mixed species. This was due to the interruption of radiant energy falling on the soil by plant canopy. The induced suction due to transpiration is probably not enough to exude further cracks as compared to bare soil. Unlike the non-crop species, CIF induced in soil vegetated with crop species was higher than that in bare soil. This was attributed to the relatively low root tensile strength and tap root system of crop species. The obtained correlations can be adopted while analyzing seepage and modeling stability of slope vegetated with the selected grass species.

CHAPTER 5 MODELING SOIL-PLANT-ATMOSPHERE INTERACTION: EFFECTS OF PLANT PARAMETERS ON ROOT ZONE SOIL SUCTION

5.1 General

Vegetation canopy and root properties are known to affect evapotranspiration, which may in turn influences soil suction (or matric potential) and hence, performance of green infrastructure (slopes, landfill covers, biofilters). In previous field and laboratory studies, since these effects are coupled, any understanding of its effect on soil suction and performance of green infrastructure becomes difficult. The objective of this study is to numerically investigate the combined effects of canopy (leaf area index (LAI)) and root properties (root distribution function (R_{df}) and root area index (RAI)) on suction induced in soil-root composite under three different scenarios [i.e., influence of (1) roots under the absence of transpiration; (2) only root properties (i.e., R_{df} and RAI) for same LAI and (3) combined effect of R_{df} and LAI]. LAI is defined as the one-sided green leaf area per unit ground canopy area. The ratio of root surface area to soil surface area surrounded by roots is termed as RAI.

5.2. Methodology

5.2.1. Finite element model

The root water uptake around a *Schefflera heptaphylla* plant is assumed as an axi-symmetrical problem. Therefore, axi-symmetric of Richards equation coupled with sink term (Eq. 5.1) was used in this study (Deb et al., 2013). Richards equation in such form is broadly accepted by the scientific community and widely verified with respect to existing numerical models and reported as appropriate (Deb et al., 2013). Commercial finite element package "HYDRUS-2D" was used to numerically solve (simulate) the Richards equation coupled with sink term. Previous researchers (Šimůnek et al., 2012) validated the "HYDRUS" extensively and model simulations were found to agree with the measurements in unsaturated soil.

$$\frac{\partial \theta}{\partial t} = \frac{\partial}{\partial z}\left[K\frac{\partial \Psi}{\partial z}\right] + \frac{1}{r}\frac{\partial}{\partial r}\left[rK\frac{\partial \Psi}{\partial r}\right] - \left[\frac{\partial K}{\partial z}\right] - \left[\alpha(\psi, r, z)S_p\right] \quad (5.1)$$

where,

θ = volumetric water content (m^3/m^3),

t = time (hours),

z = vertical coordinate (m),

r = radial coordinate (m)

K = unsaturated hydraulic conductivity (m/ hour),

ψ = suction (kPa),

α (ψ, r, z) = Transpiration reduction function (varies between 0 and 1),

S_p = Potential water uptake over root zone ($hour^{-1}$),

[α (ψ, r, z) S_p] = Sink term.

The model domain is assumed to be isotropic and homogeneous to simulate the evapotranspiration in this study. Bacteria and fungi have been shown to influence the root water uptake and drought tolerance (Parke et al., 1983). In addition, root growth dynamics and activity vary with time and effect the root water uptake (Linderman, 1988). Furthermore, salinity and temperature could alter root water uptake (Aroca et al., 2011; Pardossi et al., 1992; Aroca et al., 2001). However, these factors were not considered in present study. Recent studies related to geotechnical engineering (Ng et al., 2015a. b, c; Liu et al., 2016; Feng et al., 2017) show that, microbe, root architecture and gas interaction could influence the root water uptake. However, such interaction was not considered in present study.

5.2.2 Finite element mesh and boundary conditions

A flat ground vegetated (rooted) with single plant was considered for analysis. Its finite element structured mesh along with boundary conditions is shown in Fig. 5.1. The flat ground is 10 m wide and 5 m deep. The selected dimensions are sufficient enough to minimize any boundary effects.

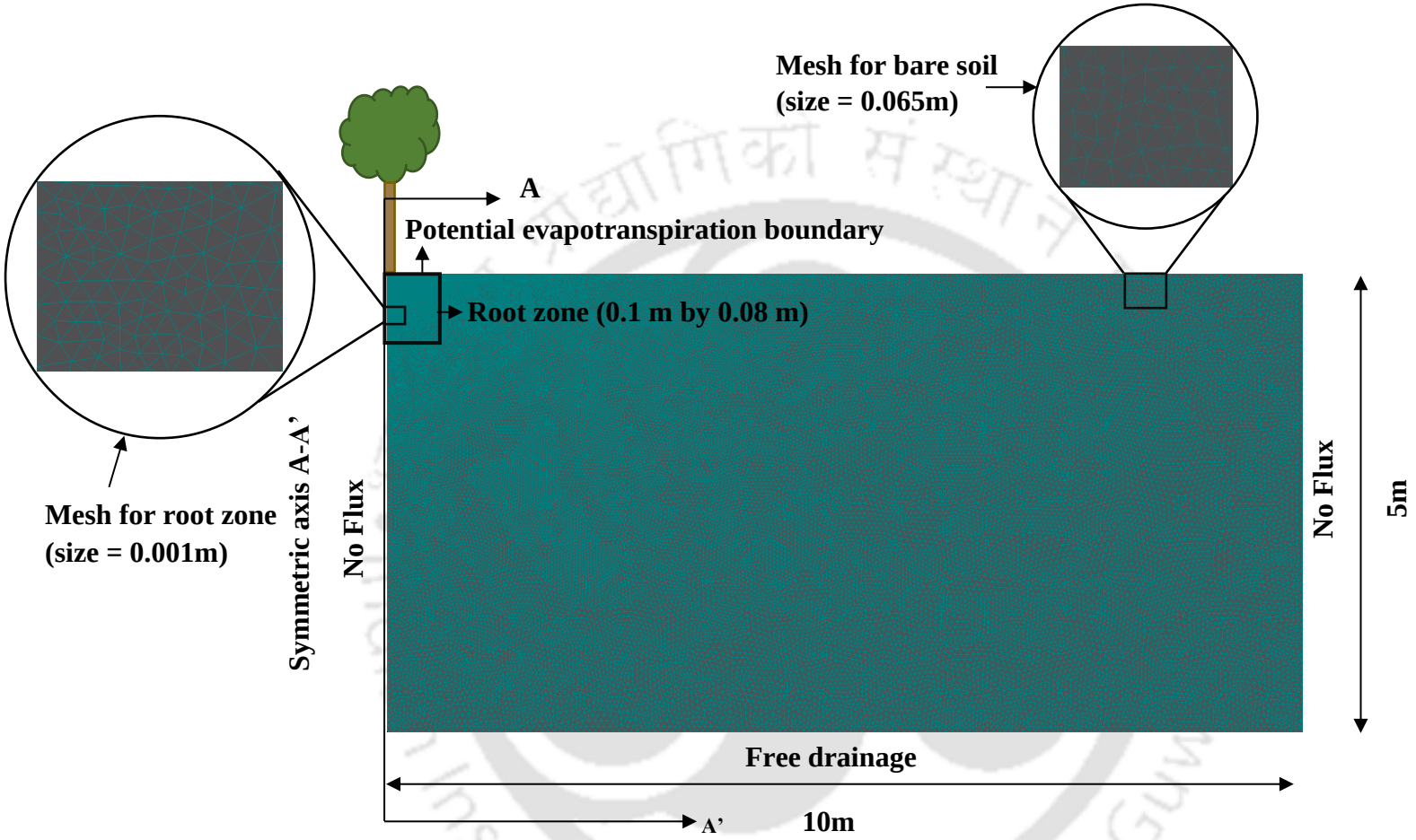

Fig. 5.1 Axi-symmetric finite element mesh and boundary conditions

The root zone of the single tree was specified beside the vertical symmetric axis (A-A'; Fig. 5.1), just below the surface. Root water uptake is simulated by applying sink term within the root zone (De Silva et al., 2008). Potential evapotranspiration was used as the upper water flow boundary conditions i.e., atmospheric boundary condition. The potential evapotranspiration (PET) is divided to potential transpiration (T_p) and potential evaporation (E_p) by using Beer-lambert law based on the LAI (Varado et al., 2006), as shown in Eq. 5.2 and Eq. 5.3

$$T_p = PET(1 - \exp(-k * LAI)) \quad (5.2)$$

$$E_p = PET(\exp(-k * LAI) \quad (5.3)$$

where:

k = constant that governs the extinction of radiation by leaves.

k was found to be 0.75 by experimental measurements for *Schefflera heptaphylla* (Leung et al., 2015b). PET was considered to be 1.5 mm/ day. In order to implement atmospheric boundary condition, limiting value of maximum allowable suction provided is 50000 kPa. This is obtained using relation between soil suction and relative humidity (Richard, 1965) for north east India under normal environmental condition (70.21 ± 2.26 %; Singh, 2009). No flux was specified along the side boundaries. Free drainage condition is specified at the bottom boundary. The numerical model represents the field condition, when water table lies far below the considered domain in vadose zone. Free drainage boundary condition has been assigned at the bottom boundary to simulate such field condition (Watson, 1966; Hillel et al., 1972; Take et al., 2015; Ng and Leung, 2011; Ng et al., 2011; Leung et al., 2016). Free drainage represents the unit total head gradient.

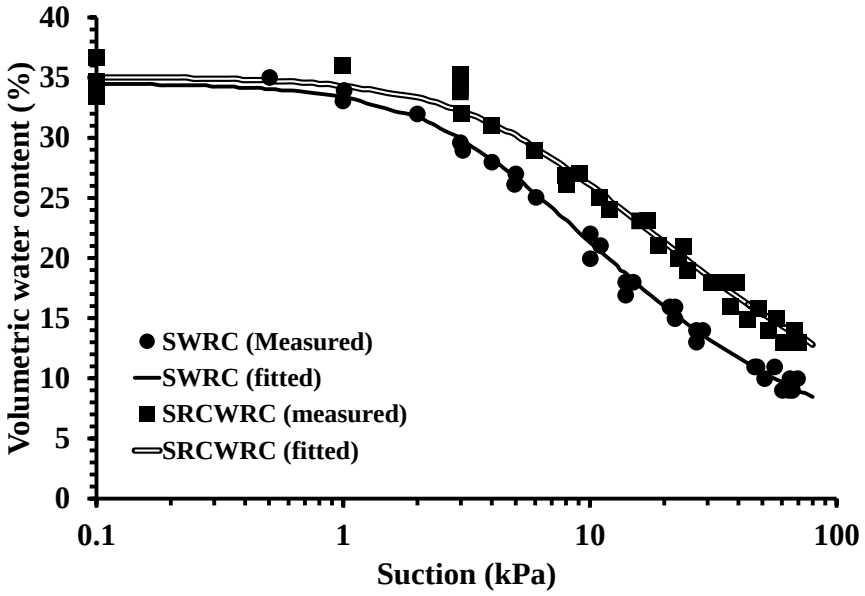

(a)

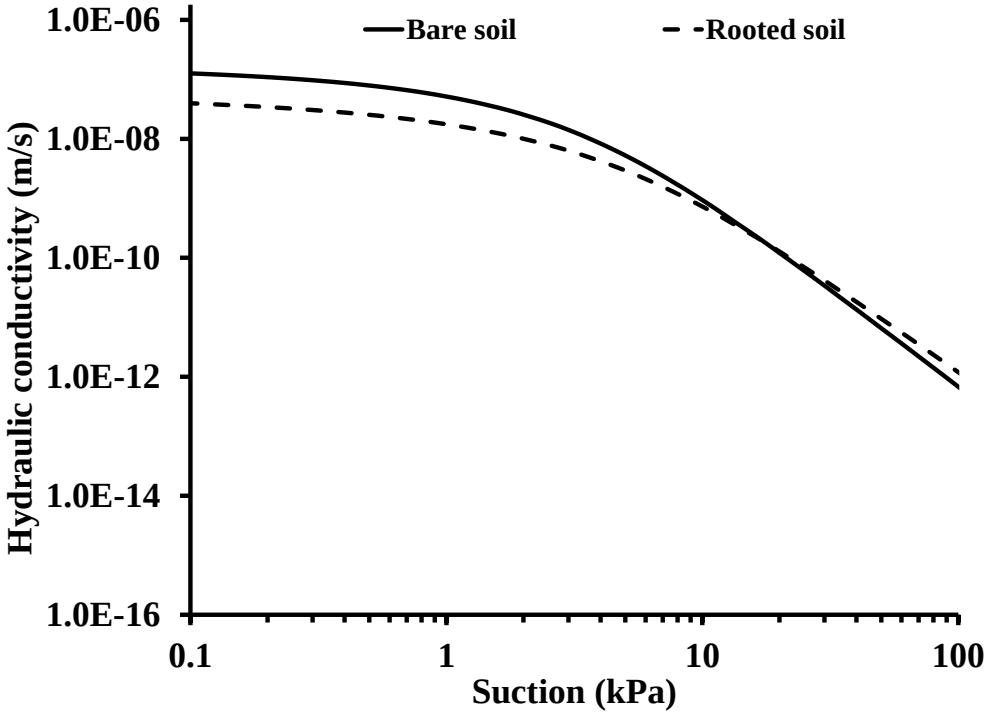

(b)

Fig. 5.2 (a) Fitted soil water retention curves (SWRCs) and soil root composite water retention curves (SRCWRCs; after Leung et al. (2015b)) and (b) deduced hydraulic conductivity using van Genuchten (1980) approach

5.2.3 Input properties of bare soil, soil-root composite and plant

5.2.3.1 Hydraulic properties of bare soil and soil-root composite

Water retention curves for bare soil and soil-root composite were fitted from experimental results. These experiments were conducted by Leung et al. (2015b), on completely decomposed granite (CDG i.e., clayey sand with gravel) specimen, corresponding to a degree of compaction of 80 %. Reference bulk density is 1.69 g/c.c. Saturated hydraulic conductivities for rooted and bare soil are 5.79×10^{-8} m/sec and 1.7×10^{-7} m/sec, respectively. Unsaturated hydraulic conductivity functions were deduced from drying water retention curves, using approach suggested by van Genuchten (1980). Fitted Water retention curves and deduced hydraulic conductivity functions were shown in Fig. 5.2 and their parameters are shown in Table 5.1.

Table 5.1
A summary of fitting coefficients for SWRCs and SRCWRCs using van Genuchten (1980) equation (after Leung et al., 2015b)

Soil type	$\boldsymbol{\theta_s}$ [m^3/m^3]	$\boldsymbol{\theta_r}$ [m^3/m^3]	$\boldsymbol{\alpha}$ [m^{-1}]	n [-]	m [-]
Bare soil	0.345	0.01	2.2	1.52	0.342
Vegetated soil	0.350	0.01	1.5	1.42	0.296

θ_s = Saturated volumetric water content

θ_r = Residual volumetric water content

α = related to inverse of air entry value

m, n = parameters related to pore size distribution

5.2.3.2 Canopy and root characteristics

Root lateral extent of 0.08 m and depth of 0.1 m, respectively, are adopted. These values were typically found for matured *Schefflera heptaphylla* grown, in CDG soil with a DoC of 80 % (Leung et al., 2015b). Although root depth is low, suction in such case was reported to effect the infiltration of green infrastructure (Leung et al., 2015a; Garg et al., 2017a,b,c) and erosion of vegetated soil (Lee et al., 2005; Zhu and Zhang, 2015b).

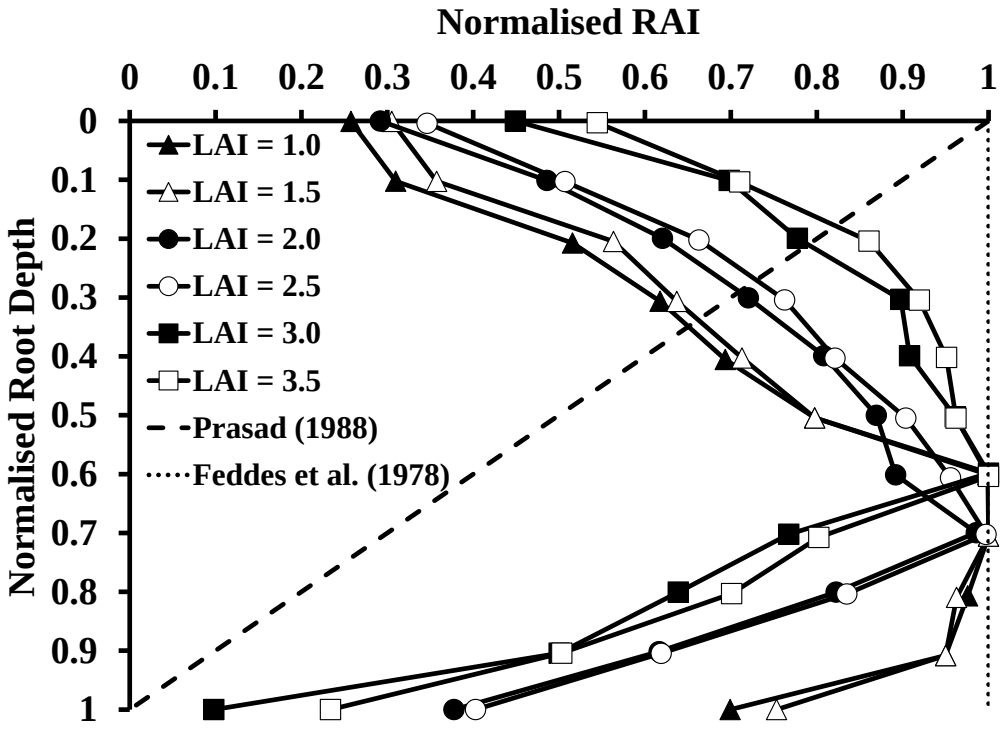

Fig. 5.3 Measured R_{df}s corresponding to different leaf area index (LAI) values (after Garg et al. 2015a)

Previous studies demonstrated the canopy area and root distributions for various types of vegetation (Garg et al., 2015a, b). However, transpiration reduction function was measured and presented corresponding to the actual LAI and R_{df} of *Schefflera heptaphylla by* Garg et al., (2015a)

recently. Hence, transpiration reduction function, LAI and R_{df} are adopted from Garg et al. (2015a) for present study. R_{df}s corresponding to different LAIs used for analysis are shown in Fig. 5.3. R_{df}s proposed by Feddes et al. (1978) and Prasad (1988) were adopted in previous studies to understand the suction induced in soil-root composite (Zhu and Zhang, 2015a, b). Hence, uniformly distributed and linearly decreasing R_{df} were adopted as reference. The main focus of the present study is to investigate the combined effects of canopy (LAI)) and root properties (R_{df} and RAI) on suction induced in soil-root composite. Hence, the selected LAI and R_{df} values are found to be sufficient for objective of present study. Garg et al., 2015a shows that, ψ_1, ψ_2 and ψ_3 vary with change in species type (details of ψ_1, ψ_2 and ψ_3 can be seen in section 2.3). In their study, ψ_1, ψ_2 and ψ_3 were found to be 1 kPa, 90 kPa and 1500 kPa. ψ_1, ψ_2 and ψ_3 were not found to vary significantly with change in LAI between 1.0 and 3.5 (Garg et al., 2015a). Hence, same transpiration reduction function was considered for all LAI values.

5.2.4. Analysis plan and procedures

Three series of simulations were conducted to systematically investigate three scenarios as shown in Table 5.2. Two simulations were conducted to investigate the first scenario. These illustrate the effect of roots on suction induced in soil-root composite, during the absence of transpiration. Water retention curve (SRCWRC) and hydraulic conductivity used for soil-root composite are different from those of bare soil (see Fig. 5.2). For second scenario, three simulations were conducted to analyze the effect of change in only R_{df} on suction induced in soil-root composite due to evapotranspiration. Three types of R_{df}s i.e., uniformly distributed along the depth of root zone (Feddes et al., 1978); linearly decreasing root distribution from top to bottom along the depth of root zone (Prasad, 1988); and Nonlinear R_{df} (Garg et al., 2015a) are considered as shown in Table

5.2. LAI was kept same as 1.5. These simulations of second scenario help to understand the importance of change in R_{df} on suction induced in soil-root composite due to evapotranspiration.

Table 5.2

Numerical analysis plan to study effects of canopy and root properties on suction induced in soil-root composite[a]

Scenario	Numerical simulation ID[b, c]	Water retention curve considered	LAI	Root distribution	Evaporation (mm/day)	Transpiration (mm/day)
1. Influence of roots in the absence of transpiration	S1-B	SWRC	N	N	1.50	N
	S1-A	SRCWRC	1.0	Nonlinear	1.50	0.00
2. Influence of root properties with same LAI	S2-U	SRCWRC	1.5	Uniform	0.49	1.01
	S2-L	SRCWRC	1.5	Linearly decreasing	0.49	1.01
	S2-C	SRCWRC	1.5	Nonlinear	0.49	1.01
3. Influence of root properties and LAI	S3-1.0	SRCWRC	1.0	Nonlinear	0.71	0.79
	S3-1.5	SRCWRC	1.5	Nonlinear	0.49	1.01
	S3-2.0	SRCWRC	2.0	Nonlinear	0.33	1.17
	S3-2.5	SRCWRC	2.5	Nonlinear	0.23	1.27
	S3-3.0	SRCWRC	3.0	Nonlinear	0.00	1.50
	S3-3.5	SRCWRC	3.5	Nonlinear	0.00	1.50

[a] N- Not considered

[b] S1- scenario 1; S2- scenario 2; S3- scenario 3; B- bare soil; R- soil-root composite; A- soil-root composite under the absence of transpiration; U- uniform root distribution in root zone (Feddes et al. (1978)); L- Linearly decreasing root distribution along the rooting depth from top to bottom

(Prasad, 1988); C- Curvilinear root distribution in root zone (nonlinear root distribution; Garg et al., (2015a))

[c] In numerical simulation ID of scenario 3 (i.e., S3-1.0, S3-1.5, S3-2.0, S3-2.5, S3-3.0 and S3-3.5), the numbers 1.0, 1.5, 2.0, 2.5, 3.0 and 3.5 represents leaf area index (LAI), respectively.

Third scenario consists of three simulations, for investigating the combined effect of change in LAI and R_{df}. In this analysis variation in both LAI and R_{df} is considered. This scenario specifies the importance of LAI and its corresponding R_{df} consideration. Initial suction (initial condition) for the domain was taken as 50 kPa at 0 hours of time for all the simulations.

5.3. Results and discussions

5.3.1 Effect of roots on suction induced in soil-root composite during the absence of transpiration (scenario 1)

Fig. 5.4 shows the computed suction profiles at cross section A-A' (see Fig. 5.1) for scenario 1 simulations (S1-B and S1-A) for a period of 10 hours of evaporation. Suction variation has been plotted to compare suction profile only up to 0.2 m depth. This is because variation of suction below depth of root zone (0.1 m) is negligible with respect to initial condition. After 10 hours, suction for both cases at surface (0 m depth) has increased 50,000 kPa due to evaporation. A nearly constant suction profile below 0.015 m depth was observed. This may be due to negligible change in soil moisture due to the absence of transpiration. This depth represents EDZ, which is same for both cases. In this case, depth of SIZ is also 0.015 m. Although suction profiles seems to be similar, computed suction for case S1-A is found to be slightly higher (1 % to 20 %) than that of S1-B within 0.01 m depth from surface. The reason for such difference between computed suctions may be attributed to dissimilar hydraulic properties of bare soil and soil-root composite (Leung et al.,

2015b). The findings implies that during unfavorable conditions of root water uptake (i.e., abiotic stress; Aroca et al., 2011), any influence of roots is only near surface. However, below root depth, such influence is negligible.

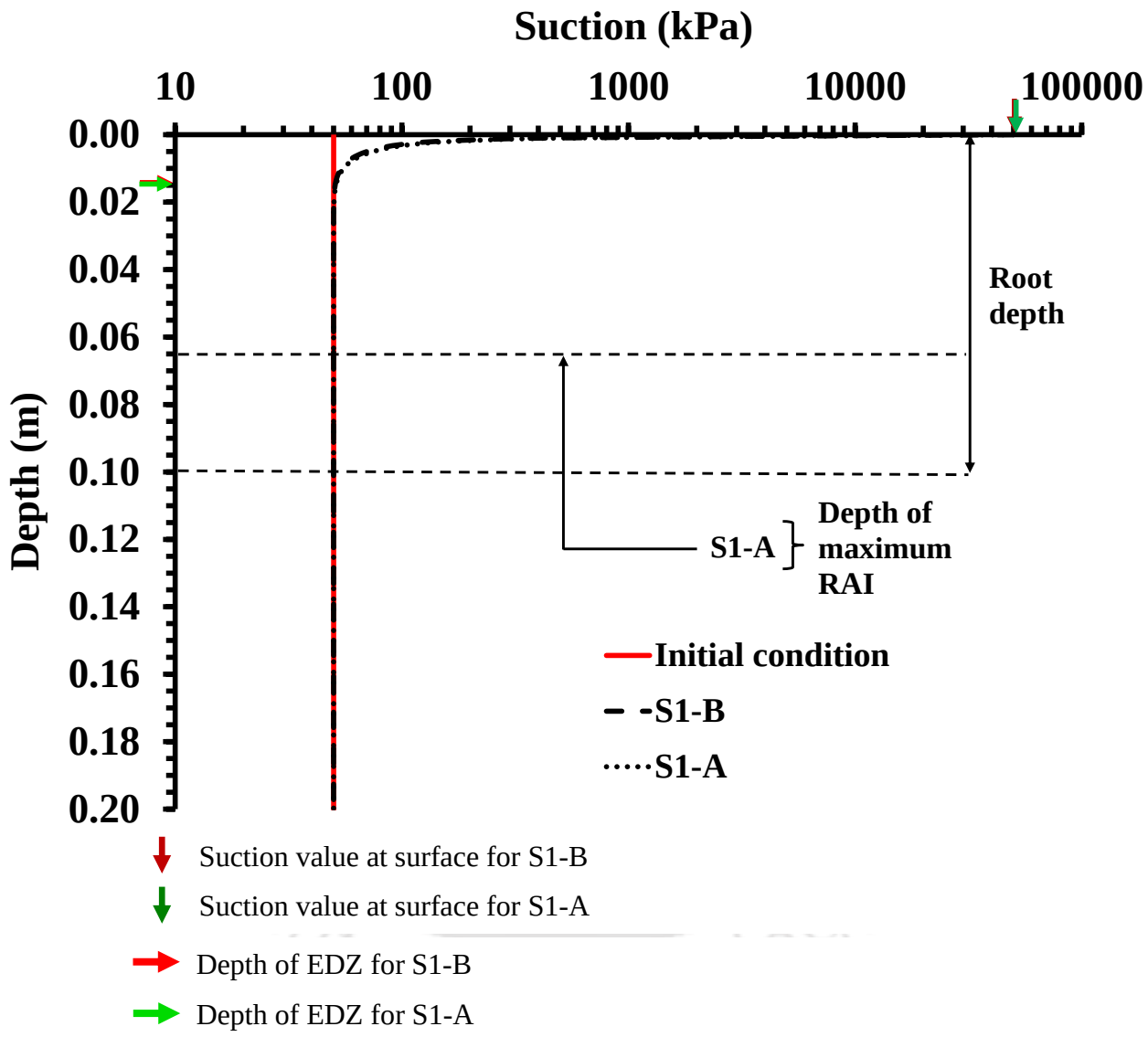

Fig. 5.4 Effect of roots on suction profile under the absence of transpiration

5.3.2 Effect of root properties on suction induced in soil-root composite (scenario 2)

Fig. 5.5a shows the computed suction profiles at cross section A-A' (see Fig. 5.1) for simulations corresponding to scenario 2 i.e., S2-U (uniform R_{df}), S2-L (linearly decreasing R_{df}) and S2-C (Non-linear R_{df}). These were simulated for 10 hours of drying. Depths of EDZ and suction value at surface are highlighted in the figure. Midpoint of root zone depth (i.e., 0.05 m), depth of maximum RAI and maximum rooting depth (i.e., 0.1 m) are also marked for reference. Depth of EDZ can be identified from the large difference between suction values within and below the EDZ (i.e., 695 – 49571kPa). In addition, it can also be identified from the suction profile trend in cases of curvilinear and uniformly distributed R_{df}s. Suction profile trend of S2-U and S2-C within EDZ is not found to be consistent with trend of R_{df}s.

Value of suction at depth of maximum RAI in case of S2-L is higher than that of S2-U and S2-C. Such finding is also consistent with that observed by Garg and Ng (2015). Within 0.044 m depth, suction is observed to be higher for linearly decreasing R_{df} as compared to other two R_{df}s. Below this depth, higher suction is found in case of non-linear R_{df} than linearly decreasing R_{df} and uniform $R_{df.}$ This is because roots are mostly concentrated near surface for linearly decreasing R_{df}s whereas, it is mostly concentrated at subsurface for non-linearly decreasing R_{df}s.

Depth of SIZ for uniform R_{df} and non-linear R_{df} is observed to be 11 % and 13 % higher than that of linearly decreasing R_{df}. This implies that species with uniform or nonlinear root distribution are more relevant for providing stabilization of slopes at deeper depths than species with linearly decreasing root distribution. Hence, SIZ is likely to be one of the crucial parameters in governing the depth of slip surface for slope instability. Fig. 5.5b shows the temporal variation of depth of EDZ and its corresponding suction. Depth of EDZ is found to increase with time. This indicates the movement of drying front toward deeper depths during drying. It also implies that

with time, the influence of soil moisture loss through evaporation can be dominant even at deeper depths, where roots are present. Depth of EDZ for S2-U and S2-C is observed to be 1.08 to 3 times higher than that of S2-L. However, interestingly, suction at the depth of EDZ is found to be 1.39 to 2.71 times higher in case of S2-L, as compared to S2-U and S2-C. This is obvious for the case of S2-L, where the combined effects of evaporation and maximum root density is more than that of other two cases within EDZ. Unlike in Fig. 5.4, suction at the end of EDZ remained higher than 50 kPa (initial condition) for all types of R_{df}s, due to transpiration. This implies that in long term (with time), the magnitude of soil suction in case of S2-L will not only be higher than other R_{df}s near surface but also at deeper depths. It implies that in long term, drying front in case of S2-L will propagate downward at lower rate but with higher soil moisture loss. This has implications especially in case of landfill covers, where it is not advisable to have deeper drying front but rather higher suctions near shallower surface. Similarly, for erosion resistance, it is more advisable to have higher resistance (suction) near surface than a moderate suction at deeper depths. Depending on the engineering problem, it is important to select species with particular type of root distribution.

Fig. 5.5c compares the suction profiles at cross section A-A' (see Fig. 5.1) at the end of respective wilting point attaining time periods between cases, S2-U, S2-L and S2-C. The time to reach wilting point was first attained by linearly decreasing R_{df} (i.e., 4.90 hours), followed by uniform R_{df} (i.e., 9.40 hours) and non-linear R_{df} (i.e., 10.75 hours). This observation implies that there might be a concern of long term performance of vegetation and hence infrastructure (slope, biofiltration, landfill cover) while using species with linear root distribution as compared to that of uniform and non-linear root distribution. This also implies that frequent irrigation supply may

be required for smooth maintenance of green infrastructure with species corresponding to linear root distribution.

Depths of EDZ of S2-U (nearly 0.015 m) and S2-C (nearly 0.013 m) are found to be higher than that of S2-L (nearly 0.008 m). Non-linear R_{df} is observed to induce higher suction within 70 % of the rooting depth, than linear and uniform R_{df}s. This suggests that non-linear R_{df}s is highly suitable for stabilization of slope against failures at deeper depths. Root density distribution is an important parameter that can influence stability of slope at deeper depths. Depths of SIZ of uniform R_{df}, linearly decreasing R_{df} and non-linear R_{df} are 0.108 m, 0.093 m and 0.109 m, when the wilting point was attained.

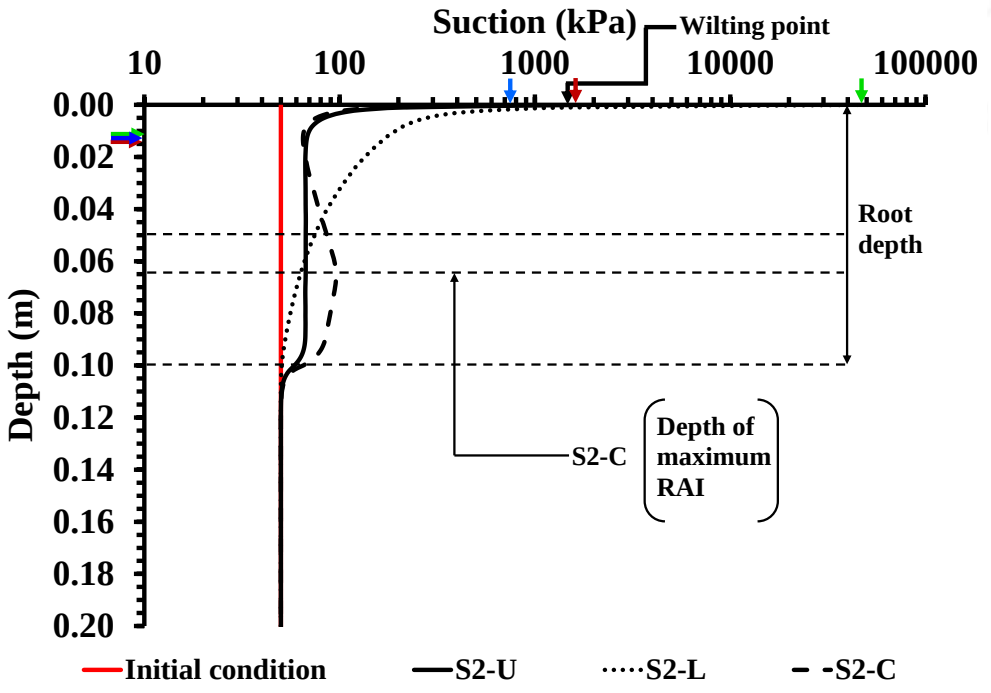

(a)

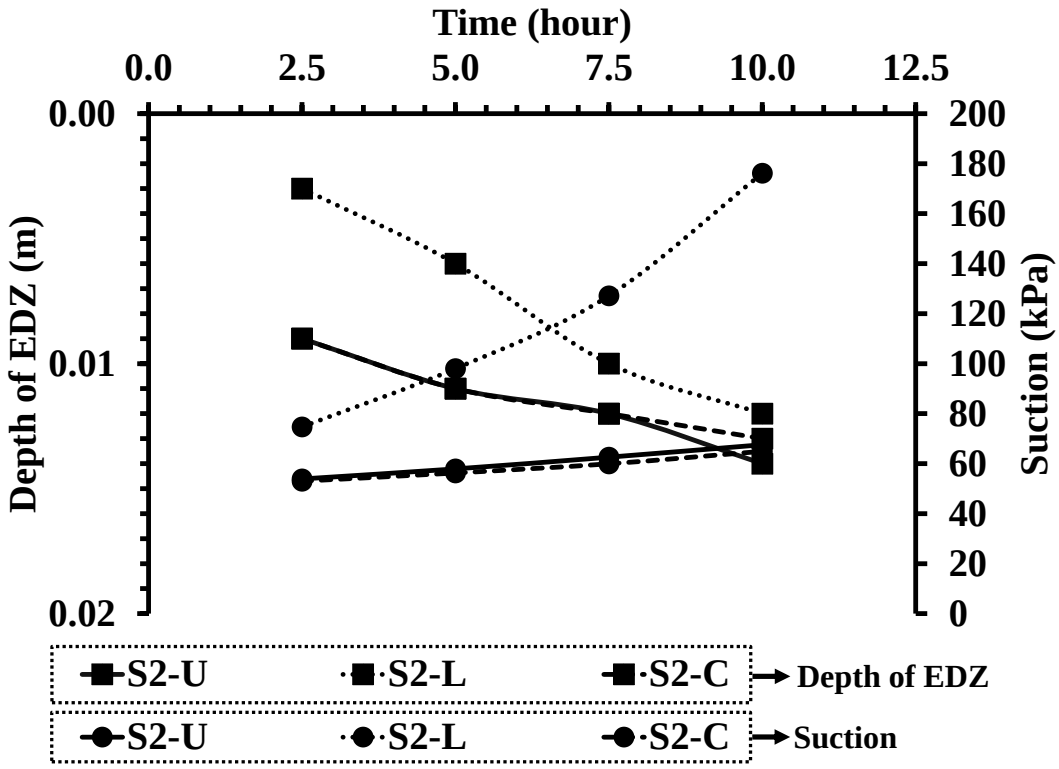

(b)

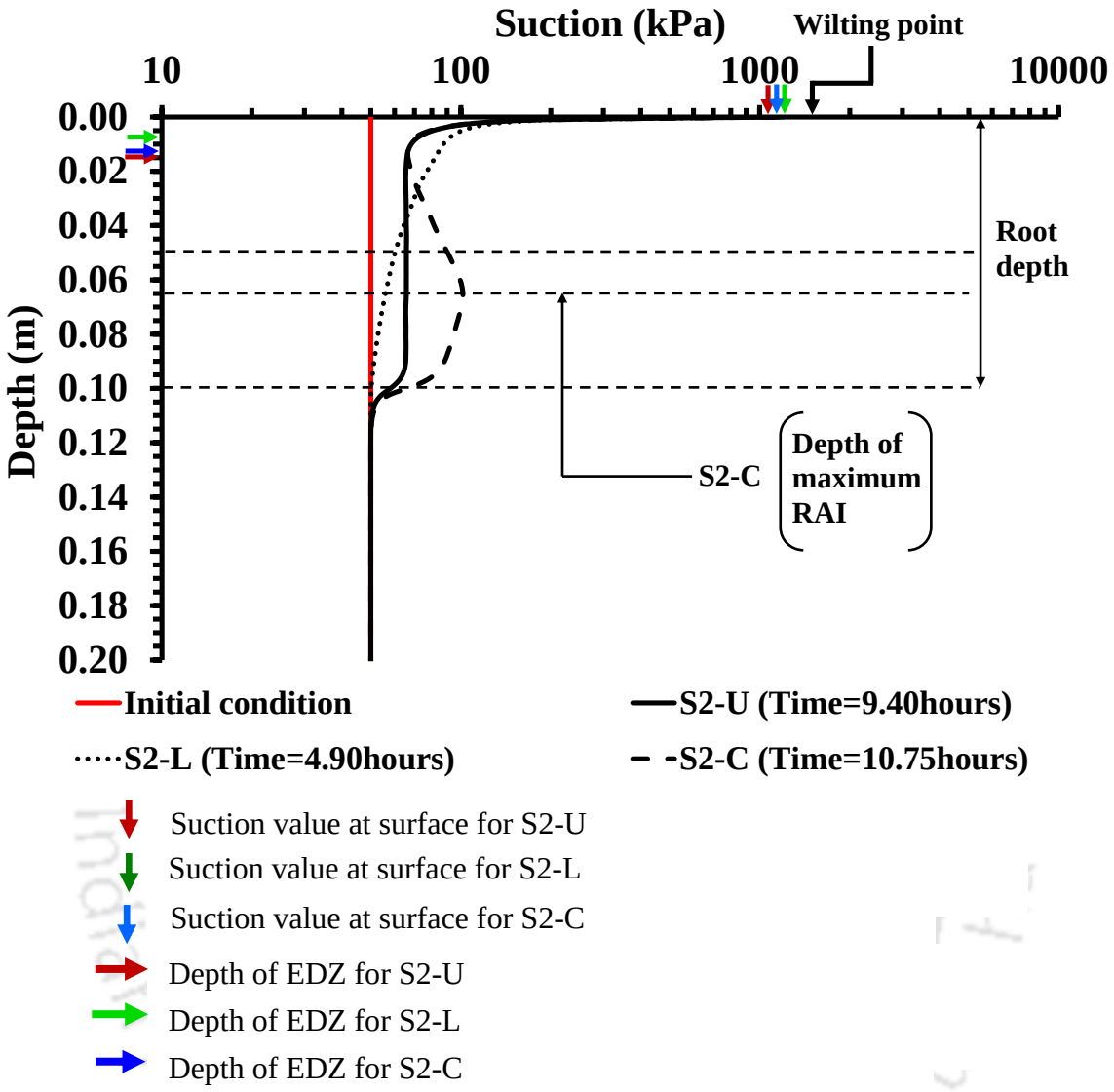

(c)

Fig. 5.5 Effect of R_{df}s on (a) suction profile at time t = 10 hours, (b) temporal variation of depth of EDZ and its corresponding suction and (c) suction profile at time t= wilting point attaining time

5.3.3 Influence of canopy and root properties on suction induced by soil-root composite (scenario 3)

Fig. 5.6a shows the computed suction profiles at cross section A-A' (see Fig. 5.1), for the simulations i.e., S3-1.0, S3-1.5, S3-2.0, S3-2.5, S3-3.0 and S3-3.5 of third scenario. These were analyzed for 10 hours of drying. Suctions induced in soil-root composite with three different LAIs and their corresponding R_{df}s were compared. Depth of EDZ can be identified from the large difference between suction values within and below the EDZ (119 – 15343kPa; for evaporation > 0). In addition, it can also be observed from the suction profile trend of S3-1.0, S3-1.5, S3-2.0, S3-2.5, S3-3.0 and S3-3.5. Suction profile trend within EDZ is not found to be consistent with R_{df}s. Despite higher evaporation in case of LAI of 2.5 than that of LAI of 3.0 and 3.5, suction induced at surface is observed to be lower in former than latter. This shows that effect of excess transpiration in case of LAI of 3.0 and 3.5 dominates the influence of higher evaporation due to LAI of 2.5. Highest suction at surface is found to be induced in case of LAI = 1.0, among the six LAI values.

It can also be seen from Fig. 5.3 that though RAI decreases with increase in LAI, still higher suctions was found for case with higher LAI. This difference in suction can be explained by the fact that, influence of higher LAI is able to dominate the effect of greater RAI. Any variation in depth of SIZ due to change in LAI was not found to be significant. This implies that as compared to R_{df}s, LAI seems to have negligible impact on depth of SIZ. This suggests that the depth of slip surface for slope may not be influenced by change in LAI. Fig. 5.6b shows the temporal variation of depth of EDZ and its corresponding suction values. The depth of EDZ is found to decrease with increase in LAI. It is observed to be negligible for LAI = 3.0 and 3.5. It can also be observed that, suction at depth of EDZ is increasing with increment in LAI. Suction at depth of EDZ for LAI of 1.5 - 3.5 is observed to be 1.13 - 5.25 times higher than that of LAI=1.0 at the end of 10 hours.

One of the reasons for these variations can be, difference in evaporation values among three different LAIs (see Table 5.2; Tratch, 1996).

Fig. 5.6c compares the suction profiles at cross section A-A' (see Fig. 5.1), for simulations of third scenario (i.e., S3-1.0, S3-1.5, S3-2.0, S3-2.5, S3-3.0 and S3-3.5) when wilting point was attained. Soil-root composite covered with relatively low leaf area (i.e., LAI = 1.0) is observed to reach wilting point earlier than others, near the surface. This may be due to the higher evaporation for LAI = 1.0 (see Table 5.2; Tratch, 1996). However, it can be observed from the suction values that, soil-root composite with maximum leaf area (i.e., LAI = 3.5) reaches wilting point earlier than others at depth of maximum RAI. One reason for this may be relatively higher transpiration undergone by greater RAI below the surface. Furthermore, LAI = 2.5 induces higher suction than LAI = 3.0 and 3.5 below 0.06 m depth, within the root zone.

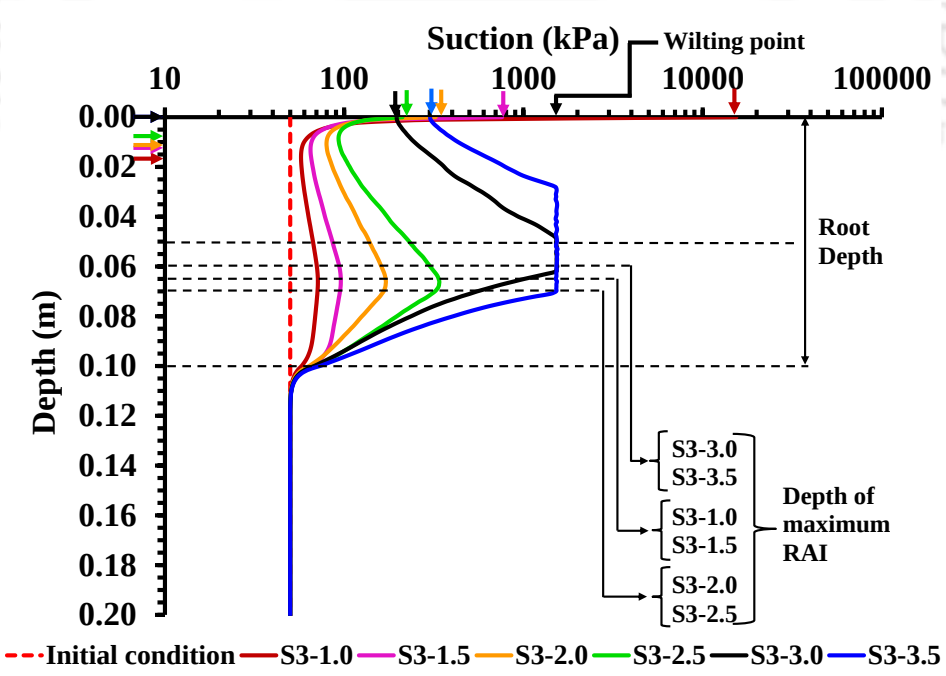

(a)

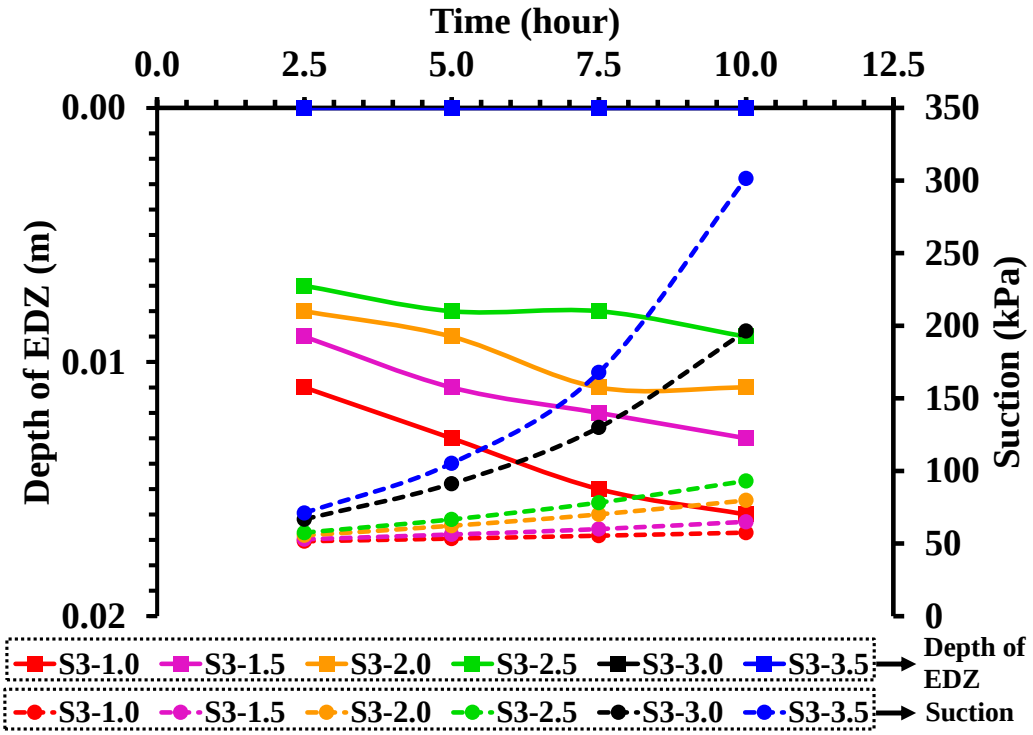

(b)

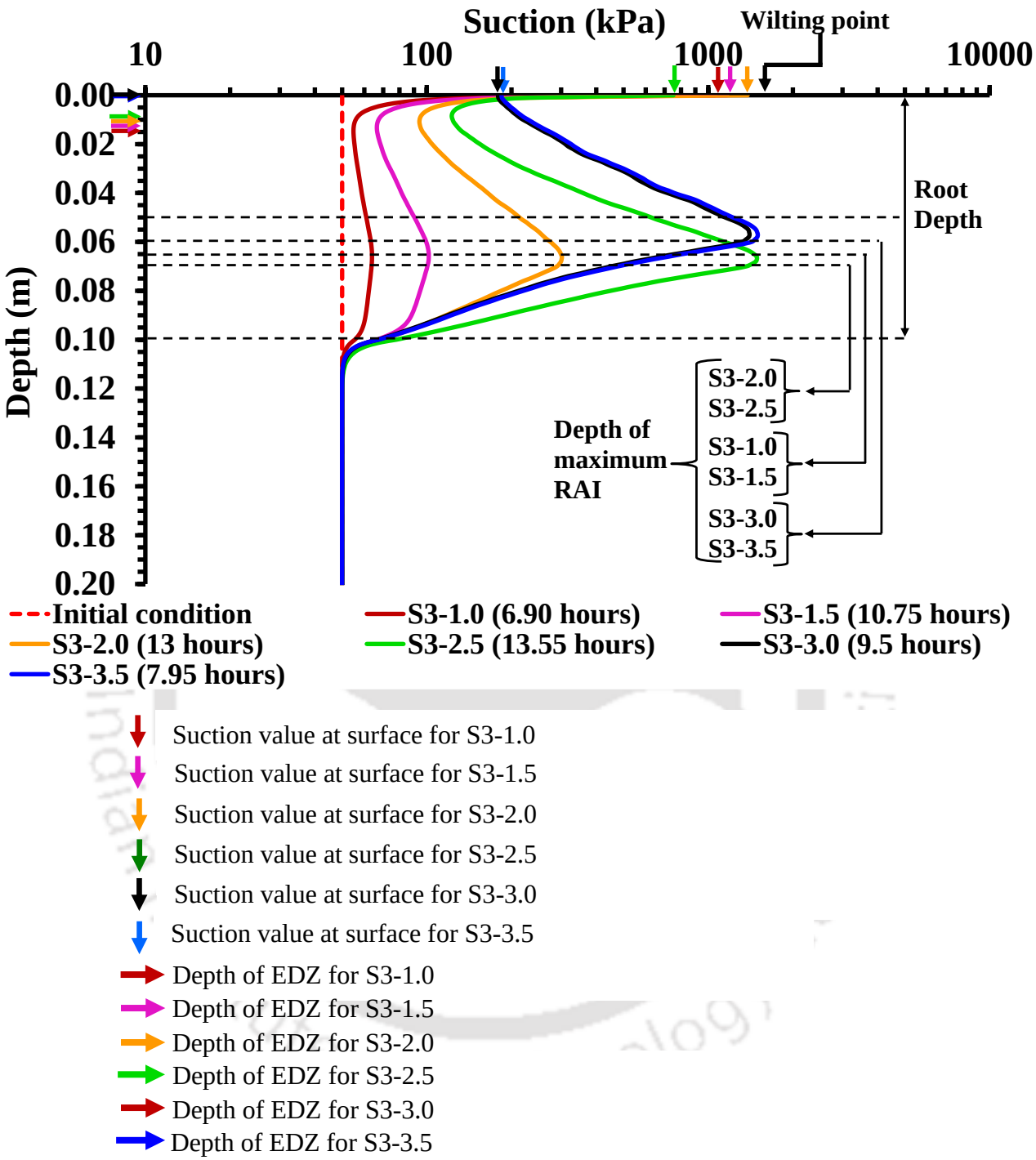

(c)

Fig. 5.6 Effect of canopy (LAI) on (a) suction profile at time t = 10.0 hours, (b) temporal variation of depth of EDZ and its corresponding suction and (c) suction profile at time t = wilting point attaining time

5.4 Summary and Conclusions

This study investigates the canopy and root properties effect on suction induced in soil-root composite using a systematic parametric study under three different scenarios. In addition to SIZ, a new parameter (Evaporation dominant zone; EDZ) was proposed in this study to improve the understanding of suction profile. Scenario 1 confirms that, soil-root composite induces 1 % – 20 % higher suction than bare soil when transpiration was absent. This was attributed to change in water retention properties due to roots. It is evident from scenario 2 that, value of suction at depth of maximum RAI in case of linearly decreasing R_{df} is higher than that of uniformly decreasing R_{df} and non-linear R_{df}. However, depth of SIZ for uniform R_{df} and non-linear R_{df} was 10 % and 11 % higher than that of linearly decreasing R_{df}. Furthermore, depth of EDZ for uniformly decreasing R_{df} and non-linear R_{df} is 1.08 to 3 times higher than that of linearly decreasing R_{df}. Although linearly decreasing R_{df} and uniform R_{df} attain wilting point early, non-linear R_{df} induces relatively high suction within 70 % of the rooting depth. This was due to long exposure of non-linear R_{df} to evapotranspiration. Scenario 3 reveals that depth of SIZ was not influenced by change in LAI. One of the reasons for this may be, less difference among R_{df}s of three different LAIs. Influence of higher LAI dominates the effect of greater RAI on suction induced in soil-root composite. Depth of EDZ decreases with increase in LAI. Soil-root composite covered with relatively low leaf area (i.e., LAI = 1.0) reaches wilting point earlier than others (i.e., LAI = 1.5 – 3.5), near the surface. Whereas, LAI = 3.5 reaches wilting point earlier than others at the depth of maximum RAI.

Overall, results of present study reveal that, consideration of the variation in canopy and root properties enables the root water uptake modelers to understand the variation in suction explicitly. Furthermore, results obtained by such consideration help modelers to analyze

subsequent infiltration, runoff and erosion, which usually occurs at shallower depths in green infrastructures

CHAPTER 6 A NOVEL COLOUR ANALYSIS TECHNIQUE TO QUANTIFY THE SPATIAL HETEROGENEITY IN MIX GRASS COVER

6.1 General

The spatial heterogeneity of mix grass species in the selected site was categorized into three different portions i.e., 1) mix grass cover under tree shade (MUT); 2) mix grass cover under self-shade (MUS) and 3) mix grass cover without shade (MWS). Field monitoring was conducted for about six months to validate the colour analysis technique. A java based image analysis tool ImageJ was used for colour analysis. Lab colour space is adopted for the present study, which identifies the spatial heterogeneity of mix grass cover based on lightness variation of green colour.

6.2 Materials and Methods

6.2.1 Site description

Location of selected site for validation of colour analysis technique (i.e., *Pongamia pinnata tree* vicinity) is shown in Fig. 6.1. This tree vicinity is located in front of the academic building in IIT Guwahati campus. The tree vicinity consists of mix grass cover on a flat ground. Mix grass cover consists of *Cyperus, Poaceae* and *Bauhinia purpurea* species. *Cyperus, Poaceae* and *Bauhinia purpurea* species were selected based on their (i) wide availability in urban areas of sub-tropical regions (Jim and Lui, 2001; Vaio et al., 2005; Ghosh et al., 2003) and also (ii) drought tolerance, which may be appropriate for slope stabilization and land rehabilitation (Allen, 1986; Reubens et al., 2011). In this study, field monitoring was conducted on mix grass cover in the tree vicinity. This field monitoring is intended to better understand the proportion of mix grass cover variation in the tree vicinity.

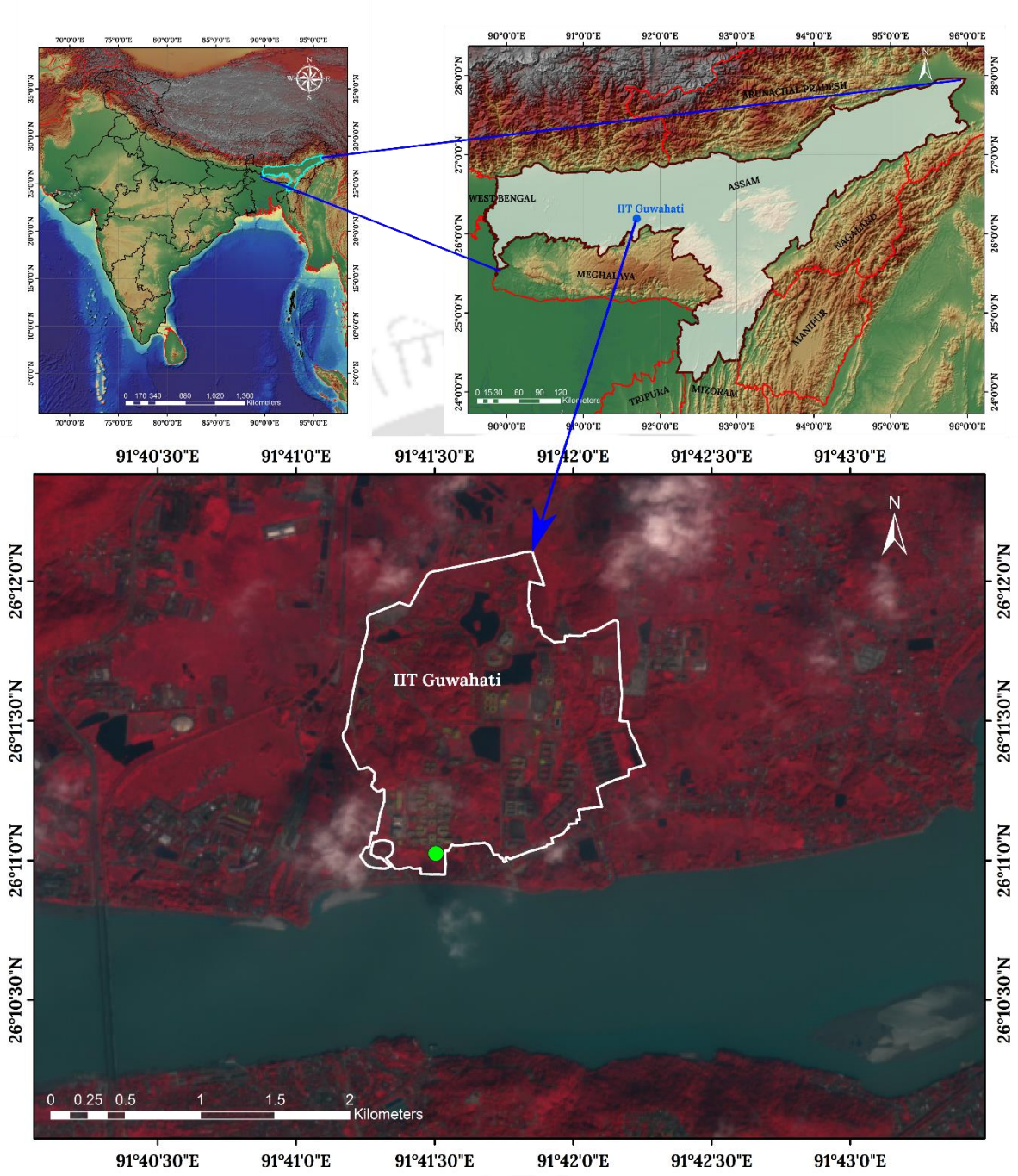

Fig. 6.1 Location of the selected site for the current study

6.2.2 Soil properties

Ten disturbed soil samples were collected from four different locations i.e., five samples from right side of tree stem and another five were collected from left side of tree stem. Among these ten samples, five samples were collected within 2.5 m radial distance from tree stem and remaining five were collected in between 2.5 m and 5 m radial distances from tree stem. Field tests were conducted to determine soil density according to procedure outlined in literature (ASTM D4914, 2016). Soil dry density (ρ_d) is defined as the mass of soil solids (M_s) per unit volume (V). It was found that in situ dry densities of the four soil samples varied between 1319 kg/m^3 and 1367 kg/m^3, with an average value of 1343 kg/m^3. The average in situ dry density of soil is approximately equal to 78.4 % of the maximum dry density. The average contents of gravel (particle size $D_0 \geq 2$ mm), sand (particle size 0.063 mm $\geq D_0 \leq 2$ mm), silt and clay (particle size $D_0 \leq 0.063$ mm) are found to be 0 %, 98 % and 2 %, respectively. According to the Unified Soil Classification System (USCS), the soil in the tree vicinity is classified as poorly-graded sand (SP; ASTM D2487, 2010), based on the measure particle size distribution.

6.2.3 Overview of test site comprising mix grass cover in tree vicinity

Fig. 6.2a shows overview of the tree vicinity with mix grass cover. It can be seen from Fig. 6.2b that tree vicinity is categorized into five rectangular areas. This categorization is aimed to quantify the spatial variation of shoot growth. The rectangular areas are of 6 m long and 1 m wide. Dimension of rectangular areas (6 m by 1 m) are considered based on visual observation, within which shoot length appears to be less variable. Non-uniform shoot length and shredded leaves can be observed over the tree vicinity.

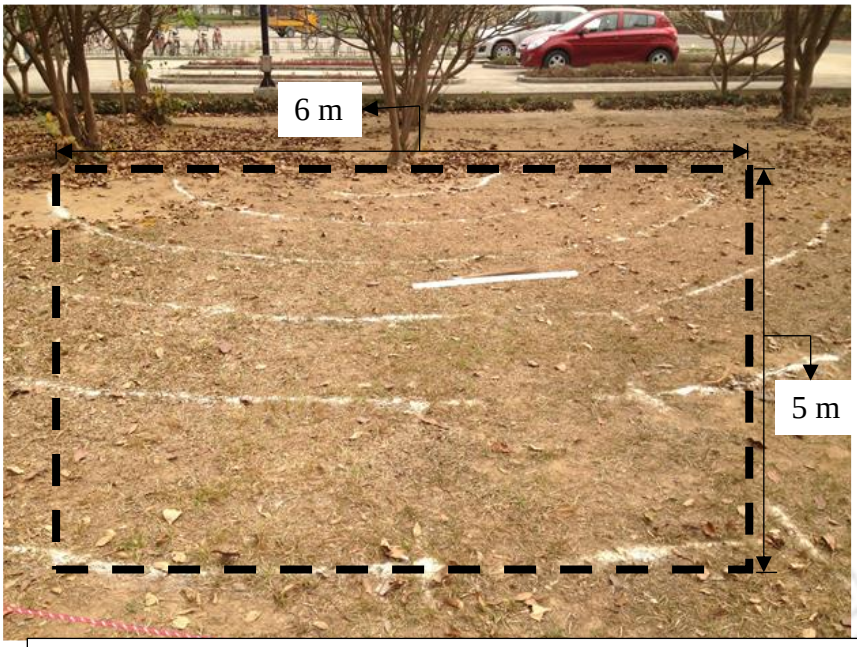

* Area shown in rectangle is considered for present

(a)

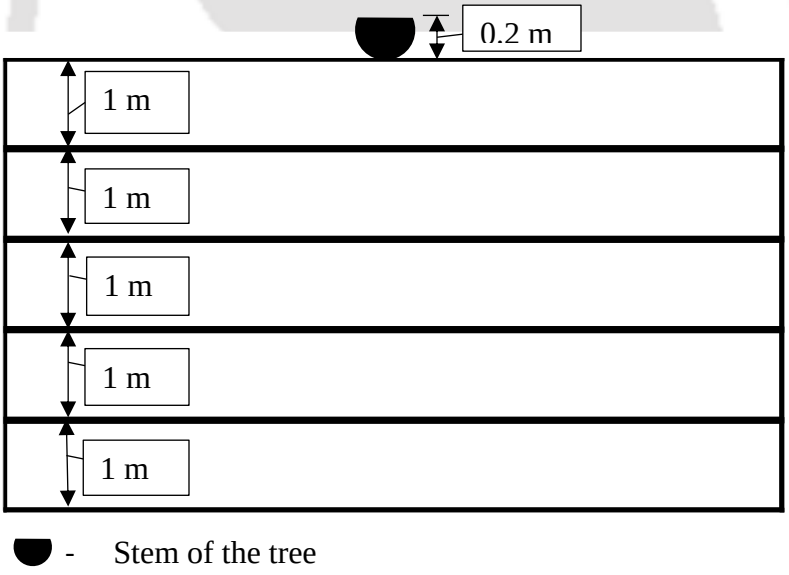

- Stem of the tree

(b)

Fig. 6.2 (a) Overview of tree vicinity with *Cyperus and Poaceae* species and **(b)** categorization of selected site for measuring shoot growth in the tree vicinity

6.2.4 Instrumentation on the vegetated soil in the tree vicinity

A commercial camera model CANON EOS 600D was used to capture mix grass cover images with lens range 18-55 mm and horizontal/vertical resolution of 72 dpi. The exposure time, focal length and ISO speed were maintained at 1/30 sec, 23 mm and ISO-640 respectively. Resolution of camera is 18 megapixels. Images were captured by keeping a constant angle (15°) between base of tree stem and lens of camera. Camera was fixed at a height of 2m to avoid any observational errors. Constant number of pixels was achieved for all captured images by maintaining same height, angle, exposure time, focal length and ISO speed. Constant number of pixels in the images is essential to compare the colour analysis results of captured images accurately (Feirra and Rasband, 2012).

It should be noted that the angle of incidence of sun rays on the selected site varies from morning to evening (Solanki, 2015). It implies that proportions of MUT, MUS and MWS would change with time. Hence, only one observation in a day may not be sufficient enough to design the instrumentation plan. However, the main focus of the present study is to develop a working knowledge on the usage of colour analysis technique and understand its validity with seasonal change. Hence, only one particular time of the day was chosen in the present study. Each image analyzed in this study was captured when the radiant energy during the day was maximum. Maximum radiant energy indicates that the angle of incidence of the light rays on the ground is close to 90° (Keane, 2014). Less difference among the angles of incidence while capturing the images would assure accurate comparison of results (Feirra and Rasband, 2012; Keane, 2014). Shoot length is measured using a scale, which had a least count of 1 mm.

6.2.5 Field monitoring programme

The field monitoring programme to study the temporal variation of mix grass proportion was conducted from 1st January 2016 to 30thJune 2016 under natural atmospheric variations. It is clear that mix grass cover proportion and shoot growth are spatially uncertain (Philipp and Rath, 2002). A micro climate monitoring system (MCMS) was used to monitor the atmospheric parameters: rainfall depth, air temperature, wind speed, relative humidity and net radiation. Fig. 6.3 shows monthly rainfall depth data during the monitoring period. It can be observed that lowest rainfall depth of 5 mm occurred during February and highest rainfall depth of 275 mm occurred during April. Rainfall depths of January, February and March are much lower than those in April, May and June. This clearly shows that the first three months of observation period (i.e., January, February and March) implies relatively lower water content availability in vegetated soil, which correspond to the dry period. The three-month period of April, May and June, which implies relatively high available water content in vegetated soil can be referred as wet period. Temperature was found to vary between 9 ˚C and 36 ˚C during monitoring period.

Three categories of green colour i.e., dark green, medium green and light green can be seen in the tree vicinity which are shown in Fig. 6.6. Dark green indicates the proportion of MUT, medium green indicates the proportion of MUS and light green indicates the proportion of MWS. Mix grass proportion was determined by processing captured mix grass cover images using ImageJ.

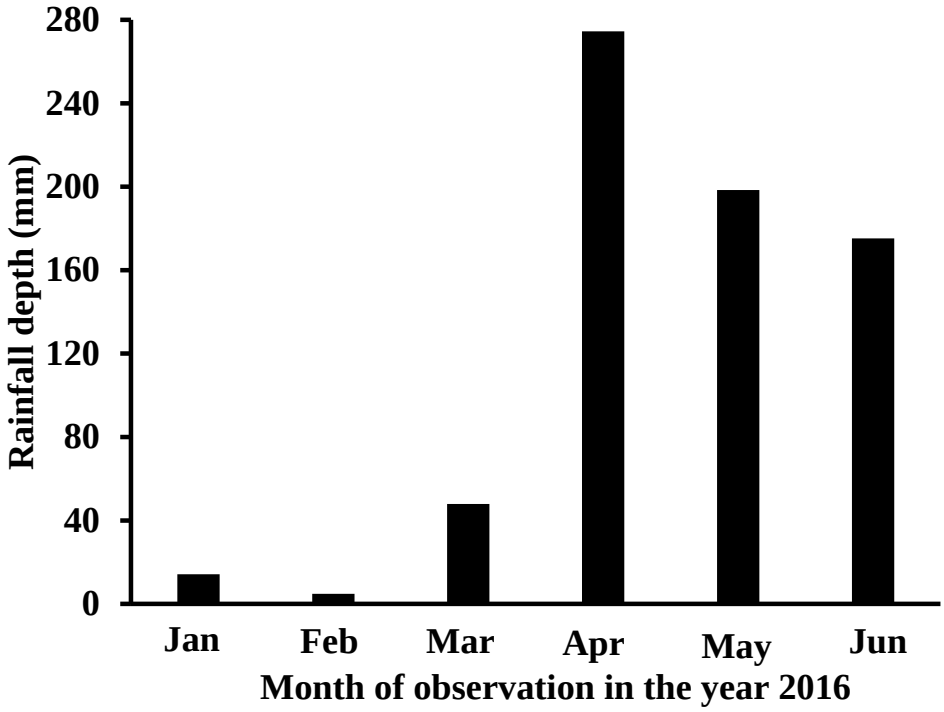

Fig. 6.3 Monthly rainfall depths in the study area during the monitoring period

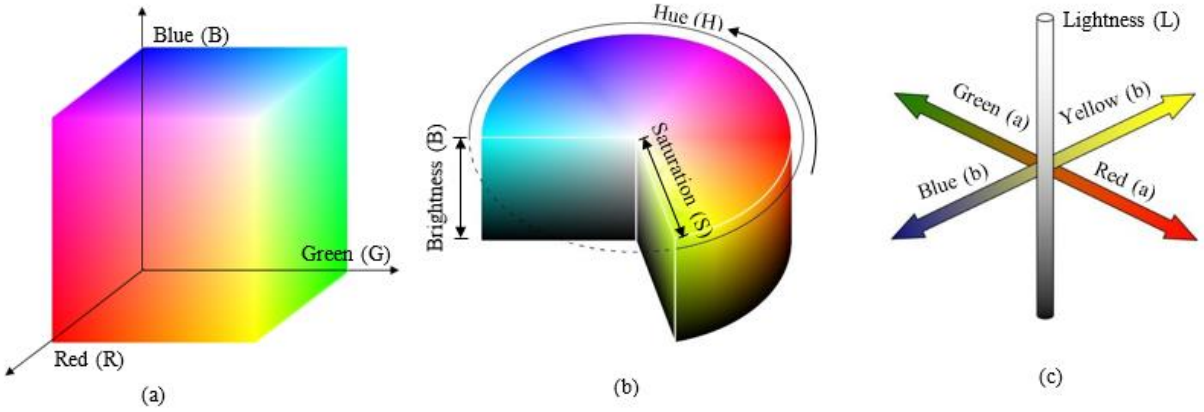

Fig. 6.4 Schematic view of (a) RGB, (b) HSB and (c) Lab colour spaces (after Russ and Russ, 2007)

6.2.6 Colour Analysis

RGB, HSB and Lab are widely used colour spaces in green infrastructure studies to differentiate vegetation cover on the basis of colour. Colour space is a mathematical model, which describes colour as a finite ordered list of elements (Russ and Russ, 2007). RGB colour space describes colour as chromaticities (percentage of hues; Fig. 6.4(a)) of red (R), green (G) and blue (B). However, it is a device-dependent colour space. Colour produced in device dependent colour space depends on parameters (i.e., R, G and B; Russ and Russ, 2007) and the device used for display. Unlike RGB, HSB (Hue saturation Brightness; Russ and Russ, 2007) and Lab colour spaces replicate the human perception of colour. HSB colour space represents RGB colour model in cylindrical coordinates (see Fig. 6.4(b)). In HSB colour space, H represents the type of colour i.e., violet, indigo, blue, green, yellow, orange and red. It ranges between 0° and 360°. S represents colourfulness of object or area with respect to brightness i.e., proportion of white added to the pure colour. B represents brightness. S and B range from 0 % and 100 %. In Lab colour space (Fig. 6.4(c)), L represents Lightness, which ranges between 0 % and 100 % brightness, a extends between two opponent colours red and green and b axis represents from blue to yellow. ImageJ is adopted to process the images using various colour spaces (Ferreira and Rasband, 2012). ImageJ displays 256 segments for the parameters in various colour spaces i.e., R, G, B, H, S, B, L, a and b. Colour of image is characterized using these 256 segments.

Lab colour space is adopted for the present study to investigate the spatial heterogeneity of mix grass cover. This is because spatial heterogeneity of mix grass can be identified by the difference in lightness among mix grass cover. In general, HSB colour space can also be used to identify the lightness difference. However, HSB categorizes the difference in lightness between light green and dark green using 42 segments, whereas Lab colour space categorizes it using 123 segments

(Ferreira and Rasband, 2012). This shows that, Lab colour space is appropriate for present study as compared to other colour spaces. In addition, colour differentiation of entire mix grass in the selected area is found to be possible in Lab colour space. Hence, Lab colour space is adopted for this study.

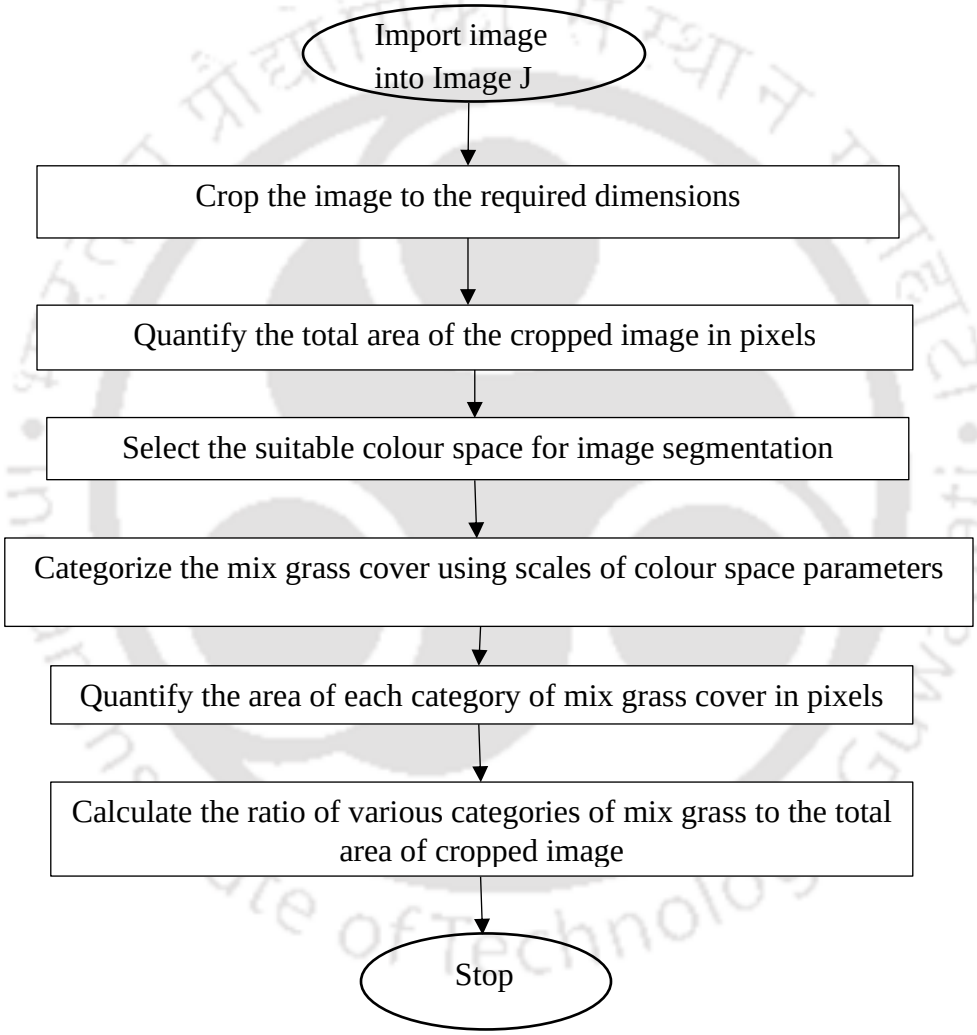

Fig. 6.5 Flow diagram to differentiate various colours of mix grass

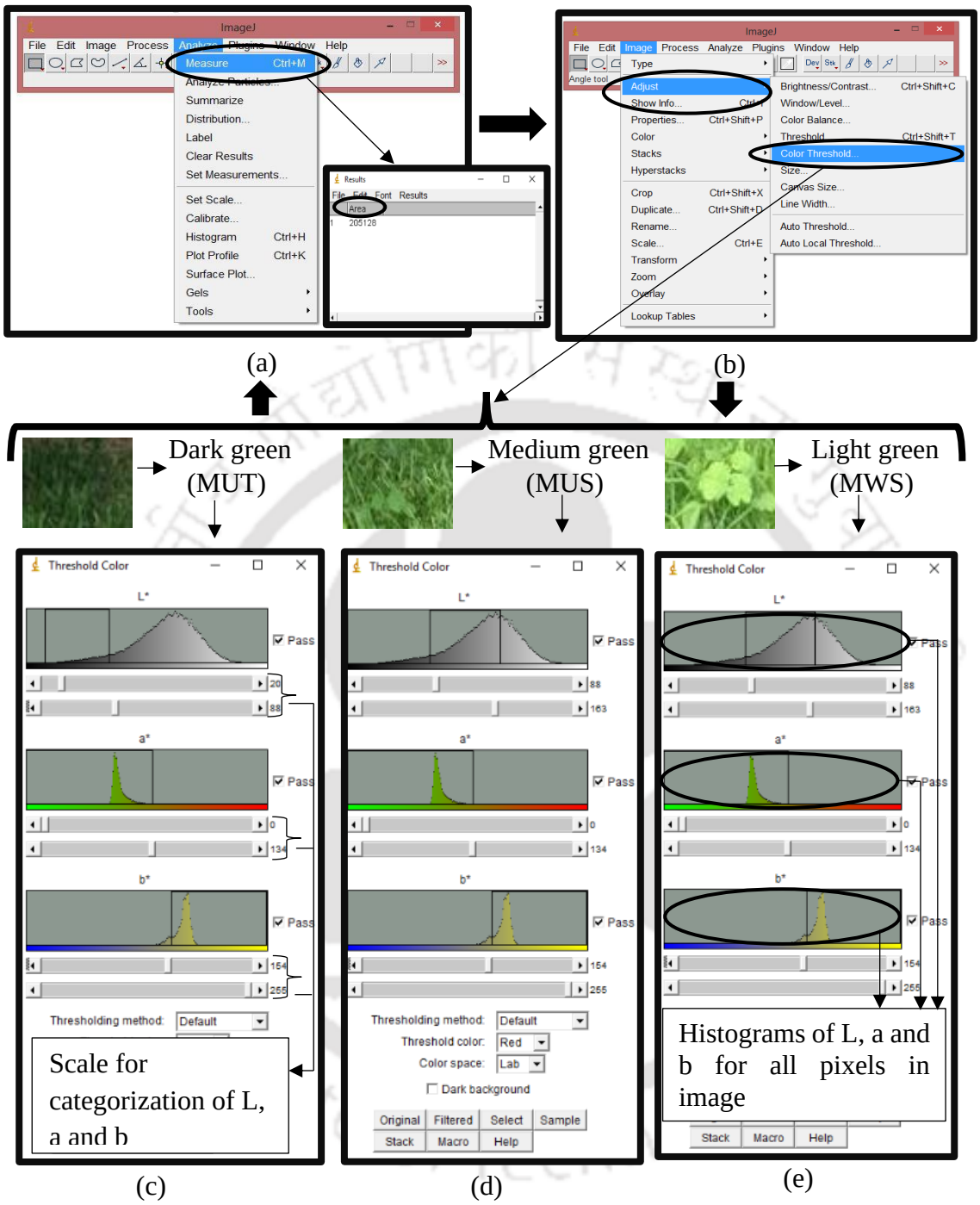

Fig. 6.6 Procedure for (a) measuring the area of selected portion in image and (b) categorization of mix grass i.e., (c) MUT, (d) MUS and (e) MWS

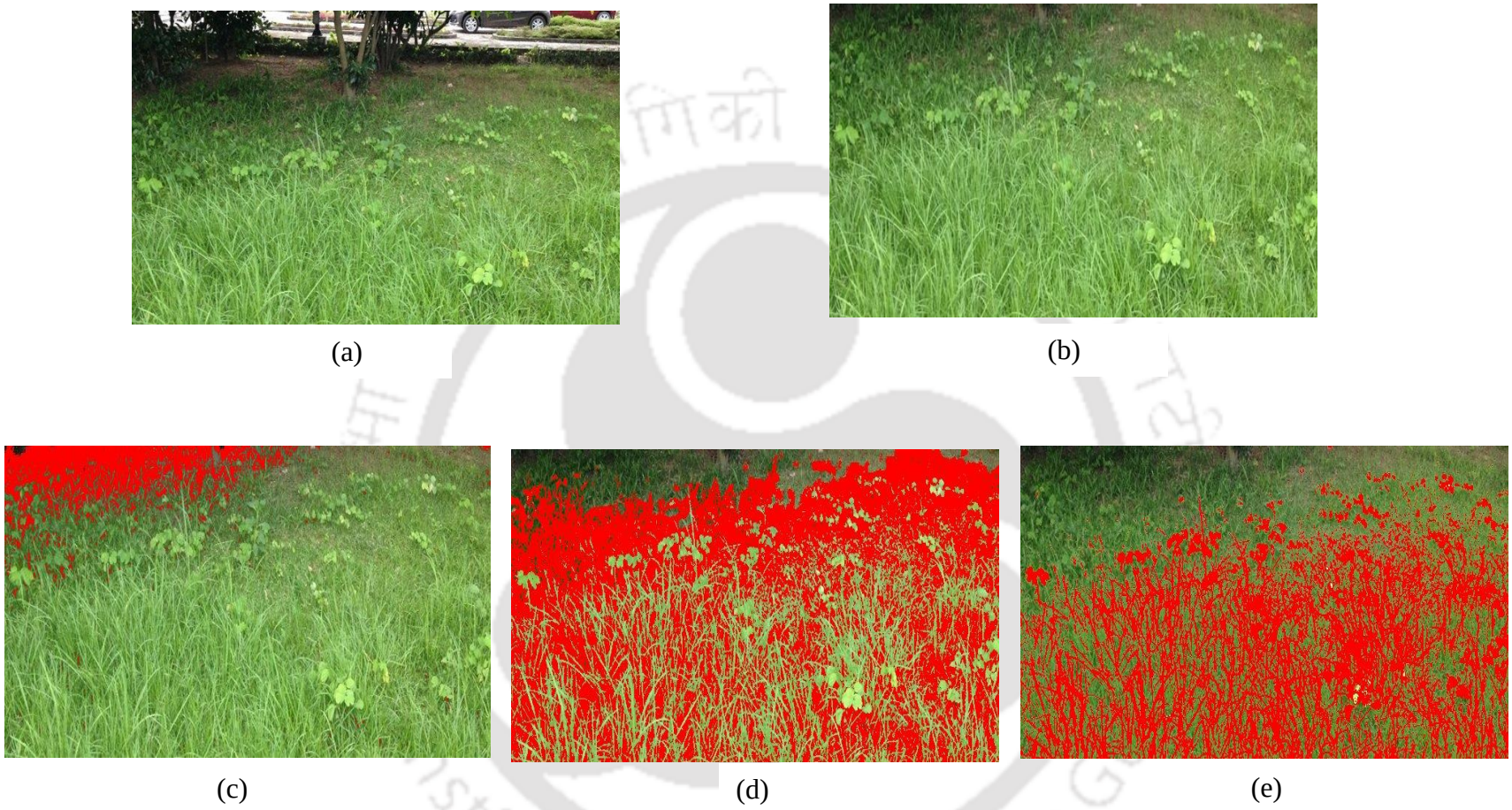

Fig. 6.7 Overview of (a) original image captured at the end of April, (b) cropped image and processed images for determination of area of (c) MUT, (d) MUS and (e) MWS

6.2.7 Colour Analysis Procedure

Fig. 6.5 shows the flow chart of colour analysis procedure. Fig. 6.6 shows the colour analysis procedure in ImageJ. Processed images of MUT, MUS and MWS can be seen in Fig. 6.7. The captured images were imported into ImageJ and digitized (see Fig. 6.7 (a)). Thereafter, digitized images were cropped to only account the desired portion or size (6m length and 5 m wide; see Fig. 6.7 (b)) of vegetation cover. Area in pixels of cropped image was quantified using area measurement option. This measure option and window showing quantified area in pixels can be seen in Fig. 6.6 (a). MUT, MUS and MWS can be differentiated by using the lightness variation of the green colour. The lightness difference among those is shown in Fig. 6.6. In order to quantify surface area occupied by MUT, MUS and MWS separately, the mix grass cover is categorized using colour threshold option (see Fig. 6.6 (b)). This option enables ImageJ to display the histogram of L, a and b values for the all pixels of image. ImageJ displays 256 values of L, a and b parameters, which are marked in Fig. 6.6 (c). This shows that L, a and b parameters are categorized using a scale of range 0-255.

The three categories of mix grass can be identified separately by adjusting the values of L, a and b on scales marked in Fig. 6.6c. For the mix grass cover in the selected site, ranges of a and b values were found be 0-134 and 154-255, respectively. Within the lightness scale of green (L), values between 20 and 91 are found to indicate dark green i.e., MUT (Fig. 6.6c), whereas, medium green i.e., MUS is found to be in the range of 92-162 (Fig. 6.6 d). MWS is observed to be indicated by L values ranging from 163 to 233 (Fig. 6.6 e). The processed images for three types of mix grass cover i.e., MUT, MUS and MWS occurred in the month of April as shown in Fig. 6.7 c, d and e (red portion). These pixel values of selected mix grass covers are converted into area and

taken into account as surface area covered by the respective type of mix grass. Proportions of MUT, MUS and MWS were quantified using following formulae.

$$\text{Proportion of MUT (\%)} = \frac{Surface\ area\ of\ MUT}{Toatl\ surface\ area\ considered}\ x\ 100 \quad (6.1)$$

$$\text{Proportion of MUS (\%)} = \frac{Surface\ area\ of\ MUS}{Toatl\ surface\ area\ considered}\ x\ 100 \quad (6.2)$$

$$\text{Proportion of MWS (\%)} = \frac{Surface\ area\ of\ MWS}{Toatl\ surface\ area\ considered}\ x\ 100 \quad (6.3)$$

6.3 Results and discussion

6.3.1 Mix grass cover variation during monitoring period

Fig. 6.8a – f show the overview of surface area variation in selected site during monitoring period. It can be seen that, minor area of selected site in tree vicinity is covered with vegetation during initial stage (see image captured in January, 2016; Fig. 6.8a). Fig. 6.8b (Image captured on 28th February 2016) shows yellow shredded leaves with relatively low vegetation growth in February. Fig. 6.8c (31st March 2016) shows vegetation regrowth and greening during March. Majority region of selected site is observed to be covered densely by vegetation at the end of April (Fig. 6.8d). Growth of *Bauhinia purpurea* species is also found during April. This reveals additional growth of new vegetation species, which were not present during dry period. Mix grass growth is observed to continue during May and June, which can be observed from Fig. 6.8e and Fig. 6.8f.

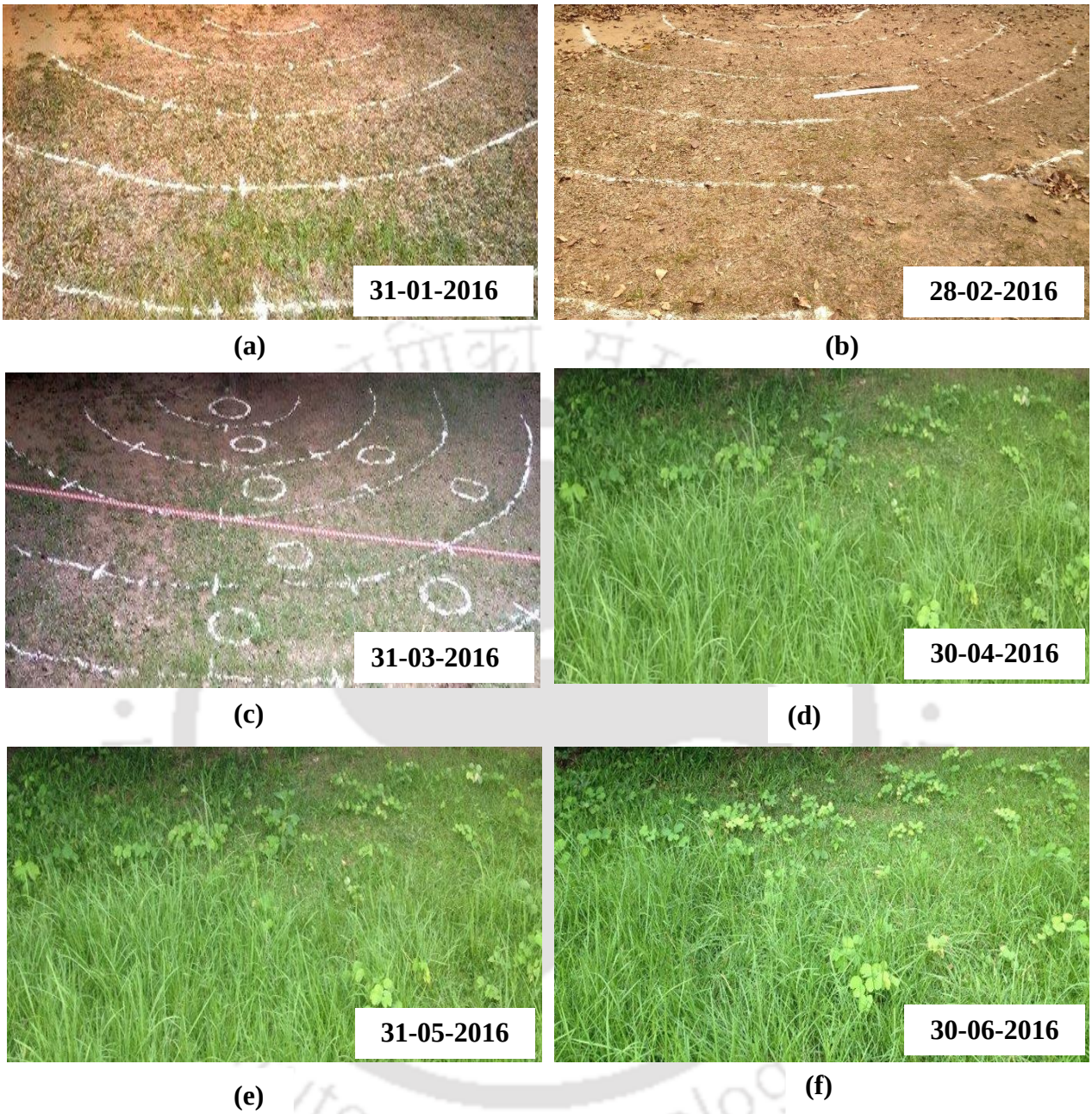

Fig. 6.8 Vegetation cover at the end of six consecutive months: (a) 31 January 2016 (b) 28 February 2016 (c) 31 March 2016 (d) 30 April 2016 (e) 31 May 2016 (f) 30 June 2016

6.3.2 Temporal variation of shoot growth and mix grass proportion

6.3.2.1 Comparison of average shoot growth among various rectangular areas in the vicinity of tree

Fig. 6.9 shows the variation of average shoot length in the various rectangular areas in the tree vicinity. Three types of species i.e., *Cyperus*, *Poaceae* and *Bauhinia purpurea* are considered for measuring average shoot length. It can be observed that, no significant spatial heterogeneity of shoot growth is found during dry period. Average shoot length is found to vary between 5 mm and 15 mm during dry period. Unlike dry period, shoot length is found to be higher in rectangular areas at greater radial distances from tree stem as compared to that in rectangular areas nearer to the tree stem. This may be attributed to presence of tree roots and tree shading at near distance from tree stem. Root growth would be slow when mix grass root system overlap with tree roots (Casper and Jackson, 1997). Lack of photosynthetically active radiation, which occurs due to tree shading effect may also be a reason for relatively less shoot growth rate near tree stem (Fitzpatrick and Kirkman, 1995).

Fig. 6.10 (a) and (b) show shoot growth rate variation with time in rectangular areas at 0.2 m and 4 m due to occurrence of various rainfall depths. Shoot growth rate is observed to change with rainfall depth variation. Average shoot growth rates in rectangular area at 0.2m longitudinal distance from tree stem are found to be 5mm/month, 3mm/month, 7mm/month, 49mm/month, 70mm/month and 60mm/month during January, February, March, April, May and June, respectively. Average shoot growth rates in rectangular area at 4 m longitudinal distance from tree stem are found to be 40mm/ month, 20mm/month, 60mm/ month, 184mm/month, 334mm/month and 280mm/month during January, February, March, April, May and June, respectively. These results show that, greater shoot growth rate is found during the months in which, relatively high

rainfall depths occurred over majority of monitoring period. This may be attributed to increase in available water content due to raise in rainfall depth. This trend is not found to hold true during April. This may be due to regrowth of vegetation in the tree vicinity during April.

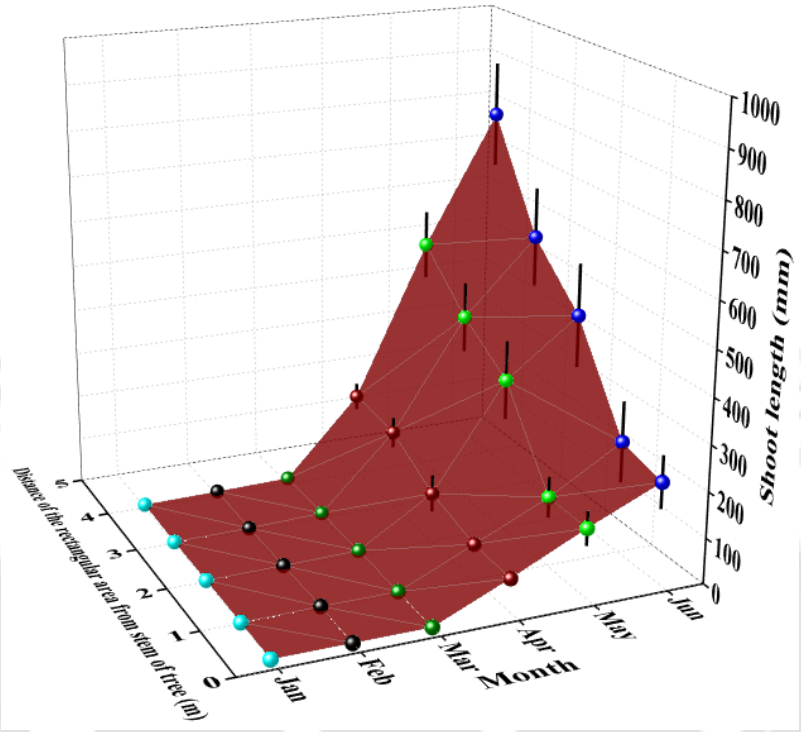

Fig. 6.9 Comparison of shoot length among various rectangular areas over six months of the observation period

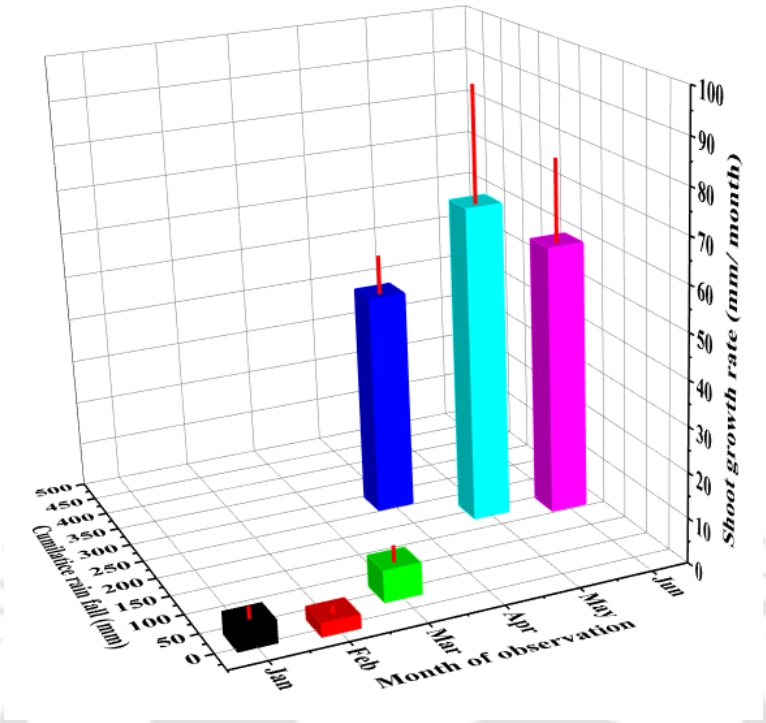

(a)

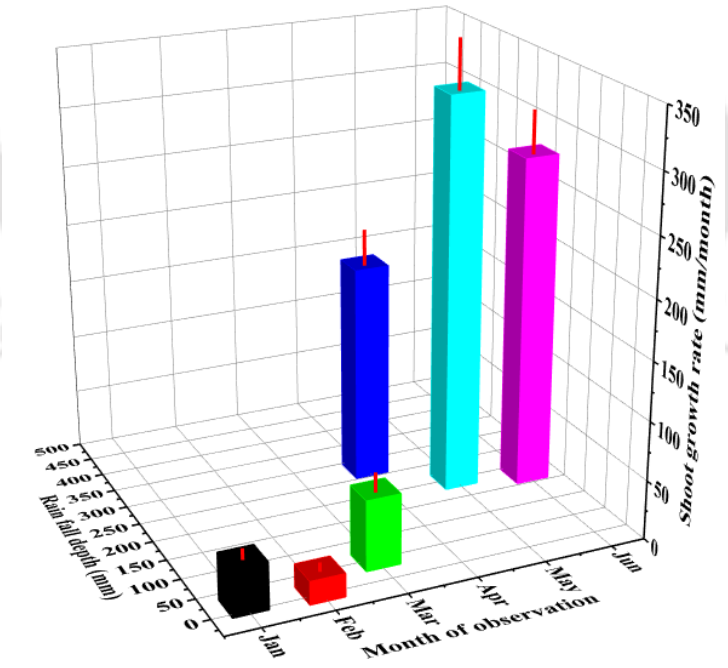

(b)

Fig. 6.10 Average shoot growth rate variation with change in rain fall depth in rectangular areas at (a) 0.2 m longitudinal distance from tree stem and (b) 4 m longitudinal distance from tree stem, during monitoring period

6.3.2.2 Comparison among various types of mix grass proportions occurred during monitoring period

Fig. 6.11 depicts the mix grass proportions variation with respect to change in rainfall depth. Rainfall depth is considered instead of month of observation in the horizontal axis for the better interpretation of results. Total mix grass proportion is found to vary between 13 % and 97 %. Only two types of mix grass cover i.e., MWS and MUT are found during dry period. The reason for the absence of MUS during dry period is very low shoot length (i.e., 5mm to 15mm). Maximum mix grass proportion (49 %) is found at the end of March during dry period. One reason for this may be, rainfall depth in March is higher than that in January and February.

The proportion of MWS is found to vary between 12 % and 47 % during dry period. Proportion of MWS is observed to increase with rainfall depth increment during dry period. In addition to the low rainfall depth, shredding of leaves during February is also a reason for relatively low proportion of MWS occurred at the end of February. Furthermore, relatively high proportion of MWS was found at the end of March due to regrowth of mix grass. MUT proportion varies between 0.2 % and 2.0 % during dry period. Lowest proportion of MUT is found at the end of February during which, shredding of leaves occurred. MUT proportion is found higher at the end of March as compared to that at the end of January and February. This may be due to tree leaves regrowth and relatively high rainfall depth during March.

All the three types of covers i.e., MUS, MWS and MUT can be observed during wet period. Ranges of MUS, MWS and MUT are found to be 45 % - 53 %, 37 % - 49 % and 2 % - 3 % during wet period. MUS variation is not found to be consistent with rainfall depth or shoot length. At the end of May, MUS proportion is found 2 % higher than that at the end of April. However, at the

end of June, MUS proportion is found 10 % lower than that at the end of May. Unlike during dry period, trend of variation of MWS proportion is not observed to be effected by change in rainfall depth. However, MWS is found to increase with shoot growth during wet period. MUT is found to increase with shoot growth during wet period. This is due to growth of tree leaves. Such increase in tree leaves widens the area under shading.

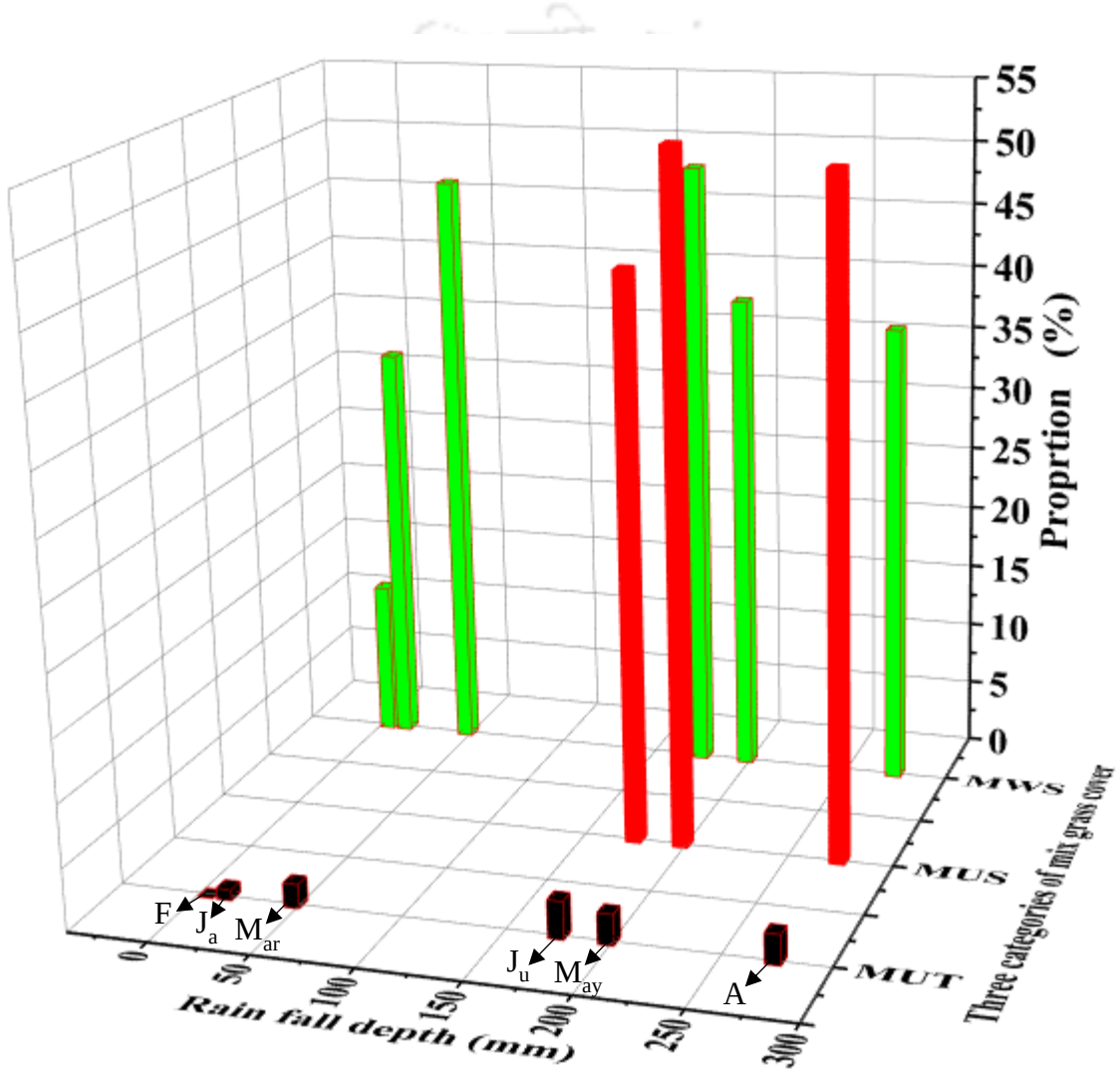

J_a- January; F- February; M_{ar}- March; A- April; M_{ay}- May; J_u- June

Fig. 6.11 Comparison among three types of mix grass proportions during the monitoring period

6.4 Summary and Conclusions

Low cost non-invasive technique (colour analysis) was demonstrated to differentiate the MUT, MUS and MWS in the selected site. Lab colour space was suitable for this differentiation. Reason for this is, higher number of segments (i.e., 123) can be identified between light green and dark green using lightness parameter (L) of Lab colour space. “a” lies between two opponent colours red and green. Whereas, “b” lies between blue to yellow. ImageJ displays 256 segments for L, a and b. Ranges of L values for MUT, MUS and MWS lie within 20 - 91, 92 - 162 and 162 – 233. The ranges of “a” and “b” for three categories of mix grass are 0 – 134 and 154 – 255, respectively. Ranges of MUT, MUS and MWS proportions during monitoring period lie within 0.2 % - 3.0 %, 0 % - 53 % and 12 % - 49 %. Only two types of mix grass cover i.e., MWS and MUT exist during dry period. Proportions of MWS and MUT increase with rise in rainfall depth during dry period. Lowest proportions of MWS and MUT were found at the end of February. In addition to relatively low rainfall, shredding of leaves is also a reason for these lowest proportions. Unlike dry period, three types of areas i.e., MUS, MWS and MUT were observed during wet period. MUS proportion variation trend was not consistent with rainfall depth or shoot growth. Proportions of MWS and MUT increase with shoot growth during wet period. This was due to tree leaves growth, which continues with time.

The obtained results help numerical modelers to better understand the non-uniformity in vegetation cover exposed to PAR for simulation of flow through green infrastructure. Drones (unmanned air vehicles) can be programmed with colour analysis technique to differentiate and quantify the MUT, MUS and MWS in relatively large areas. Such fusion helps to avoid the human interference on the site while capturing images regularly. In addition, drones programmed with

colour analysis technique could be remotely connected to automatic mix grass mower. This helps to establish efficient and cost effective unmanned landscape maintenance system.

CHAPTER 7 EFFECT OF HIGH SUCTION ON PLANT PARAMETERS

7.1 General

This chapter focuses on suction induced in root zone of mix grass used in green infrastructure. Most of the previous studies focused on evapotranspiration induced suction < 100 kPa measured using tensiometers. For investigating the drought condition necessitate suction data > 100 kPa. It was noted that the response of plant parameters such as stomatal conductance and surface area were not considered holistically with root zone evapotranspiration induced suction. This chapter presents the effect of evapotranspiration induced suction on stomatal conductance and surface area for a mix grass species used in green infrastructure subjected to drought stress for suction > 100 kPa.

7.2. Materials and methods

7.2.1 Soil properties

The engineering properties of the selected soil were described in section 3.2.1.

7.2.2 Selected plant species and transplantation condition

Mix grass, which is combination of two species namely, *Axonopus Compressus* and *Cynadon Dactylon* were selected for the study. The description about these species and transplanting condition is stated in section 4.2.1.

7.2.3 Experimental setup and instrumentation

7.2.3.1 Soil sample preparation

Test setup used to demonstrate the measurement of stomatal conductance and surface of mix grass is schematically portrayed in Fig. 7.1. The experimental setup consists of a cylindrical PVC (poly

vinyl chloride) mould of 300mm diameter and 250mm length with prefabricated holes at sides to accommodate suction and moisture content sensors. The locations of the instrumentation can be seen in Fig. 7.1. Soil excavated from nearby hill site was compacted up-to 170 mm height in three layers corresponding to 0.9 MDD as per previous literature for grass species (Ng et al., 2014; Li et al., 2016). The procedure of compaction is explained in section 4.2.1.

7.2.3.2 Installation of instrumentation

Dummy tubes were placed during compaction at the locations of VWC and suction sensors. The tubes of relatively less diameter as compared to sensors were inserted to ensure contact between soil and instruments after installation. Two MPS-6 sensors (METER Group, USA) were installed at diametrically opposite ends at a depth of 40mm to capture the suction (range of 9-10000 kPa) induced due to root water uptake. In addition, a tensiometer (UMS BMGH, 2016) was installed to capture the suction range below 9 kPa. A moisture content sensor (SM 200; Delta-T devices, 2006) was installed diametrically opposite to tensiometer. The minor gap between sensor and soil was backfilled with soil to prevent the preferential flow. A layer of anabond adhesive was applied in the clearance between sensor and PVC at the predrilled holes. The MPS-6 sensors were connected to EM 50 data logger (METER Group, USA) for data logging. Tensiometer and SM 200 were connected to GP2 (Goodchild et al., 2014) and DL-6 data loggers (Delta-T devices, 2013), respectively. Soil root composite water retention curve was obtained using measured suction and VWC.

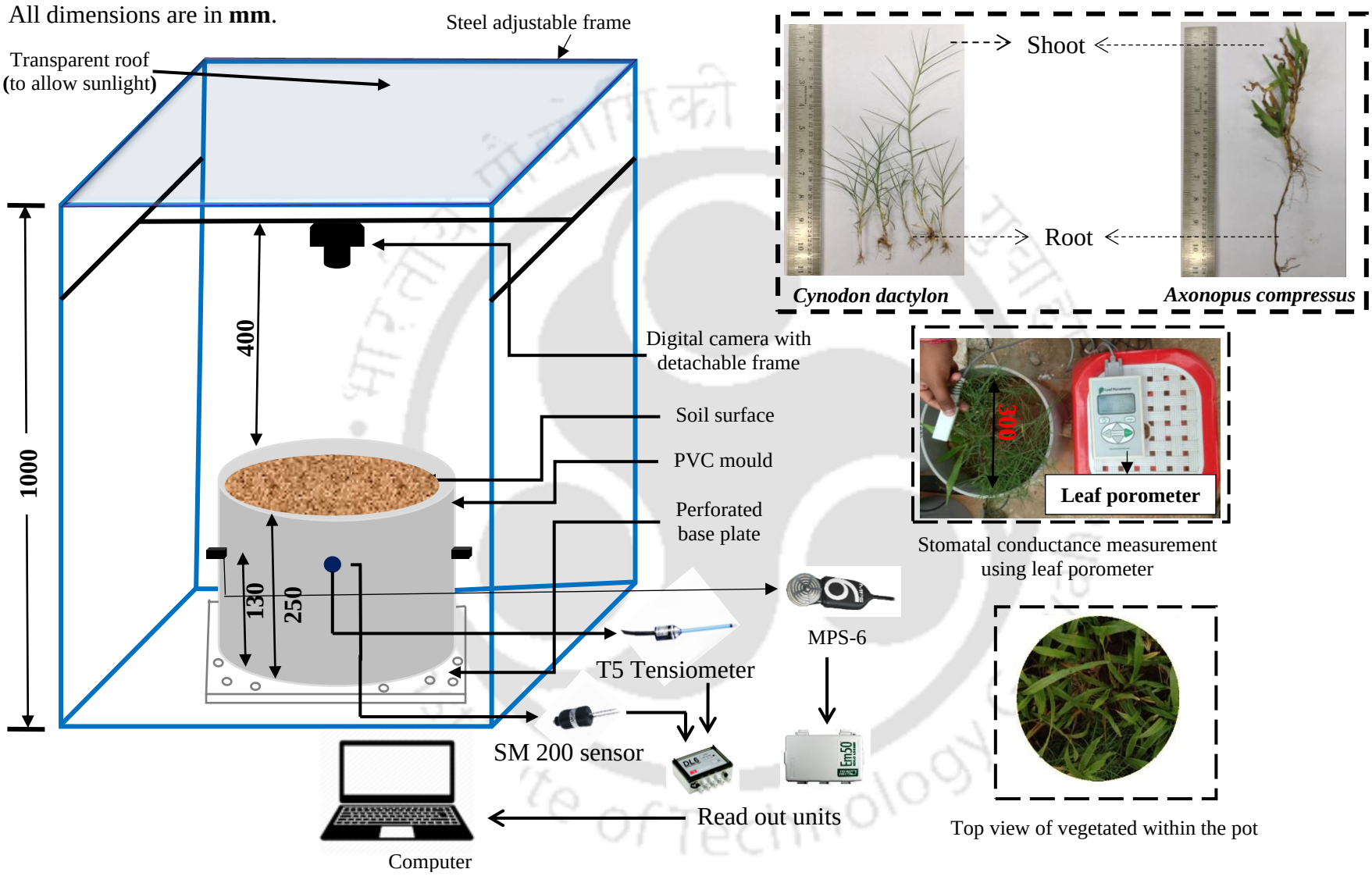

Fig. 7.1 Schematic representation of experimental setup used to measure area of vegetation cover, suction, volumetric water content (VWC) and stomatal conductance

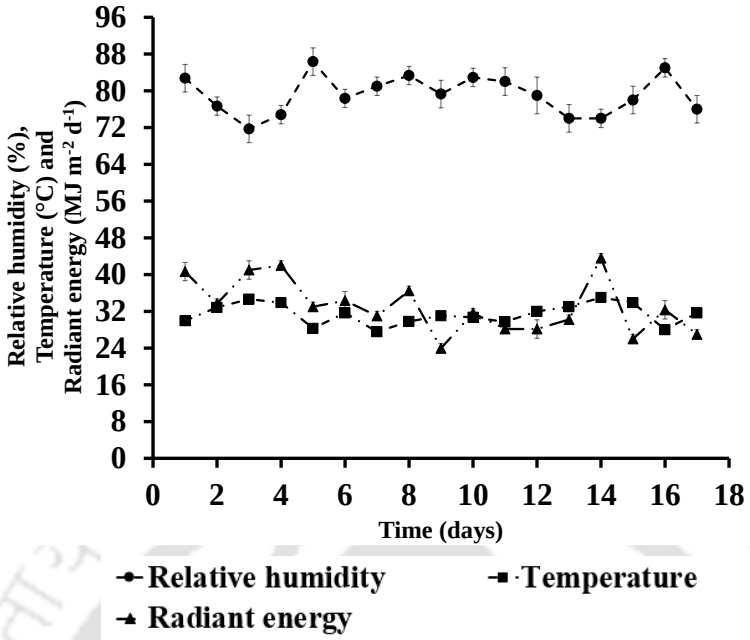

Fig. 7.2 Weather condition during the test period

7.2.3.3 Environmental conditions during plant growth

The specimen was placed under transparent roof and exposed to natural environmental condition during monitoring period. Transparent roof was arranged to avoid effect of natural precipitation during monitoring period while the mould is subjected to drying. Controlled irrigation was applied using a sprinkler system to nurture the mix grass. A digital camera with a detachable frame was mounted above the PVC mould to obtain the images of mix grass periodically. Mix grass was transplanted to the pot after the installation of instruments. Vegetated pot was irrigated regularly for a period of 72 days. The irrigation period was maintained at 4 day interval to ensure the suction below the wilting point reported by previous researchers (1500 kPa; Feddes, 1982). Area of green grass cover (live grass cover in the pot) was found to reach inner area of pot at the end of 73 days. Thereafter, mix grass cover was exposed to evaporation until it completely wilts. Methodology to quantify the surface area of grass cover has been explained in section 2.5. The meteorological

parameters such as solar radiation, air temperature and air relative humidity were monitored using micro-climate monitoring system (MCMS, METER Group, USA). Meteorological parameters observed during test period are shown in Fig. 7.2 (explained in next section).

7.2.3.4 Camera settings for capturing images of mix grass cover

A commercially available camera (CANON EOS 600D) was mounted on a detachable frame above the PVC mould to capture the images of mix grass cover periodically. The lens range and horizontal/vertical resolution were maintained at 18-55 mm and 72 dpi. The focal length, ISO speed and exposure time were maintained at 23mm, ISO-640 and 1/30sec respectively. Resolution of camera model is 18 megapixels. Images were captured from same height (400mm) using an adjustable frame (see Fig. 7.1). Maintenance of same focal length, ISO speed and exposure time and height minimizes observational errors, and enable constant number of pixels. In order to compare the image analysis results accurately, constant pixel area is essential. Images were captured in ambient light during measurement period of stomatal conductance.

7.2.3.5 Measurement of stomatal conductance

GGL, GGS and CWG were categorized by visual observation to measure stomatal conductance. It is evident that, large number of leaves are available for testing. Measurement of stomatal conductance for all existing leaves in pot requires relatively long duration. In such case, measured stomatal conductance could not be compared accurately (Pietragalla and Pask, 2012). Hence, five locations of each category were selected for measurement of stomatal conductance using leaf porometer (METER Group, USA). Stomatal conductance refers to ratio of flux density and the water vapor concentration difference between surrounding and leaf surface (Pietragalla and Pask,

2012). Leaf is clamped to the open chamber in leaf porometer. Relative humidity gradient is developed between surroundings of chamber and leaf surface. Leaf porometer calculates stomatal conductance from the relative humidity gradient. A standard procedure (METER Group, USA) was adopted for the calibration of leaf porometer. The instrument was calibrated using a known conductance value of filter paper moistened with distilled water. The accuracy of the leaf porometer was found to be around 90 %. As the stomata is sensitive to physical alteration, any physical stress or human contact with the leaf is avoided as much as possible. Measurements were performed quickly, as the porometer usage may alter surface of leaf.

Variation in relative humidity, temperature and radiant energy is found to be very low during 10:00 A.M. - 12:00 A.M. Hence, stomatal conductance and surface area was monitored under ambient light during this time period. Relative humidity, temperature and radiant energy are observed to be 79 % ± 4 %, 31°C ± 2°C and 33 MJ m^{-2} d^{-1} ± 6 MJ m^{-2} d^{-1} (see Fig. 7.2). It must be noted that light, relative humidity and temperature would change with time (Koyama and Takemoto, 2014). Changes in light, relative humidity and temperature affect stomatal conductance and surface area of mix grass ((Bytnerowicz and Fenn, 1996; Bytnerowicz et al., 2003; Mooney et al., 1983). As a result of change in stomatal conductance and surface area, the correlations developed in present study may not be same for different environmental conditions. The main focus of present study is to explore the high evapotranspiration induced suction in soil root composite and, changes in stomatal conductance and surface area of canopy at higher suctions. Hence, measurements taken at only one point of time suffice the purpose of the study. It is evident that, age of grass effects the stomatal conductance (Buchanan-Wollaston et al., 2005; Lee et al., 2011). Hence, the mix grass of relatively less age difference was considered for the measurement. In addition, mix grass wilts gradually (McGechan, 1990). Therefore, measurement of stomatal

conductance for a single leaf could not be possible during entire monitoring period. Leaf considered for stomatal conductance measurement has been changed when the mix grass at selected location approaches wilting point.

7.2.3.6 Quantification of surface area of GGL, GGS and CWG

Colour analysis procedure to differentiate and quantify the surface area covered by GGL, GGS and CWG is shown in Fig. 6.6 (chapter 6). It is known that fewer shoots exist below the mix grass. As the captured images are two dimensional, the surface area of above mentioned fewer shoots could not be categorized. Surface area of shoots below the mix grass was found to be 6 % - 7 % of total surface area of mix grass. Surface area of shoots below the mix grass could be relatively high in case of few species. In such case, analysis of two dimensional images may not suffice the purpose. Hence, three-dimensional images are required to quantify and categorize the mix grass accurately. 3D lidar imaging could be the possible solution to capture the high resolution three-dimensional images (Omasa et al., 2006).

7.3. Results and discussions

7.3.1 Gradual wilting of mix grass cover during monitoring period

Fig. 7.3 shows the water retention curve of soil root composite (SRCWRC). Water retention curve was fitted using van Genuchten (1980) model. Fitting coefficients related to curvature (α) and pore size distribution (n) were found to be 0.27 and 1.45, respectively. VWC is observed to reduce noticeably from about 30 % to 7 % with increase in suction by 90 kPa from 8 kPa. Volumetric field capacity is found to be 24 %-26 %. It refers to the VWC held in soil after excess water drained away due to gravity. Suction corresponding to volumetric field capacity is observed to be around

11 kPa. Fig. 7.3a-f shows the gradual wilting of mix grass with respect to suction during monitoring period. Visibly identifiable change is not found in surface area covered by green grass up to 103 kPa (see Fig. 7.3 (a-c)). Noticeable change in surface area covered by green grass at suction values beyond 103 kPa can be seen. Completely wilted grass is observed over major region at suction around 2431 kPa.

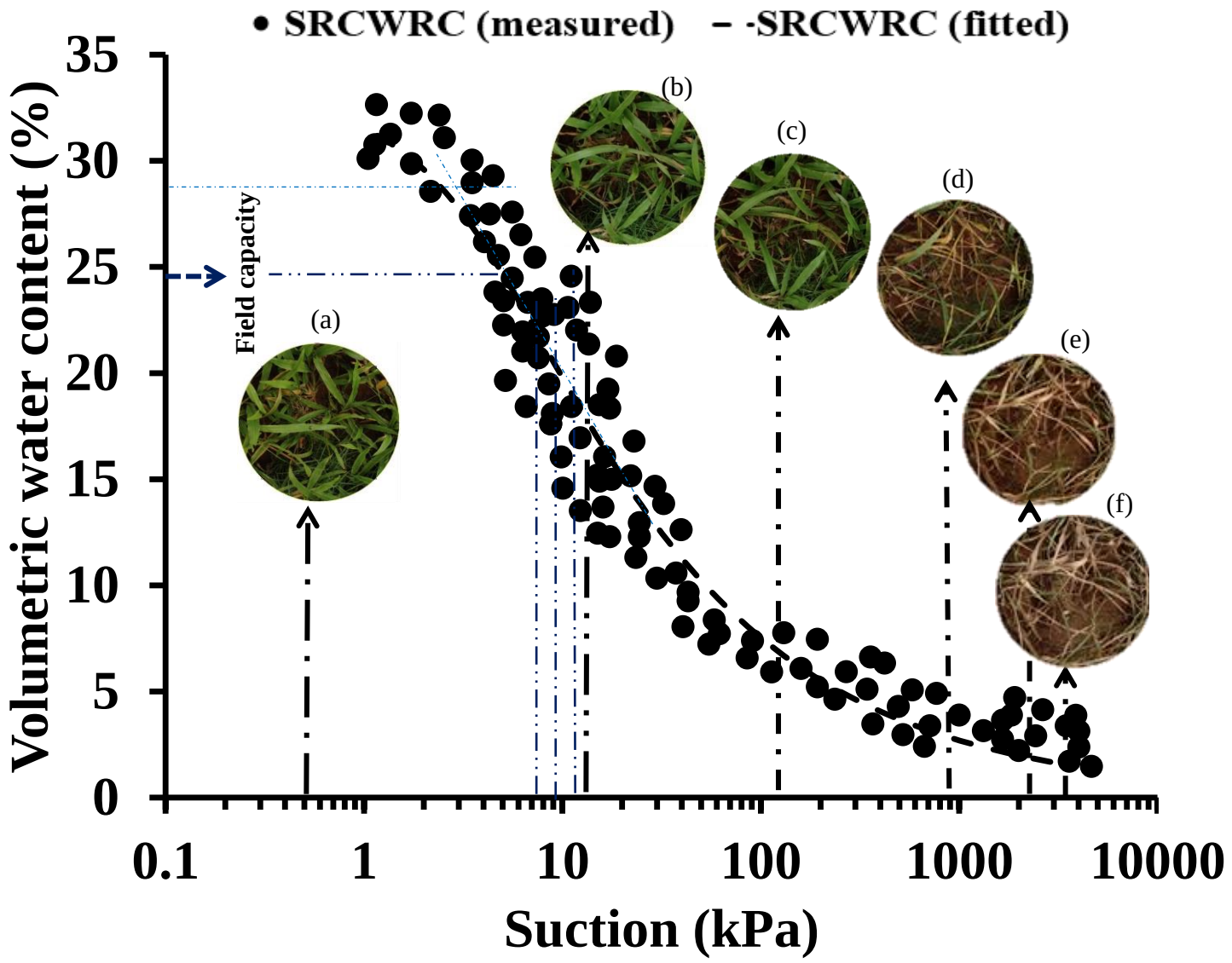

Fig. 7.3 Measured and fitted soil root composite water retention curve (SRCWRC) and pictorial view of gradual wilting of mix grass when it was subjected to continuous drying

7.3.2 Stomatal conductance variation during monitoring period

7.3.2.1 Comparison of stomatal conductance measured at various suction values

Fig. 7.4 shows the average stomatal conductance at the selected locations of GGL and GGS. Stomatal conductance is observed to vary between 681 m mol m^{-2} s^{-1} and 0 m mol m^{-2} s^{-1}. Stomatal conductance of GGL and GGS is observed to increase with rise in suction from 1 kPa to 6±1 kPa during monitoring period. Stomatal conductance of GGL and GGS is observed to increase by 54 % and 101 % with 5 kPa rise in suction. It can also be observed that, peak stomatal conductance occurs near to the suction corresponding to volumetric field capacity. Relatively less stomatal conductance at low suction can be explained on the basis of oxygen available in soil root composite. Low suction represents the situation, when oxygen available in pores of soil root composite is very limited due to high saturation (Raes and Deprost, 2003). In such case, stomatal conductance would be relatively low (Thomas et al., 2016). Thereafter, stomatal conductance is found to decrease up to suction around 1340 kPa. Such decrease is observed to be around 90 % for GGL and GGS. Furthermore, stomatal conductance variation is observed to be relatively low (around 21 %) with increase in suction from 1340 kPa to 2431 kPa. This is due to relatively low available water content. Stomatal conductance is observed to be zero at suction around 2431 kPa. This suction value can be termed as typical wilting point for the selected combination of grass species. Wilting point was reported to be 1500 kPa by Feddes (1982). In addition, a recent study (Garg et al., 2015a) also presented the wilting point for *Schefflera heptaphylla* according to Feddes (1982). However, results of the current study show that, stomatal conductance values and wilting point may vary for different species. Predicted stomatal conductance values were presented in a recent study (Tobin and Kulmatiski, 2018) corresponding to a wide range of suction (1-500 kPa). However, applicability of the predicted stomatal conductance was not presented in the context of

soil type or density in their study. In addition, stomatal conductance was not monitored from anaerobiosis point to wilting point for the selected non-crop species.

Decrement in stomatal conductance due to increase in suction from 6 kPa to 2431 kPa can be explained using phenomena of partial and complete stomata closure. Partial and complete closure of stomata occur when plant is subjected to drought stress (i.e., large suction). A plant hormone i.e., abscisic acid, which exists in guard cell mediates the adaptation of mix grass to drought stress through partial and complete closure of stomata (Tipple and Pagani 2007). Abscisic acid changes the pH and concentration of Ca^{2+}, Cl^{-} and K^{+} in leaf to respond drought (Wilkinson and Davies, 1997). These changes cause partial closure of stomata and increase the suction in leaf (Pei et al., 2000; Munimesa et al., 2015). This partial closure of stomata results in less stomatal conductance. It can be observed from Fig. 7.4 that, partial closure of stomata occurs typically at suction between 6 kPa and 1340 kPa. Further water loss through stomata at very large suction and less available water content damages the chloroplast and guard cells. Hence, major number of stomata exist in leaf will be completely closed and results in very low stomatal conductance. Such low stomatal conductance can be observed between 1340 kPa and 2431 kPa. Stomatal conductance becomes 0 when stomata system is completely damaged at suction around 2431 kPa.

Stomatal conductance of mix grass under light is observed to be 19 % - 64 % higher than that under shade up to suction around 1340 kPa. This can be attributed to difference in stomata opening corresponding to radiant energy variation (Gross et al., 1996). Stomata closes partially under the presence of low light for photosynthesis (Miyazawa et al., 2005). Stomata opens completely in the presence of adequate radiant energy (Schymanski and Zwieniecki 2013). Difference between stomatal conductance of GGL and GGS is minimal beyond the suction value of 1340 kPa. Stomatal conductance of GGL is observed to be only 2 % - 4 % higher than that of

GGS at suction beyond 1340 kPa and below the wilting point. Reason for this may be complete closure of major number of stomata exist in GGL as well as GGS due to large suction. This shows that, effect of suction dominates the influence of light when suction lies between 1340 kPa-2431 kPa. Previous studies (Ackerson, 1980; Bréda et al., 1993; Tardieu and Simonneau, 1998; Gomes et al., 2004; Warren, 2008) show that decrease in stomatal conductance by 95 % is possible due to water stress in soil.

7.3.2.2 Establishment of correlation between stomatal conductance and suction

Visual assessment suggests that the stomatal conductance-suction relation mirrors water retention curve at suction values beyond 7 kPa (see Fig. 7.3 and Fig. 7.4). A new model was proposed to characterize the relationship between stomatal conductance and suction:

$$SC(\Psi) = sc_{min} + \frac{sc_{max} - sc_{min}}{[1+(a_{sc}(\Psi))^{n_{sc}}]^{1-\frac{1}{n_{sc}}}} \quad (7.1)$$

SC (Ψ) = stomatal conductance corresponding to suction (mol m^{-2} s^{-1}/mol m^{-2} s^{-1})

sc_{max}= maximum stomatal conductance (mol m^{-2} s^{-1}/mol m^{-2} s^{-1})

sc_{min}= minimum stomatal conductance (mol m^{-2} s^{-1}/mol m^{-2} s^{-1})

a_{sc} is related to the suction corresponding to peak stomatal conductance ($a > 0$)

n_{sc} = fitting coefficient associated with the curvature (n>1)

All the fitting parameters are tabulated in Table 7.1. It should be noted that the fitting parameters are valid for the suction range beyond the corresponding suction of peak stomatal conductance. The curves fitted can be referred as stomatal conductance characteristic curve (SCCC). It must be noted that drought response of various evergreen or deciduous vegetation may be dissimilar to that of the species tested in preset study (Smith et al., 2001; Niinemets and Valladares, 2006).Therefore, SCCC may also vary for various evergreen or deciduous species.

Table 7.1 A summary of fitting coefficients for correlating stomatal conductance and suction using a novel approach

	SCCC					
	Upper limit [mol m^{-2} s^{-1}/mol m^{-2} s^{-1}]	Lower limit [mol m^{-2} s^{-1}/mol m^{-2} s^{-1}]	a_{sc} [kPa^{-1}]	n_{sc} [-]	m [-]	R^2 (%)
GGL	0.91	0.08	0.08	1.45	0.31	98
GGS	0.63	0.07	0.10	1.39	0.28	98

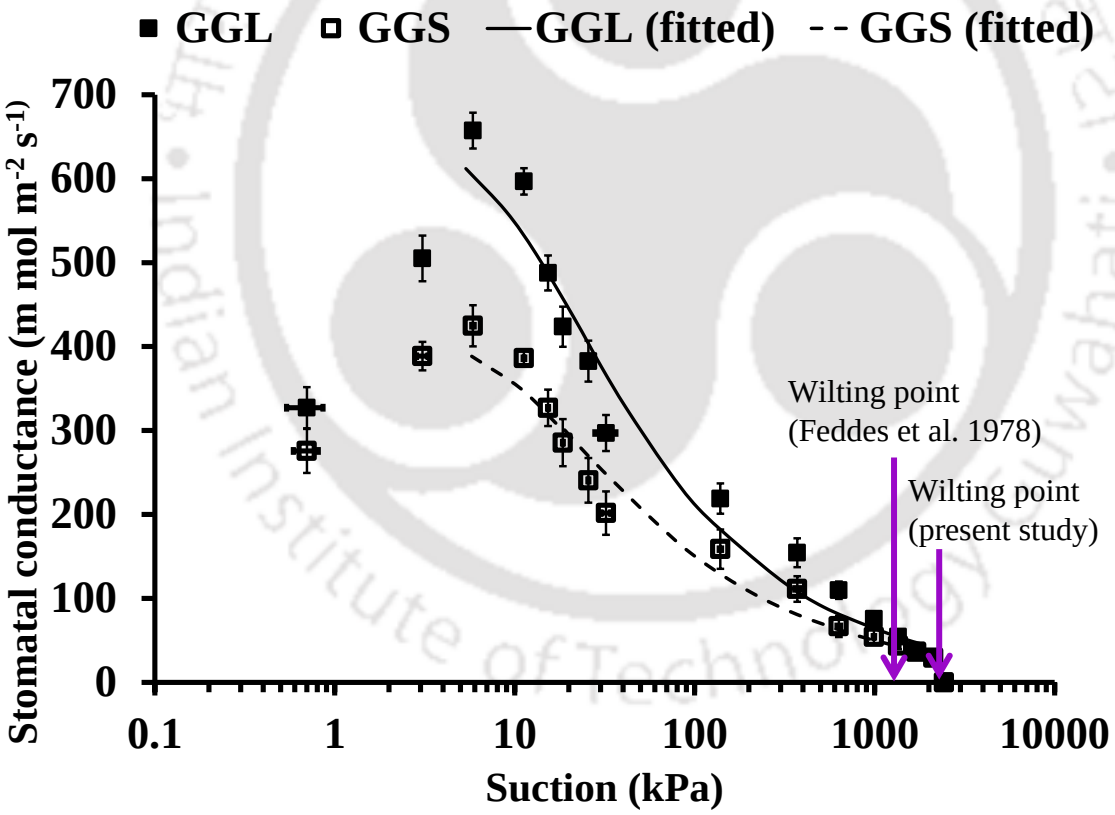

Fig. 7.4 Effect of suction on stomatal conductance

7.3.3 Surface area variation during monitoring period

7.3.3.1 Comparison of normalized surface area of mix grass cover at various suction values

Surface areas of entire mix grass, GGL, GGS and CWG were obtained in pixels using Image J. Thereafter, it was normalized by maximum surface area of entire mix grass cover for better representation. Fig. 7.5 shows the variation of normalized surface area of entire mix grass cover, GGL, GGS and CWG with respect to suction. Normalized surface area of entire mix grass is observed to vary between 1.00 and 0.38. Normalized surface area of entire mix grass cover is observed to increase with rise in suction from 1 kPa to 6 kPa. This is due to growth of mix grass. Thereafter, normalized surface area of entire mix grass is observed to decrease with increase in suction up to 3642 kPa. Reason for such decrease is shrinkage of mix grass when it is exposed to continuous evapotranspiration (Chartzoulakis et al., 2002; Scoffoni et al., 2011). Normalized surface area of GGL is found to vary between 0.00 and 0.79. Normalized surface area of GGL is observed to increase with suction from 1 kPa to 18 kPa. This is due to growth of new leaves of mix grass. However, normalized area of entire mix grass is not found to increase between 6 kPa and 18 kPa. Reason for this is increase in normalized area of wilted grass due to shrinkage of existing mix grass. Normalized surface area of GGL is found to decrease with increase in suction from 18 kPa to 3624 kPa. Normalized surface area of GGL is observed to reach 0.00 at suction around 3624 kPa. Range of normalized surface area of GGS is found to be 0.00-0.18. Normalized surface area of GGS is found to decrease with increase in suction up to around 3013 kPa. Although green grass exists, normalized surface area of GGS is found to be 0 at 3013 kPa.

Variation in normalized surface area of entire mix grass and three categories of mix grass is observed to be relatively low (i.e., within ±15 %) up to 138 kPa. Reason for this can be explained on the basis of favorable suction range for root water uptake. Feddes (1982) reported that, root

water uptake could be significant between 5 kPa to 100 kPa. Such high root water uptake implies more vegetation growth (Sharp and Davies 1985). Large decrease (around 47 % and 66 %) in normalized surface areas of entire mix grass cover and GGL can be observed with increase in suction from 138 kPa to 2431 kPa. In addition, large increase in CWG (around 31 %) also can be observed due to increase in suction from 138kPa to 2431 kPa. Reason for these may be increase in water stress and reduction in root water uptake. Normalized surface area of entire mix grass is found to decrease by 2 % with increase in suction from 2431 kPa to 3624 kPa. Whereas, any variation was not found in normalized surface area of CWG within 2431 kPa-3624 kPa. Unlike GGL and CWG, difference between maximum and minimum normalized surface area of GGS is relatively low i.e., 18 %. Reason for such low difference is decrement in normalized surface area of mix grass due to shrinkage (Jeong et al., 2013). Previous research (Jeong et al., 2013) shows that surface area change observed in the current study could be possible due to continuous drying. In addition, suction variation with time was monitored during drying period in vegetated soil widely (Somma et al., 1998; Wu et al., 1999; Vrugt and Hopmans 2001; Javaux et al., 2008). However, normalized surface area decrement was not correlated to the suction in their studies.

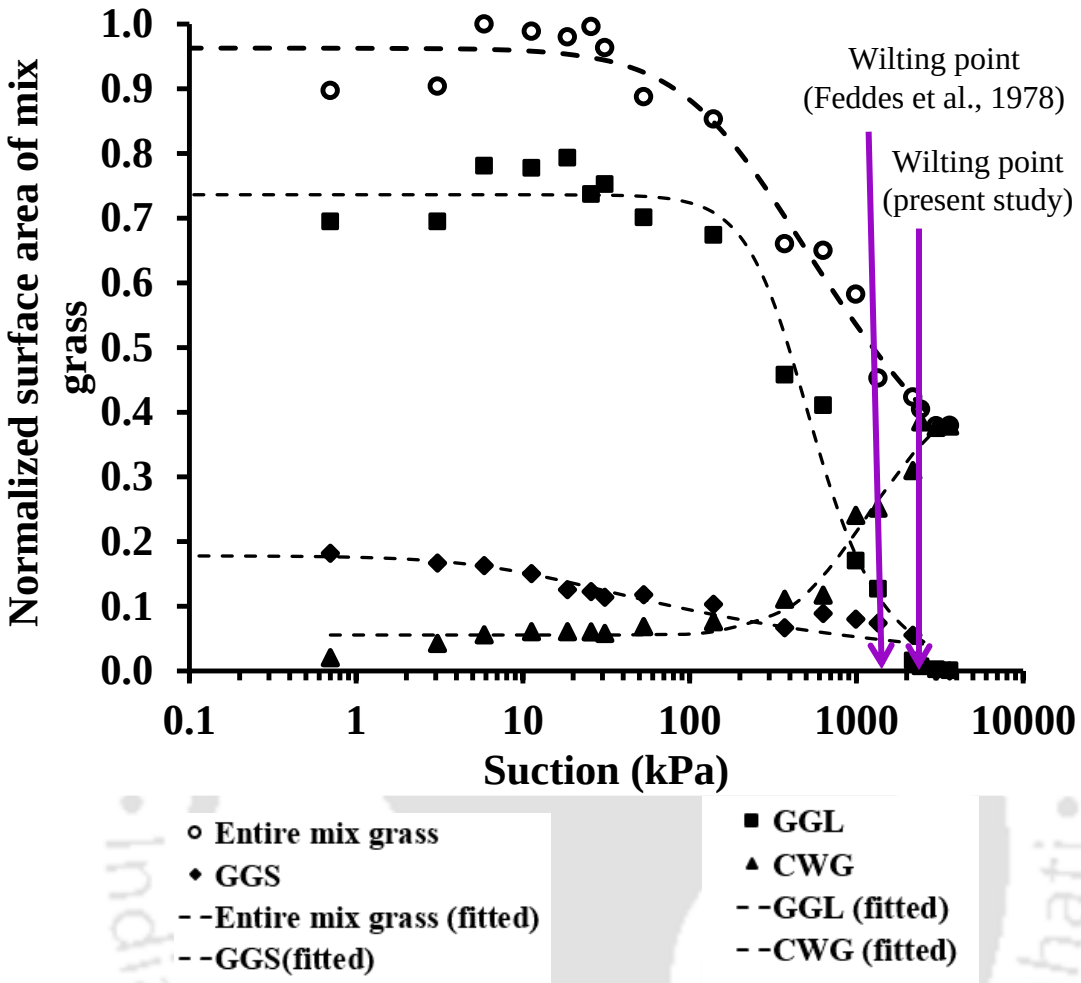

Fig. 7.5 Effect of suction on normalized surface area of entire mix grass cover, GGL, GGS and CWG

7.3.3.2 Establishment of correlation between normalized surface area of mix grass and suction

Visual assessment advises that the trend of variation of normalized surface area of grass-suction relation also emulates water retention curve (see Fig. 7.3 and Fig. 7.5). A new equation is proposed to describe the normalized surface area of grass-suction relation:

$$\text{ns}(\Psi) = ns_{min} + \frac{ns_{max} - ns_{min}}{[1+(a(\Psi))^n]^{1-\frac{1}{n}}} \quad (7.2)$$

ns (Ψ) = normalized surface area corresponding to suction (m^2/m^2)

ns_{max}= maximum normalized surface area (m^2/m^2)

ns_{min}= minimum normalized surface area (m^2/m^2)

a is related to the suction corresponding to maximum normalized surface area ($a > 0$)

n = fitting coefficient associated with the curvature (n>1)

All the fitting parameters are tabulated in Table 7.2. The curves fitted can be referred as SACC. It must be noted that small increase in surface area up to 18 kPa was not considered by the fitted curve. It is known that drought response of evergreen or deciduous vegetation may be dissimilar to that of the species tested in preset study (Ackerly, 2004; Hallik et al., 2009; Bartlett et al., 2012). In addition, change in colour of evergreen or deciduous vegetation would be dissimilar to that of species monitored in the current study (Damesin and Rambil, 1995; Rambal, 1993; Werner et al., 1999). Therefore, SACC varies for various evergreen or deciduous species. Previous studies (Quan and Liang, 2017; Beckett et al., 2017; Herbel et al., 1972) show that soil texture affects the stomatal conductance and surface area. Hence, soil type may also influence the SCCC and SACC.

Table 7.2 A summary of fitting coefficients for correlating normalized surface area of mix grass and suction using a novel approach

	SACC					
	Upper limit (pixels/pixels)	Lower limit (pixels/pixels)	α [kPa^{-1}]	n [-]	m [-]	R^2 (%)
Entire mix grass	1	0.38	0.006	1.83	0.453	95
GGL	0.74	0.05	0.005	2.70	0.63	98
GGS	0.17	0.04	0.113	1.26	0.21	87
CWG	0.39	0.05	0.001	-1.41	1.71	94

7.4. Summary and Conclusions

This study aimed to investigate the variation of suction, stomatal conductance and surface area when mix grass is subjected to drought stress. Stomatal conductance increases with raise in suction from 1 kPa to 6±1 kPa (i.e., around the suction corresponding to volumetric field capacity). This increase was attributed to oxygen raise in pores of soil root composite. Stomatal conductance decreases by 90 % due to increase in suction from 6 kPa to 1340 kPa. This was due to partial closure of stomata. Stomatal conductance variation is relatively less (around 21 %) with increase in suction between 1340-2431 kPa. This was attributed to complete closure of major number of stomata exist in leaf. Stomatal conductance becomes 0 at 2431 kPa (i.e., wilting point) due to damage of stomata system. Stomatal conductance of GGL is 2 % - 64 % higher than that of GGS at suction below 2431 kPa. This may be due to partial closure of stomata under ow light.

Change in normalized surface area of entire mix grass, GGL, GGS and CWG was relative low (within ±15 %) with increase in suction up to 138 kPa. Normalized surface areas of entire mix grass and GGL decrease drastically (by 47 % and 66 %) with increase in suction from 138 kPa to 2431 kPa. Normalized area of CWG increases significantly (by 31 %) with increase in suction from 138 kPa to 2431 kPa. Normalized surface areas of entire mix grass and GGL decrease by only 2 % with rise in suction from 2431 kPa to 3642 kPa. Whereas, normalized surface area of CWG remains reasonably constant between 2431 kPa and 3642 kPa. Decrement in normalized surface area of GGS was relatively low (i.e., 18 %) before it reaches to 0 at 3013 kPa. Two novel relationships i.e., SCCC and SACC were developed to estimate the evapotranspiration and numerical analysis of suction induced in green infrastructure accurately.

CHAPTER 8 ASSESMENT OF SOIL SURFACE WATER CONTENT USING LIGHT REFLECTION THEORY

8.1 General

A novel colour analysis technique was demonstrated to assess soil water content under spatially non-uniform light condition. Six series of tests were conducted to analyze the colour of red soil at various surface water contents. In addition, six measured dry densities on the compaction curve were selected to validate the proposed colour analysis technique. Soil was compacted to the desired state of compaction in a small mould. Images of soil samples were captured using a commercially available camera model (NIKON COOLPIX L29). The brightness variation of soil samples was quantified using the change in mean gray value of the images.

8.2 Materials and Methods

8.2.1 Soil properties

The engineering properties of the selected soil is discussed in section 3.2.1. Measured compaction curve for red soil is shown in Fig. 8.1. Fig. 8.2 shows the typical SWRC of red soil selected for the present study. The curve encapsulates three distinct zones: zone of saturation, zone of desaturation and residual zone. These zones consist of three types of soil-air-water interfaces (shown in Fig. 8.2; Fredlund and Xing, 1994). Zone of saturation represents the absence of air in the voids of soil matrix. Due to the absence of air, continuous water phase can be observed in the voids of soil matrix (see A; Fig. 8.2). Suction corresponding to the gravimetric water content at which, air enters is termed as air entry value. Air entry value is the starting point of desaturation (see B; Fig. 8.2).

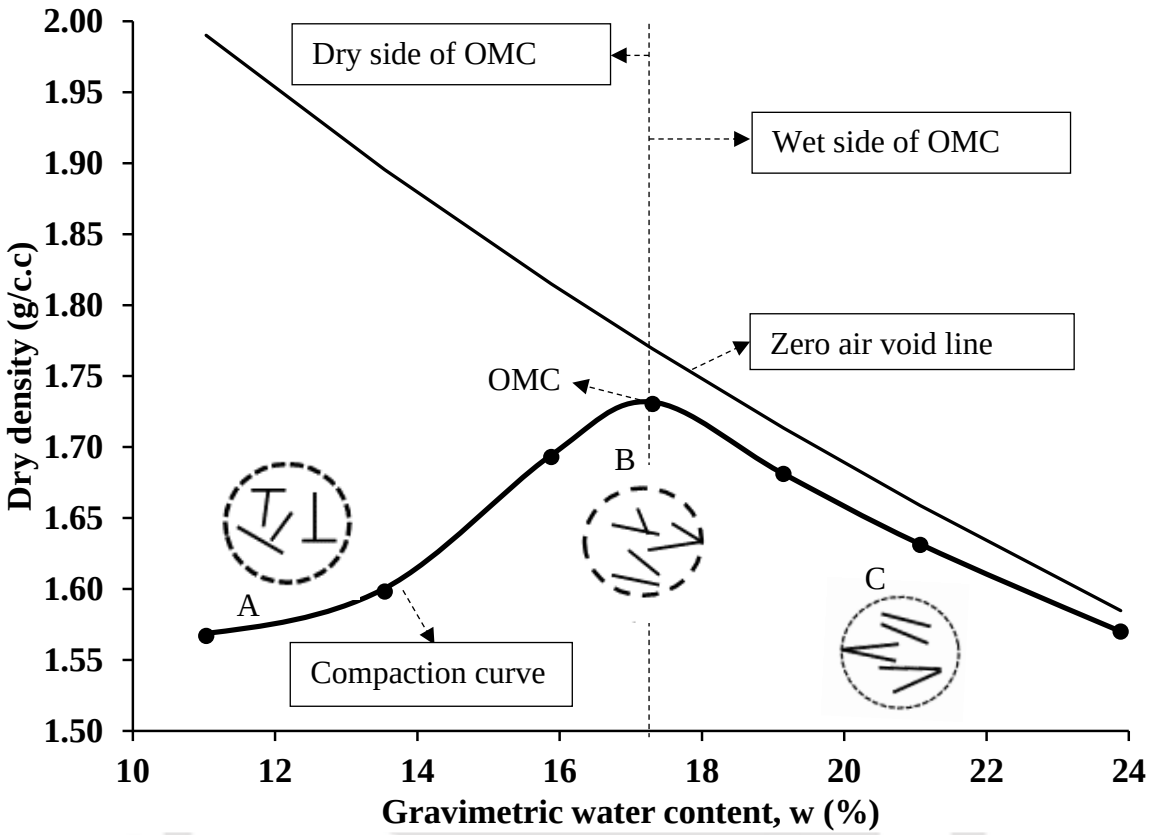

A- Flocculated structure (allows quick drainage; Lambe and Whitman, 2008)

B- Transition from flocculated to dispersed structure (allows relatively higher strength; Lambe and Whitman, 2008)

C- Dispersed structure (allows slow drainage; Lambe and Whitman, 2008)

* Points on the curve indicates the measured dry density and their corresponding water contents. Selected dry densities are 1.57g/c.c, 1.60 g/c.c, 1.69 g/c.c, 1.73 g/c.c, 1.68 g/c.c and 1.63 g/c.c

* Change in water content may alter brightness, which can be identified on a gray scale

Fig. 8.1 Measured compaction curve of red soil using standard proctor compaction test

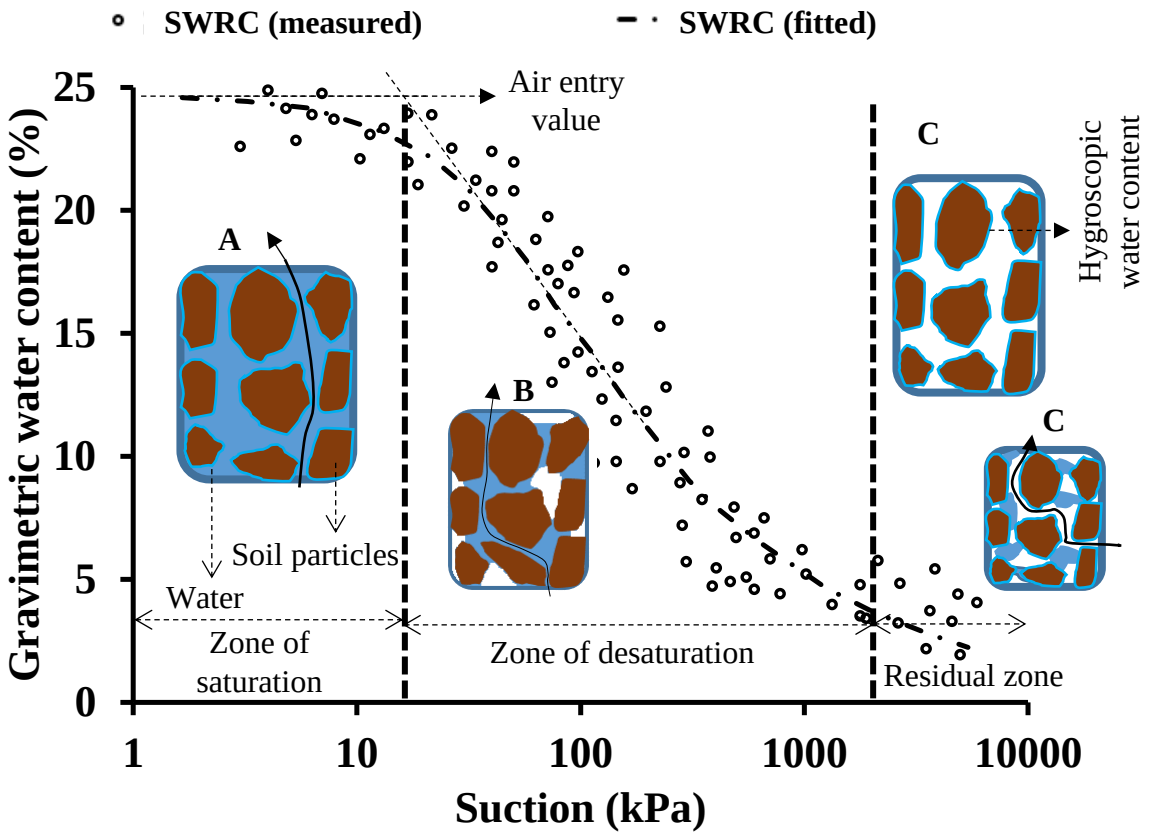

A, B and C shows the three types of soil-air-water interface, which occur at different points on SWRC (Lambe and Whitman, 2008)

A - Continuous water phase

B - Discontinuous water phase

C - Continuous air phase

- Water film (of thickness around 2 x 10^{-5} mm) adhered to the soil particle (hygroscopic water content), which can be removed only by oven drying (Leung et al., 2015)

Fig. 8.2 Soil water retention curve of red soil (SWRC)

Unlike the zone of saturation, discontinuous phases of air and water occurs in the zone of desaturation. Residual zone represents the water content and suction values at which, the rate of

desaturation is very low. Generally, two types of continuous air phase occur within this zone (see C; Fig. 8.2). The first type occurs when the water present in the voids of soil matrix is very low. Another type occurs, when the water in the voids is absent and only hygroscopic water is present around the surface of the soil (Barbu et al., 2004). Hygroscopic water refers to the water which is freely adsorbed from atmosphere that adheres to the surface of a soil particle. It can be removed only by oven drying (Barbu et al., 2004). Hygroscopic water content of the selected soil is observed to be 3 % - 5 %.

8.2.2 Test plan

In this study, six series of tests were conducted at degree of saturation (DOS) of 15 %, 30 %, 45 %, 60 %, 75 % and 90 % to demonstrate the colour analysis method. These tests are intended to differentiate the surface water contents in three zones of SWRC (see Fig. 8.2) on the basis of brightness variation. In addition, soil compacted at six dry densities was tested at selected DOS to validate the demonstrated colour analysis method. Measured dry densities on compaction curve were adopted for validation. This validation accounts the three different structures that exist in compacted soil (see Fig. 8.1). Flocculated structure of soil particles usually allows the quick drainage of water through soil pores in the subgrades (Lambe and Whitman, 2008). Dispersed structure allows less drainage. Dispersed structure of soil particles is usually preferred on land fill liners so as to minimize infiltration of water from rainfall (Lambe and Whitman, 2008). The soil on bare and vegetated slopes is compacted at maximum dry density for acquiring greater strength (Leung et al., 2015b). Furthermore, density of soil in agricultural fields and urban areas vary widely (Lambe and Whitman, 2008).

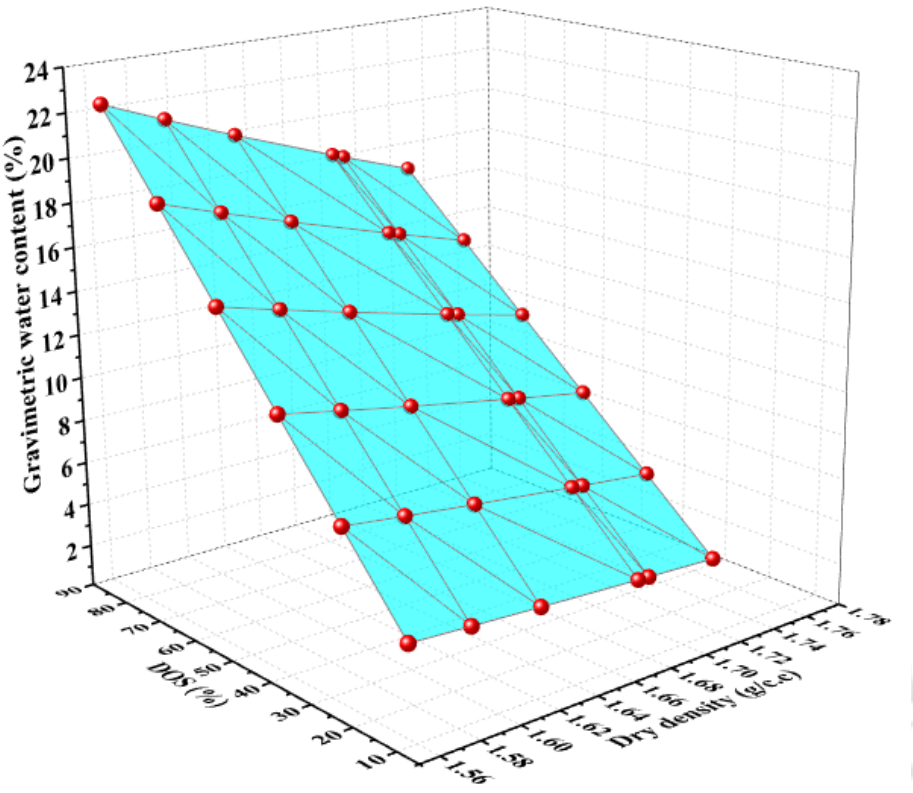

Fig. 8.3 Variation in gravimetric water content with change in degree of saturation (DOS) for soil compacted at various dry densities

The calculated gravimetric water contents are presented at various dry densities and DOS in Fig. 8.3. DOS at measured dry densities (highlighted in Fig. 8.1) in the compaction curve are observed to be 45 %, 60 %, 80 %, 91 %, 94 %, 95 % and 98 % respectively. Lowest gravimetric water content of 3% can be observed corresponding to 1.73 g/c.c dry density and 15 % DOS. Whereas, highest gravimetric water content of 22 % can be seen corresponding to 1.57 g/c.c dry density and 90 % DOS.

8.2.3 Design and development of experimental setup

Schematic representation of the experimental setup is presented in Fig. 8.4. In order to capture images from the top, a commercially available camera model (NIKON COOLPIX L29) was attached to the top of a holding stand. Resolution of camera is 16.1 effective megapixels. Moist soil was compacted to the desired dry density using a rammer in a mould of 92 mm diameter and 15 mm depth. Thereafter, compacted soil sample was placed parallel to the camera at a distance of 1.2 m on plane table. This distance is sufficient enough to adopt in the field for capturing images as well. In addition, same distance and angle were maintained between camera and soil sample for all samples to avoid observational errors. It is evident that light intensity varies over a wide range (i.e., 0-60000lux; Baker and Steemers, 2014). The images were captured under ambient light. The average light intensity was found to be 167 lux during test period. The light intensity was measured using a commercially available light measurement instrument (Metravi 1331 Digital Lux Meter). A white paper was placed below the mould containing soil sample to account the colour contrast within the soil sample. Equalization of colour contrast with respect to a reference (i.e., white paper) avoids the errors that occur due to light intensity variation. In addition, it helps to adopt the proposed colour analysis technique for various engineering applications.

8.2.4 Colour analysis procedure

8.2.4.1 Gray scale image

Gray scale image is an image, which illustrates only brightness of the reflected light. Gray scale images are black and white images. However, these are dissimilar to binary images. In a binary image, only two colour values exist i.e., black and white. Whereas, a gray scale image shows many

shades of gray in between black and white (see Fig. 8.4). Gray value is determined using red (R), green (G) and blue (B) values from RGB (red green blue) colour space (Russ and Russ, 2007). Red, green and blue are added in the RGB colour space to produce various colours. Gray value of a pixel in a digitized image with a coordinate (R, G, B) in the colour space can be found using eqs 8.1 and 8.2, which are shown in Fig. 8.4. Pure green is perceived as the brightest of three colours i.e., red, green and blue, by the human eye. Pure blue is darker than pure green and pure red. Hence, green (G) receives highest weight and blue (B) receives least weight when colours are not weighted equally. Colours are not weighted equally in present study for taking brightness difference among the colours into account. In this gray scale, black has a value of 0 and white has a value of 255, which can be seen Fig. 8.4. The other gray values fall between 0 and 255 (Ferreira and Rasband, 2012; Pérez and Pascau, 2013).

8.2.4.2 Quantification of Gray value

ImageJ is a java based program, which quantifies the average gray value (mean gray value) of the selected pixels of a digital image (Pérez and Pascau, 2013). The pictorial view of procedure for quantification of mean gray value can be seen in Fig. 8.4. The image was imported into ImageJ and cropped to take the required portion of image into account. The desired portion is selected on the soil surface using "rectangular selection" option. Mean gray value of all pixels in each selected area was quantified using "histogram" option (see the cropped ImageJ window in Fig. 8.4). This option first separates the selected portion of the image into individual pixels. Thereafter, gray value of each pixel would be quantified using eq 8.1 and displayed as a histogram. In the histogram, horizontal axis shows the possible discrete gray values and vertical axis represents the normalized

number of pixels observed for each gray value. Mean gray value was quantified by dividing the weighted sum of number of pixels in each gray value by total number of pixels. It can be seen from gray scale that higher the brightness, more the mean gray value obtained (see Fig. 8.4).

The presence of non-uniform light intensity within the soil domain can be observed from the locations pointed with L1, L1, L2, L3, L4, L5, L6, L7 and L8 on white paper. Hence, effect of light intensity variation needs to be quantified first in the terms of gray value. Mean gray value at locations L1, L1, L2, L3, L4, L5, L6, L7 and L8 are found to be 215, 224, 231, 230, 229, 215, 216 and 218, respectively. The difference between mean gray values at various locations (i.e., L1 to L8) is referred to as colour contrast. It must be noted that colour contrast should be avoided to understand the change in mean gray value (i.e., brightness) solely due to variation in surface water content. The equalization method has been adopted to avoid effect of colour contrast within the soil sample due to spatial heterogeneity of light intensity. The soil sample is categorized into eight sectors (see S1 to S8 in Fig. 8.4) on the basis of colour contrast observed at various locations (L1-L8) on white paper. It should be noted that the colour of the paper is white. Mean gray value of pure white paper would be 255 (This has been discussed in "gray scale image" subsection using Fig. 8.4). The mean gray values of soil in eight sectors were equalized using the pure white paper (i.e., mean gray value of 255) as reference. The relation used to calculate the equalized mean gray value for a portion selected in S1 has been shown below

$$Equalized\ mean\ gray\ value\ of\ selected\ portion\ in\ S1 = mean\ gray\ value\ of\ selected\ portion\ in\ S1 + (mean\ gray\ value\ of\ pure\ white\ paper - mean\ gray\ value\ at\ L1) \quad (8.3)$$

In order to minimize random errors, three different portions of equal pixel area were selected within each sector for quantification of equalized mean gray values. Average of the equalized mean

gray values of these three portions was reported as the sector's mean gray value. Mean gray values of the eight sectors were in turn averaged and considered as the mean gray value of entire sample.

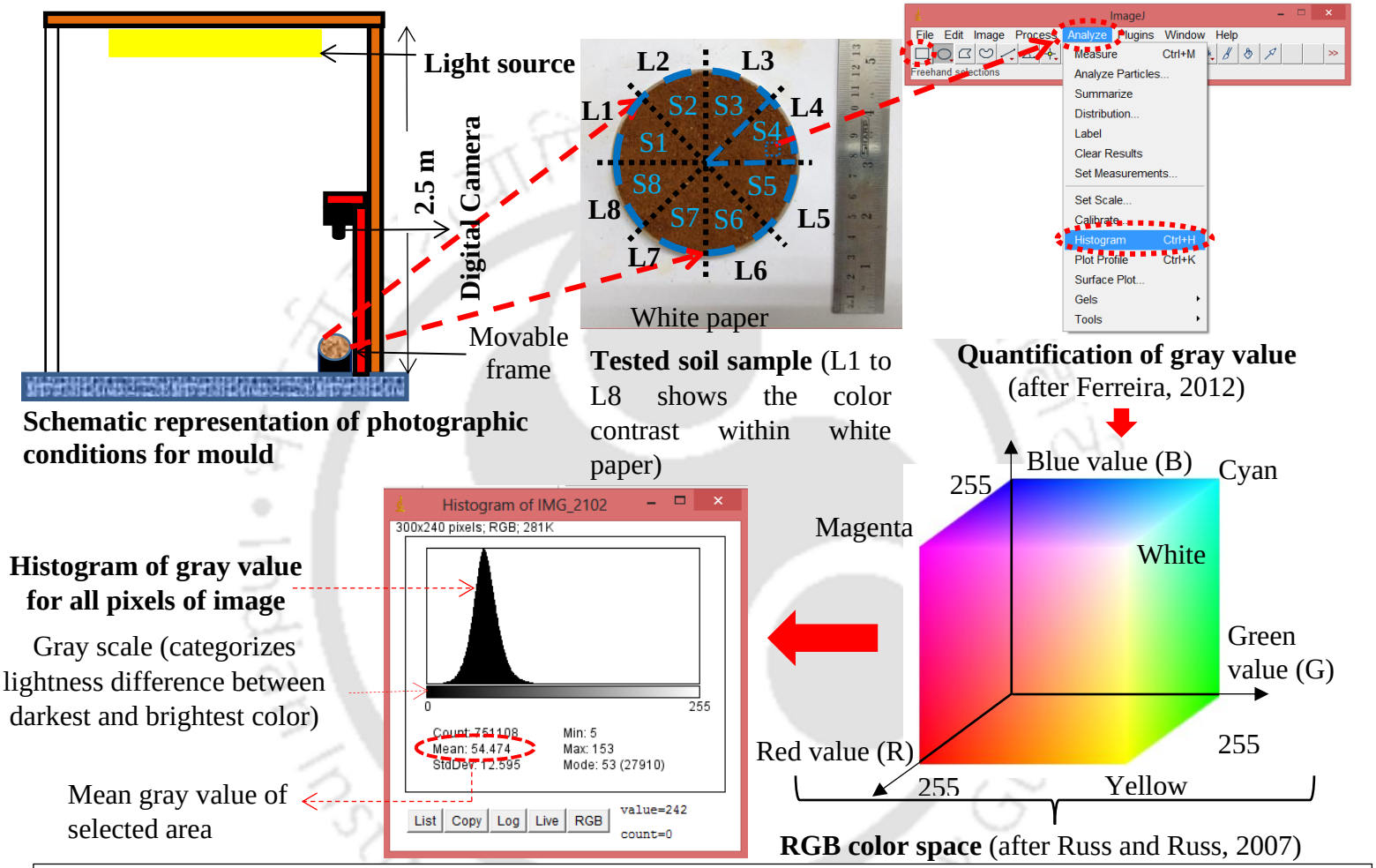

* RGB color space produces various identifiable colors by adding red, green and blue colors

Gray value (when colors are not weighted equally) = 0.299 x R + 0.587 x G + 0.114 x B (8.1)

Gray value (when colors are weighted equally) = $\frac{R+G+B}{3}$ (8.2)

Fig. 8.4 Determination of mean gray value for moist soil using colour analysis technique

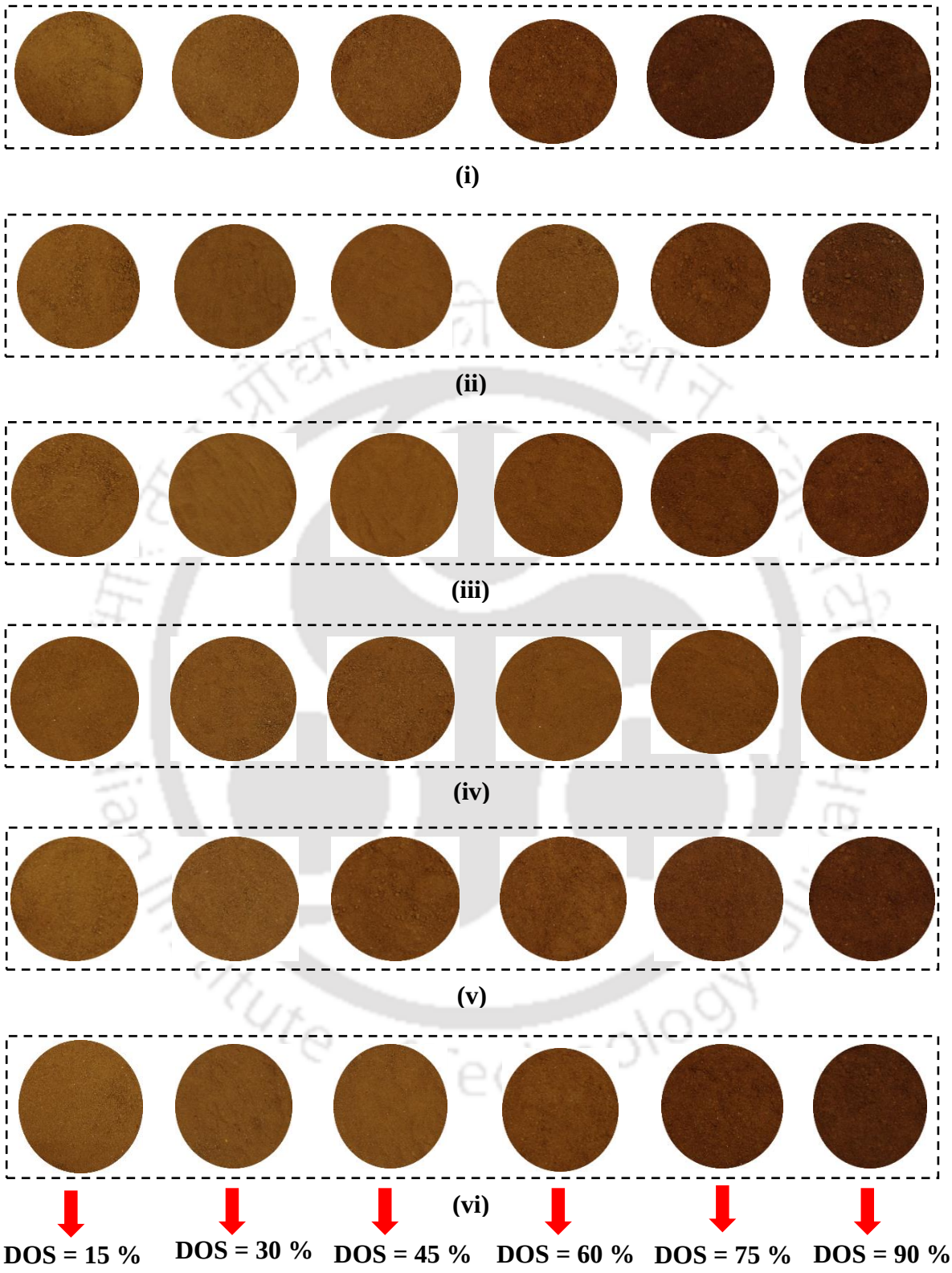

Fig. 8.5 Pictorial view of samples tested to obtain gray values for various surface water contents

8.3 Results and Discussions

8.3.1 Comparison of gray values obtained at the selected surface water contents

Soil samples tested at various dry densities are shown in Fig. 8.5. Brightness difference can be seen with the change in gravimetric water content and dry density. Brightness of all samples was quantified in terms of mean gray value of the image. Mean gray value variation with respect to change in gravimetric water content of red soil compacted at six selected dry densities has been presented in Fig. 8.6. Mean gray values are observed to vary between 27 and 87. Average mean gray value for oven dried red soil is found to be 95, which is marked in Fig. 8.6. Mean gray value is found to decrease with increase in gravimetric water content. Such decrease in mean gray value can be attributed to decrease in brightness with increase in gravimetric water content of the sample. Gravimetric water content increase causes higher refraction and total internal reflection (see Fig. 2.2b). A trend line was fitted using polynomial (Eq. 8.4) for mean gray value variation with DOS. R^2 value of Eq. 8.6 is observed to be 97 %.

Maximum mean gray values (corresponding to the water content of 3 - 4 %) are found to be 117 % to 160 % higher than those of minimum mean gray values (corresponding to the water content of 17 - 22 %). Difference between maximum and minimum mean gray values for the soils compacted at similar DOS is observed to vary between 13 % and 44 %. Lowest mean gray value is found for soil compacted to 1.57 g/c.c. Apart from the lowest mean gray value, any other trend of variation is not found between dry density and mean gray value of soils compacted at same DOS (see Fig. 8.6). One reason for this may be, difference between the considered dry densities is very less.

In saturation and desaturation zone, mean gray value is observed to decrease by 14 % - 27 % with 3 - 4 % increase in gravimetric water content. Whereas, only 3 % - 9 % decrease in mean gray value is found with such increase in gravimetric water content within the residual zone. This low decrease can be explained using soil-air-water interface. It can be observed that (Fig. 8.2), the water content in residual zone is near to hygroscopic water content. Hygroscopic water content indicates the absence of water in voids of soil matrix and presence of water film of thickness near to 2×10^{-5} mm around the soil particles (Punmia and Jain, 2005). Hence, variation in mean gray value would be mainly due to change in thickness of the film around the soil particles. Whereas, main reason for such difference in saturation zone is the change in volume of water within the voids.

Previous studies (Min and Huy, 2008; Yoshimoto et al., 2011) also showed the trend of variation observed in Fig. 8.6. Variation in the mean gray value of soil corresponding to change in water content of silt and sand was studied by Yoshimoto et al. 2011 under controlled light conditions. In their study, mean gray value of the silt and sand was found to vary between 98 and 155. Unlike present study, R, G and B values were weighted equally by Yoshimoto et al. 2011 to obtain gray value. Yoshimoto et al. 2011 shows that gray value of soil increases by 46 – 53 % due to 60 % decrease in DOS. However, gray value at DOS beyond 60 % was not measured in their study. Min and Huy, 2008 used colour number (Cn) to quantify the brightness variation due to change in water content of sand. Colour number of various shades of gray lies between 0 and 255. Typically, the two ends are white (255) and pure black (0), respectively. Min and Huy, 2008 found that the difference between colour numbers of fully saturated and dry sand would be around 37 % under controlled light conditions. However, any replicates were not considered by Min and Huy, 2008 to measure colour number for the tested samples. It can be observed from results of the

present study and Yoshimoto et al. 2011 that soil type affects the gray value. Hence, correlations obtained in the current study are applicable to the selected red soil. As the main focus of the present study is to demonstrate and validate the novel colour analysis approach, only one type of soil was considered.

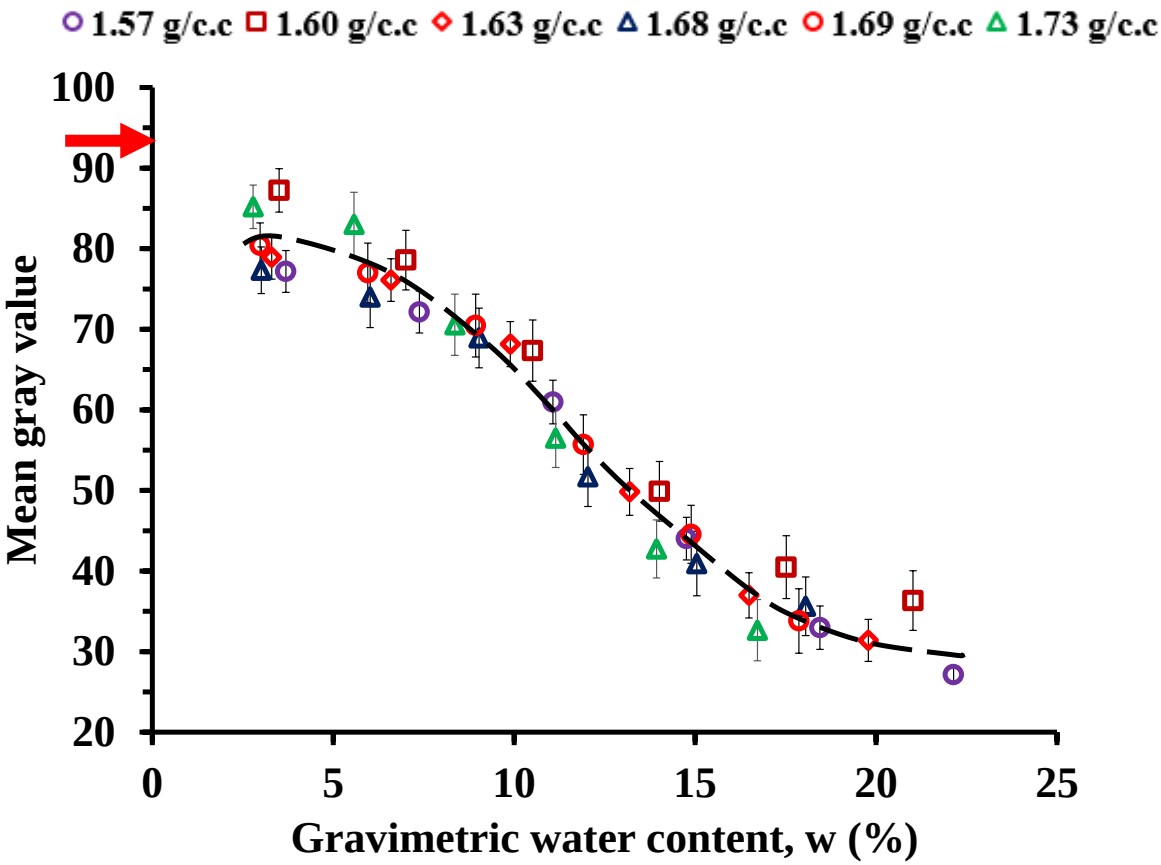

$$Mean\ gray\ value = -0.0007w^4 + 0.0546w^3 - 1.2855w^2 + 7.7548w + 67.686 \quad (8.4)$$

$$R^2 = 97\%$$

- Average mean gray value of oven dried soil

Fig. 8.6 Comparison of obtained gray values at various soil surface water contents

8.4 Summary and Conclusions

A novel colour analysis technique was demonstrated and validated to differentiate the surface water content of compacted soil. This is different from previous methods, all of which are only valid under the controlled light conditions. The proposed technique has the potential to be applied for uncontrolled light conditions and large areas. An experimental setup was designed and developed to establish the correlation between surface water content and mean gray value (from colour analysis) for the compacted soil. Mean gray value decreases with the increase of gravimetric water content for the soil considered in this study. Mean gray value decreases by 14 % to 27 % with every 3 - 4 % increase in gravimetric water content within the saturation and desaturation zones. A decrease of 3 % and 9 % in mean gray value occurs with such rise in the residual zone. Based on the results, an empirical model was developed for establishing soil surface water content as a function of mean gray value. The colour analysis technique and the obtained relation can be programmed with the UAV to quantify the surface water content. Such programming helps to monitor surface water content of large as well as densely urbanized areas at a low cost.

CHAPTER 9 SPATIAL AND TEMPORAL HETEROGENEITY OF SURFACE HYDRAULIC CONDUCTIVITY IN A GREEN SPACE

9.1 General

In this chapter, the spatial and temporal heterogeneity of hydraulic conductivity in an urban space vegetated with deciduous species is presented. Field monitoring was conducted in the green space for one year. The monitoring period is intended to understand the spatial variation of hydraulic conductivity during the vegetation growth period and gradual wilting period. The green space was categorized into 170 grids to monitor vegetation density and surface hydraulic conductivity. Changes in hydraulic conductivity were interpreted with spatial and temporal heterogeneity of vegetation density.

9.2 Materials and Methods

9.2.1 Site description

Fig. 6.1 shows the location of the selected green space. The green space consists mix grass i.e., Poacea and Bauhinia purpurea. In addition, Pongamia pinnata trees exist in the selected site. Field monitoring was conducted in the green space (at IIT Guwahati). The field monitoring program is devised to understand the spatial heterogeneity of mix vegetation density and surface hydraulic conductivity.

9.2.2 Soil properties

The engineering properties of the soil in the selected site is discussed in section 6.2.2.

9.2.3 Overview of the green space

Bauhinia purpurea is widely recognized as anti-inflammatory, thyroid hormone regulating and antidiabetic agent (Zakaria et al., 2007). In addition, Cyperus, Poacea, Bauhinia purpurea and Pongamia pinnata were considered on the basis of their (i) water stress tolerance ability (Cheplick, 2004; Cai et al., 2007), (ii) landscaping values (Bouldin et al., 2004; Arifin and Nakagoshi, 2011) and (iii) wide spread occurrence in semi-arid regions (Leishman and Westoby, 1994). The green space is categorized into five concentric half circles to quantify the spatial variation of grass growth. Spatial heterogeneity in vegetation growth and shredded leaves can be observed in Fig. 9.1. Radii of these half circles are 1 m, 2 m, 3 m, 4 m and 5 m, respectively. These radii is selected based on visual observation. The depth of ground water table was found to be around 6 m (WRIS; http://www.india-wris.nrsc.gov.in/wris.html).

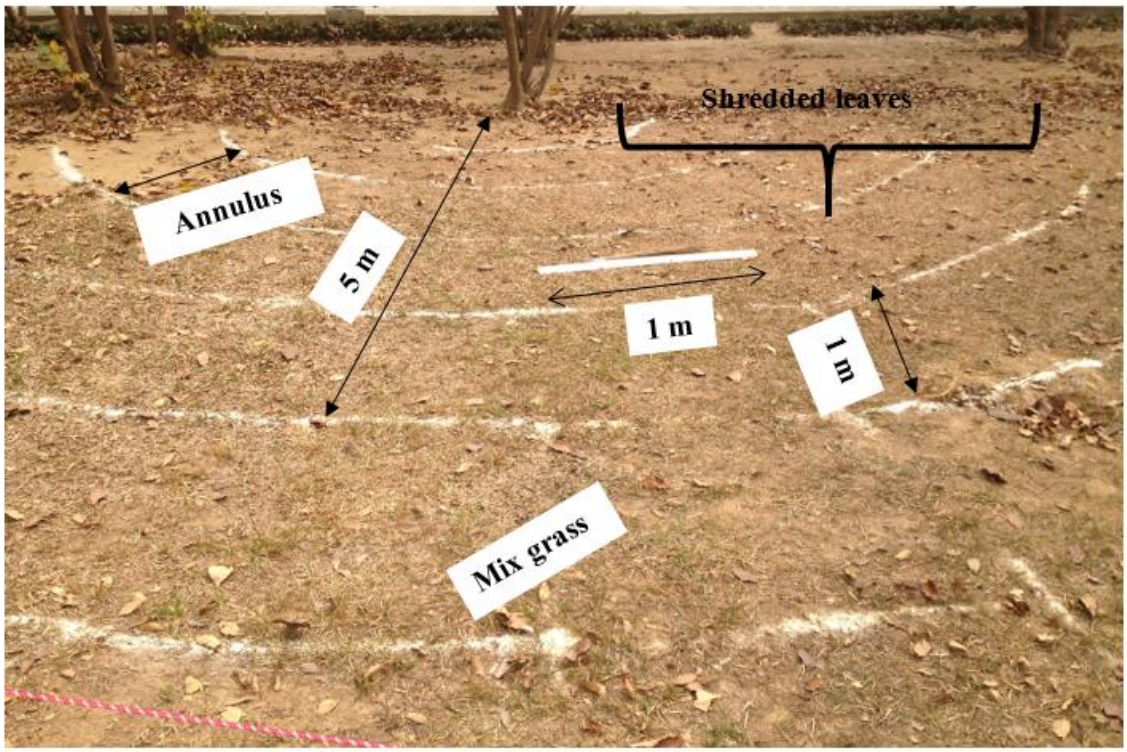

Fig. 9.1. Overview of the green space selected for testing

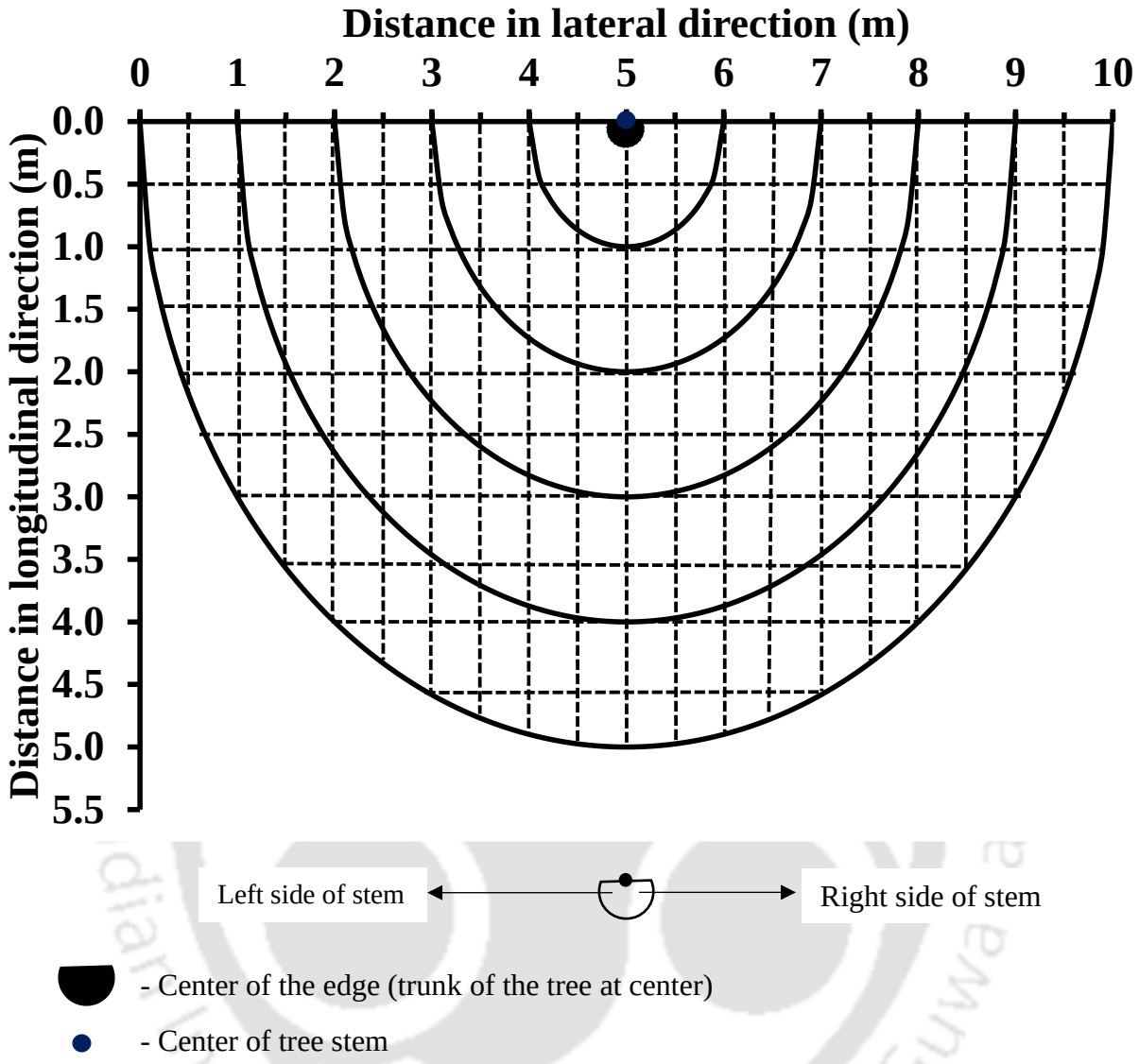

Fig. 9.2. Categorization of green space into small grids for monitoring spatial heterogeneity of vegetation cover and surface hydraulic conductivity

9.2.4 Instrumentation used in the green space

Fig. 9.2 portrays the typical layout of 170 grids, where mix vegetation density and surface hydraulic conductivity were quantified. The grid size was selected based on trial measurements of vegetation density and hydraulic conductivity. Maximum area of the grid is 0.25 m^2.

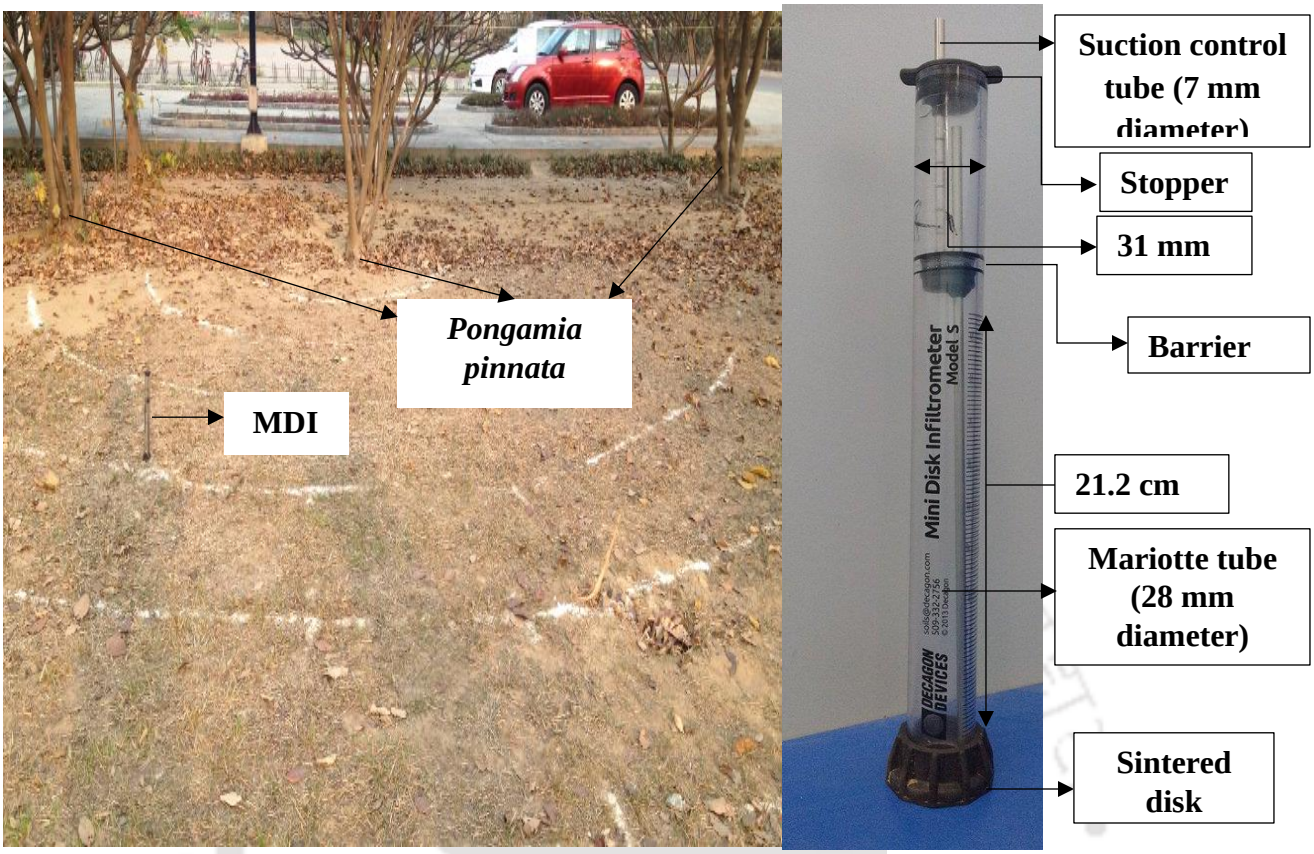

(a) (b)

Fig. 9.3. (a) Measurement of surface hydraulic conductivity in the green space; and (b) Overview of mini disk infiltrometer (MDI; after Bordoloi et al., 2017)

The images of mix grass have been captured in ambient light using commercially available unmanned air vehicle (UAV; DJI Phantom). Resolution of the camera attached to the UAV is 12 megapixels. Maximum service sealing level of UAV is 6 km above the sea level. The height of the existing tree canopies in the site is around 2.4 m. Hence, relatively low elevation of UAV was maintained to capture images. Hydraulic conductivity was measured using mini disk infiltrometer (MDI; METER Group, USA). Fig. 9.3 shows the surface hydraulic conductivity measurement in the green space. MDI consists upper and lower chambers. Suction is regulated in the top chamber. Water infiltrates into the soil through the sintered disk in the lower chamber. Flow throw

macrospores such as desiccation cracks is eliminated by the suction controlled flow. Suction in the upper chamber can be controlled between 0.5 cm and 6 cm, based the texture and void ration of soil (Zhang, 1997).

9.2.5 Field monitoring programme

The field monitoring programme was devised to understand the spatial and temporal variation of vegetation density and hydraulic conductivity in green space. Field was monitored from 2nd January 2016 to 31st Dec 2016. It is known that vegetation density and hydraulic conductivity vary spatially. Hence, these were monitored at 170 grids (see Fig. 9.2). Weather parameters such as relative humidity, rainfall depth, net radiation and air temperature were monitored using micro-climate monitoring system (MCMS, METER Group, USA). Variation in monthly rainfall depths during the monitoring period are shown in Fig. 9.4. It can be seen that rainfall depth varies from as high as 275 mm during month of April to 5 mm during month of February. Relatively low rainfall depth was found during January, February, March, August, October and December. Therefore, this duration was referred as dry period. The remaining six months duration was termed as wet period.

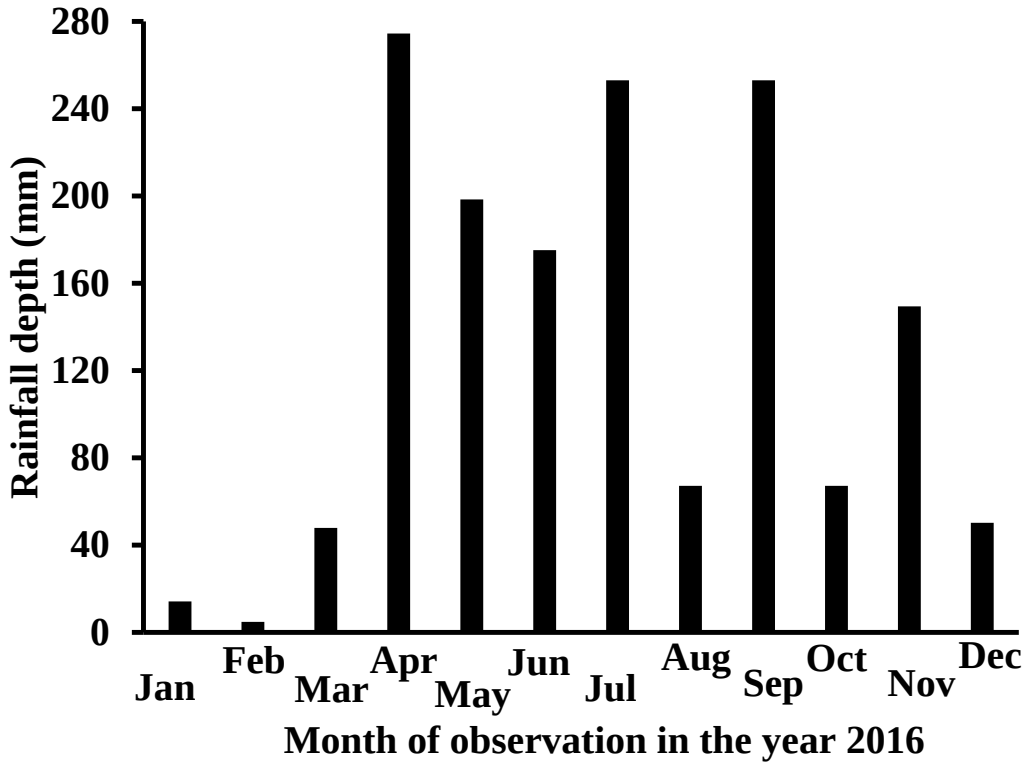

Fig. 9.4. Variation in monthly rainfall depth during monitoring period

9.2.6 Design of non-destructive image analysis approach to quantify the vegetation density in the green space

9.2.6.1 Camera settings for capturing photographs of grass in green space

Procedure of image analysis is shown in Fig. 3.3 and 4.2. Observational errors were eliminated by capturing images in ambient light. In addition, constant ISO speed, exposure time and focal length were maintained during image capturing. This helps to maintain the same pixel area for all the images. Same pixel area is needed to compare the image analysis results accurately. ISO speed, exposure time and focal length were maintained at ISO-640, 1/8000 sec and 35 mm, respectively.

9.2.6.2 Image analysis using ImageJ

Step by step procedure to quantify the vegetation density using ImageJ was shown in Fig. 4.2. Image is imported into ImageJ. The desired grid size is cropped from the imported image. Thereafter, grass and soil are differentiated using adjustable colour scales of R, G and B. Area of the grid and grass cover in the grid are quantified using "measure" option. The procedure shown in Fig. 4.2 was repeated to quantify vegetation density in 170 grids.

9.2.6.3 Surface hydraulic conductivity measurement in the green space

Good contact between sintered disk and ground was maintained to ensure axi-symmetric flow. Generally, Air bubbles accumulate in the sintered disk during measurement. These bubbles were removed by boiling the sintered disk repeatedly. Hydraulic conductivity was measured at the desired locations in three successive days at the end of every month. Water is allowed to infiltrate through sintered disk at a preset suction. Suction value was adopted according to guidelines of Zhang (1997). Cumulative depth of infiltrated water was plotted with respect to time. Infiltration rate was calculated using Eq. 9.1

$$I = at + b\sqrt{t} \tag{9.1}$$

where:

a, b = coefficients used for fitting

t = time

The near saturated hydraulic conductivity (i.e., surface hydraulic conductivity) is approximated from Eq. 9.2

$$k = \frac{a}{A} \tag{9.2}$$

Where:

"A" = Parameter deduced from Van Genuchten (VG) parameters of SWRC, suction and radius of the sintered disk

$$A = \frac{11.65\left(n^{0.1}-1\right)\exp\left[2.92(n-1.9)\alpha h\right]}{(\alpha r)^{0.91}}; \quad \text{For n > 1.9} \tag{9.3}$$

$$A = \frac{11.65\left(n^{0.1}-1\right)\exp\left[7.5(n-1.9)\alpha h\right]}{(\alpha r)^{0.91}}; \quad \text{For n < 1.9} \tag{9.4}$$

where:

n and α = the VG parameters of soil vegetated with grass,

r = the disk radius,

h = applied suction

The parameters of water retention curve (i.e., α and n) of bare soil were adopted from Carsel and Parrish (1988). It should be noted that SWRC parameters of the bare soil and vegetated soil may be dissimilar. The main focus of the current study is to understand the effect of spatial and temporal heterogeneity of vegetation density on surface hydraulic conductivity. Therefore, SWRC parameters of bare soil suffice the need.

9.3 Results and discussions

9.3.1 Grass cover change during monitoring period

Fig. 9.5(a) – (l) show the changes in grass surface during monitoring period. It can be seen that surface area of grass is relatively low during January. Thereafter, gradual wilting of grass was found during February. In addition, shredded tree leaves were also observed in the site at the end of February. Regrowth of vegetation was observed during March. Relatively small surface area of green grass can be seen in the image captured at the end of March. Unlike previous months, dense grass cover can be seen at the end of April. Only Poacea growth was observed during first three months. Whereas, Bauhinia purpurea growth was also found during April. Simultaneous growth of Poacea and Bauhinia purpurea was observed to continue from May to October (see Fig. 9.5 e – j). Thereafter, gradual wilting of grass was found. Significant proportion of wilted vegetation can be seen in Fig. 9.5 k. Grass was found to wilt completely at the end of December (see Fig. 9.5 l).

(a)

(b)

(c)

(d)

(e)

(f)

(g)

(h)

(i)

(j)

(k)

(l)

Fig. 9.5. change in mix grass cover at end of each month during monitoring period, i.e., (a) 31st Jan' 2016; (b) 28th Feb' 2016; (c) 31st Mar' 2016; (d) 30th Apr' 2016; (e) 31st May' 2016; (f) 30th Jun' 2016; (g) 31st Jul' 2016; (h) 31st Aug' 2016; (i) 30th Sep' 2016; (j) 31st Oct' 2016; (k) 30th Nov' 2016; (l) 31st Dec' 2016

9.3.2 Variation of vegetation density in the site

Spatial and temporal heterogeneity of vegetation density in the green space is shown in Fig. 9.6 a, c, e, g, i, k, m, o, q, s, u and w. Contour plots have been used to demonstrate the spatial and temporal heterogeneity of vegetation density. The difference between maximum and minimum grass densities has been categorized into eight different ranges, which can be seen in the colour scale. Tree at the center of the edge has been marked as reference to discuss the variation in vegetation density and surface hydraulic conductivity.

Vegetation density is observed to change between 0.001 m^2/ m^2 and 1.000 m^2/ m^2 in first six months. Variation of vegetation density is observed to be less significant in grids near to the tree trunk as compared to those away from the tree trunk. This can be observed from the number of vegetation density ranges that exist in the contour. Spatial heterogeneity is relatively low during February due to presence of shredded leaves. Spatial variation of vegetation density shows the non-uniformity in mix grass growth during first six months. Vegetation density in annuli at higher distance from center was found to be greater. This trend is found during the absence of shredded leaves. Relatively less vegetation density near the tree stem may be attributed to the growth competition between tree roots and mix grass roots. Unlike other months, vegetation density in the annuli near to the center is relatively high as compared to that in other annuli at the end of February. This is due to existence of shredded leaves. Vegetation density is found to increase substantially (i.e., 17 % - 590 %) during April in all the grids. Any relation between vegetation density and rainfall depth was not found. Although trees exist at 3 m lateral distance from the center, vegetation density near to the tree trunks is observed to be relatively high during April, May and June. This is due to the growth of Pongamia pinnata plants during April, May and June. Unlike first six months, vegetation density is observed to be 1.000 in last six months.

9.3.3 Spatial heterogeneity of surface hydraulic conductivity

Fig. 9.6b, d, f, h, j, l, n, p, r, t, v and x show the spatial heterogeneity of surface hydraulic conductivity in the green space during monitoring period. The difference between maximum and minimum grass densities have been categorized into eight different ranges, which can be seen in the colour scale. Unlike the vegetation density, surface hydraulic conductivity is found to vary spatially during entire monitoring period. In addition, hydraulic conductivity on right side and left side of the center are found to be dissimilar during first three months at longitudinal distance beyond 2 m from the center. Thereafter, such considerable dissimilarity was not found at longitudinal distance beyond 2 m from the center in various annuli. Hydraulic conductivity is not found to vary with change in radial distance during first three months. Whereas, variation in hydraulic conductivity with change in radial distance from the center was found in next nine months. Hydraulic conductivity is found to be relatively low in first six months as compared to that during next months. These observations imply that hydraulic conductivity around the tree vicinity is not axi-symmetrical, which is commonly presumed in numerical modeling of flow through green space (Deb et al., 2013; Garg and Ng, 2015).

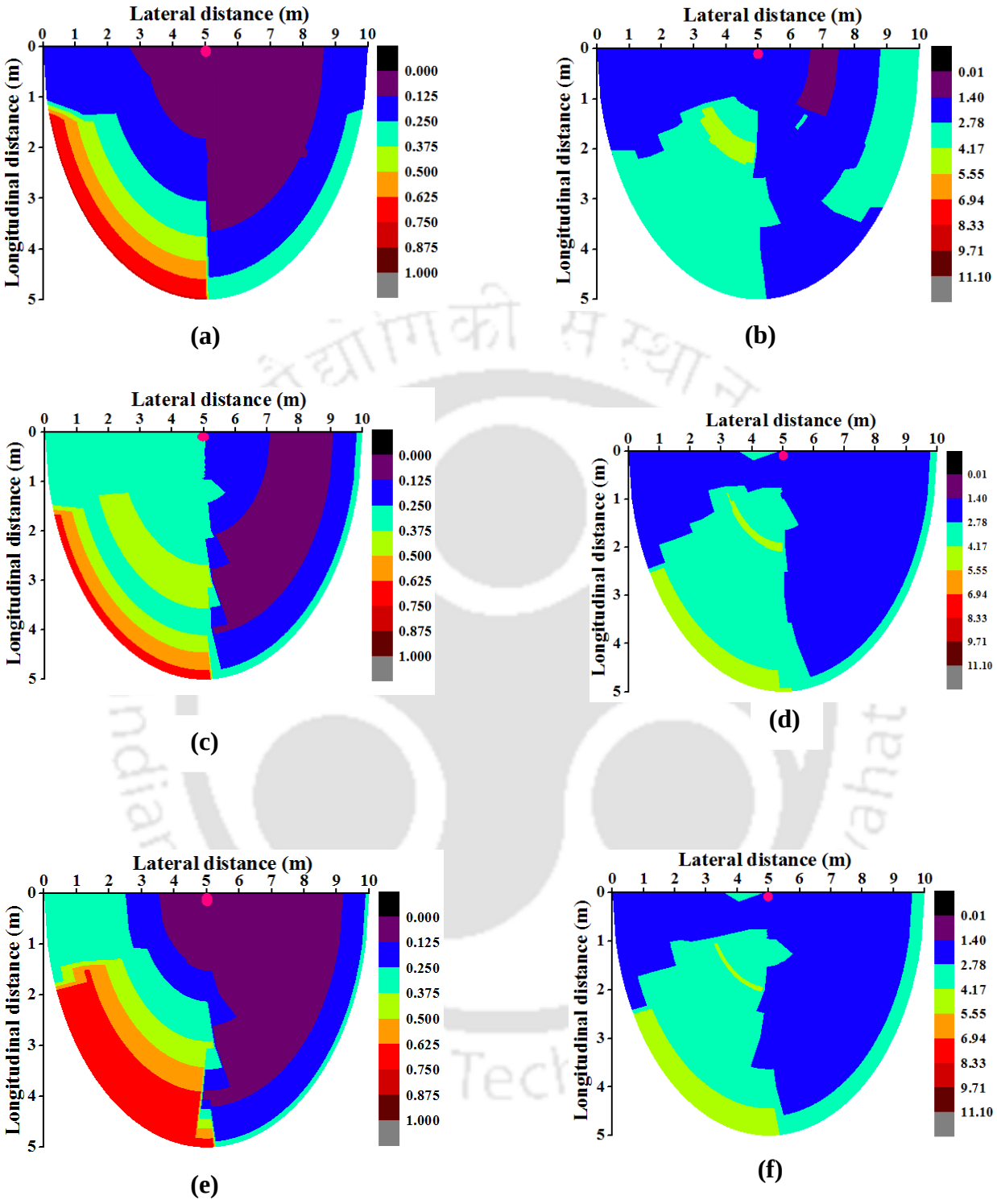

- Vegetation density (m^2/m^2)
- Hydraulic conductivity (10^{-6} m/sec)

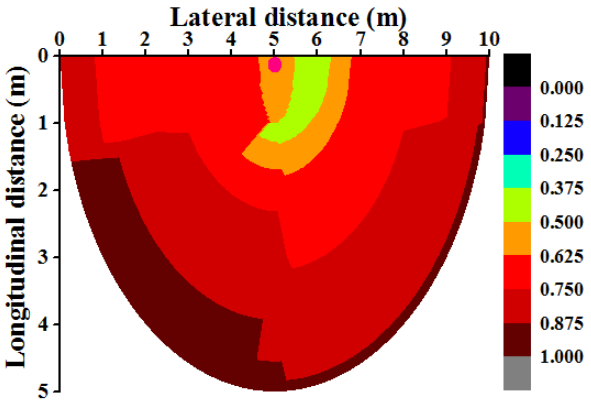

(g)

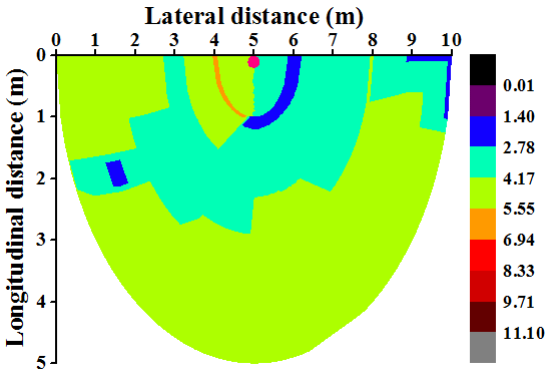

(h)

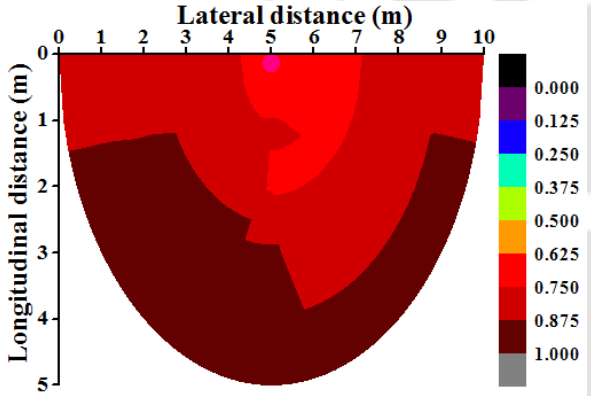

(i)

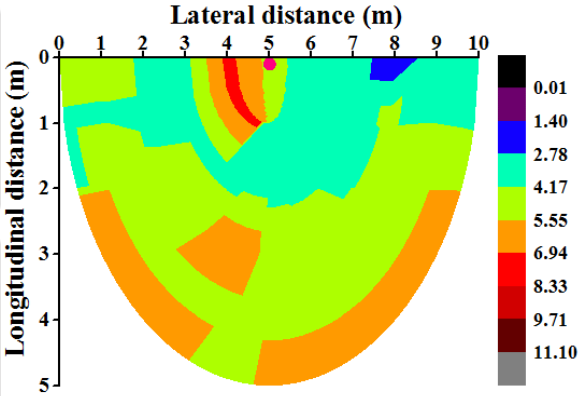

(j)

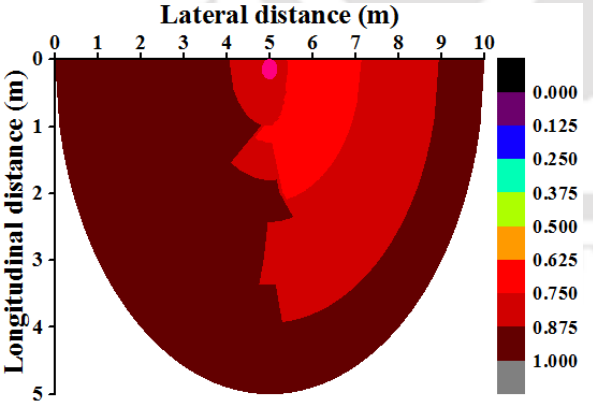

(k)

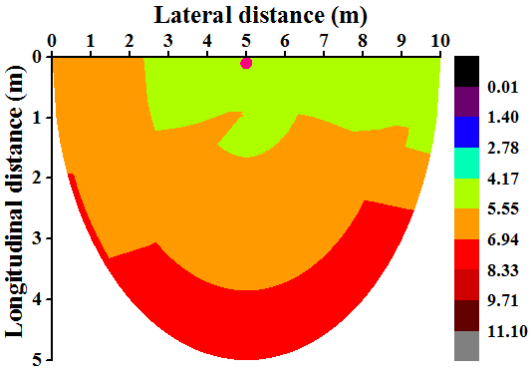

(l)

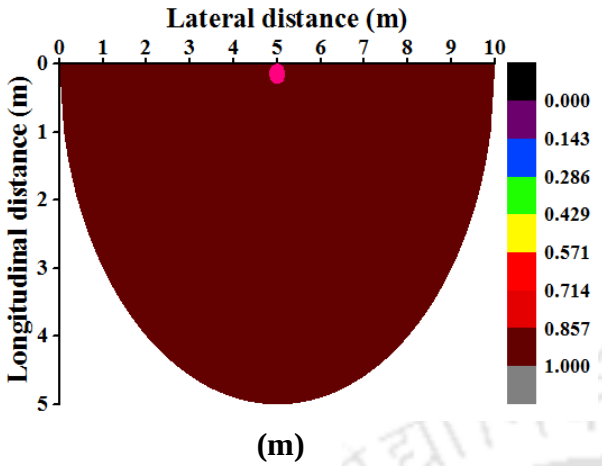

(m)

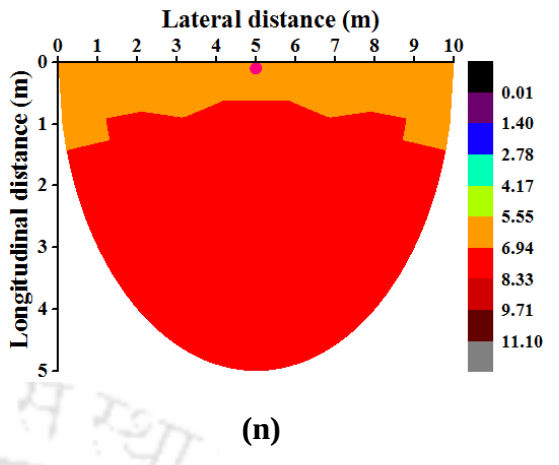

(n)

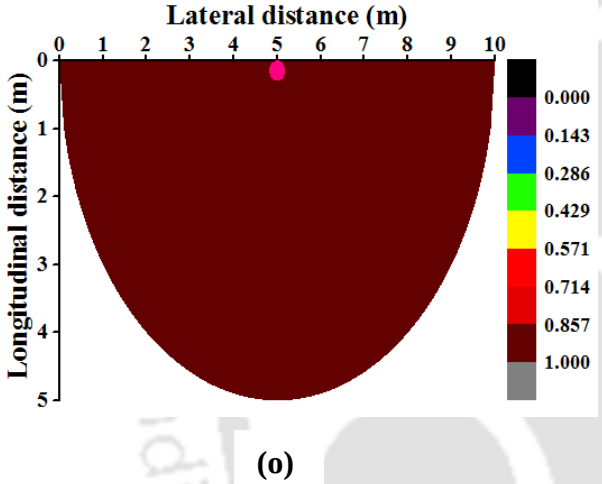

(o)

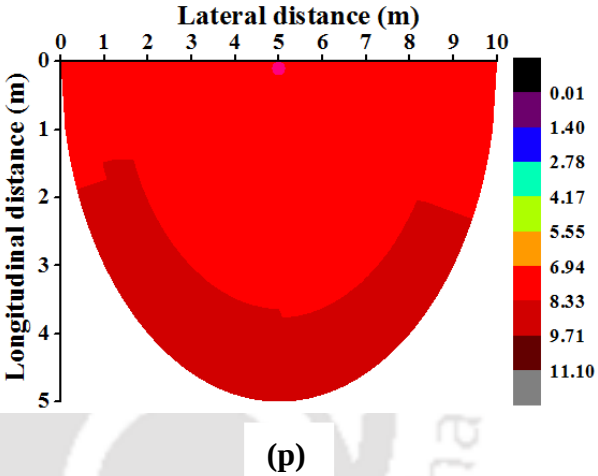

(p)

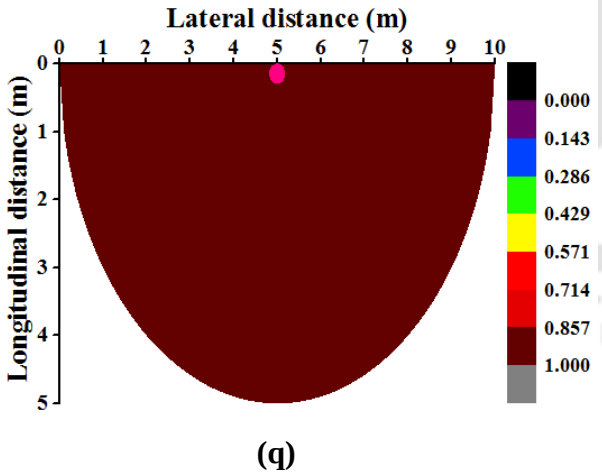

(q)

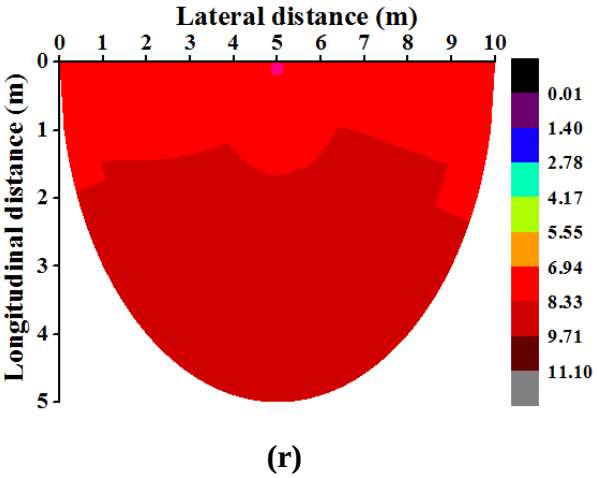

(r)

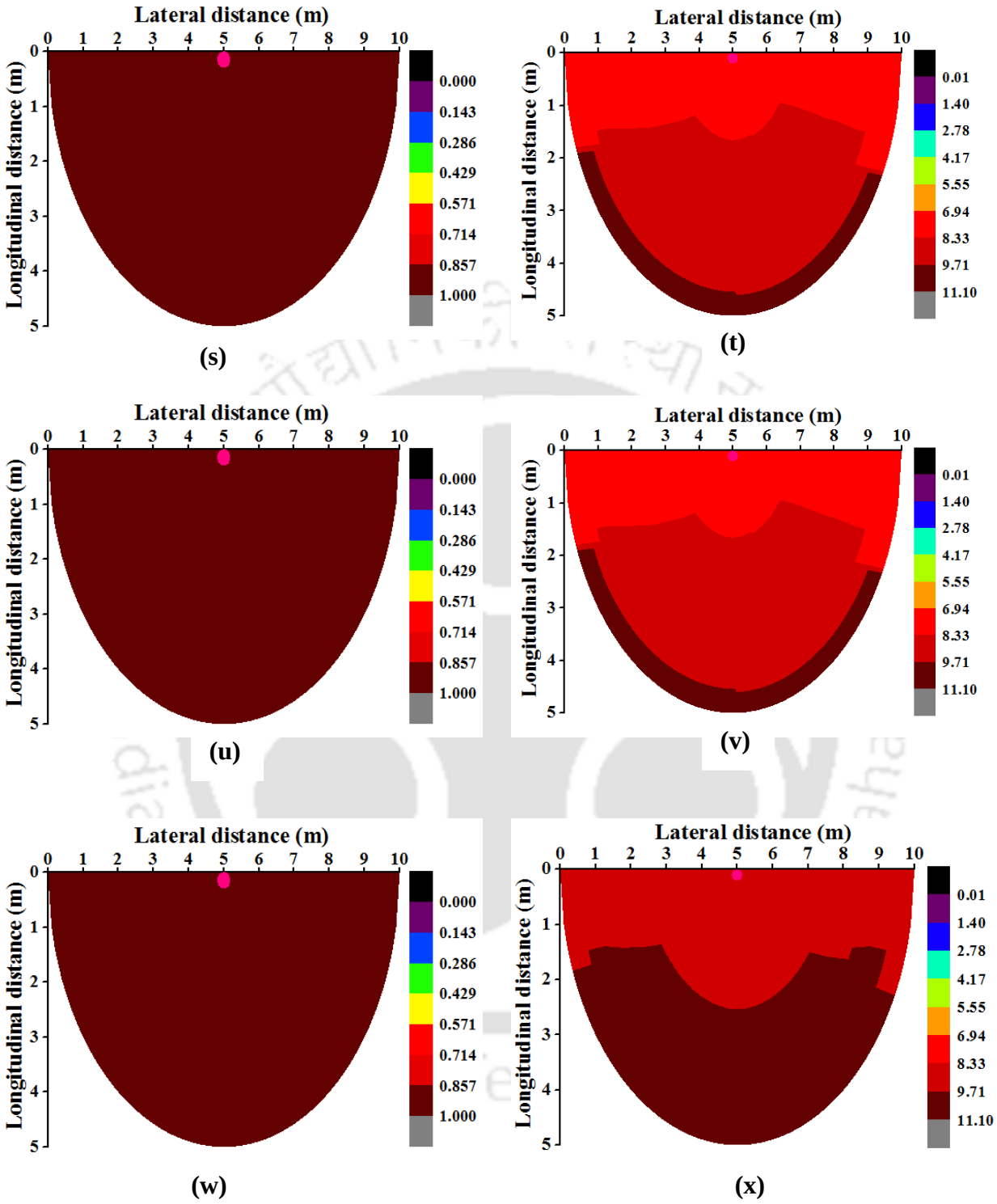

Fig. 9.6. Spatial heterogeneity of vegetation density and hydraulic conductivity at the end of: (a) & (b) January 2016; (c) & (d) February 2016; (e) & (f) March 2016; (g) & (h) April 2016; (i) & (j) May 2016; (k) & (l) June 2016; (m) & (n) July 2016; (o) & (p) August 2016; (q) & (r) September 2016; (s) & (t) October 2016; (u) & (v) November 2016; (w) & (x) December 2016

9.3.4 Effect of vegetation density on surface hydraulic conductivity

Hydraulic conductivity is observed to vary between 1.40×10^{-6} m/s and 2.78×10^{-6} m/s in the right side of the center over major region where vegetation density lies between 0.000 m^2/m^2 and 0.125 m^2/m^2 at the end of January. Hydraulic conductivity in small region at right side of tree stem is observed to vary between 0.01×10^{-6} m/s to 1.40×10^{-6} m/s. This may be attributed to relatively less vegetation density (i.e., around 0.001 m^2/m^2). Hydraulic conductivity is observed to vary between 2.78×10^{-6} m/s and 4.17×10^{-6} m/s where vegetation density lies between 0.125 m^2/m^2 and 0.750 m^2/m^2 at the end of January. Trend of variation of hydraulic conductivity at the end of February and March is similar to that of January. Difference between hydraulic conductivities through higher and lower vegetation density is observed to be 31 % - 99 %. This may be due to the difference between preferential flow rates around the roots (Nieber and Sidle, 2010).

Hydraulic conductivity is observed to increase by only 51 % due to 0.57 m^2/m^2 rise in vegetation density during first three months. Whereas, hydraulic conductivity is observed to increase by 296 % with the above-mentioned change in vegetation density during April. The difference between rates of increase in hydraulic conductivity can be attributed to presence of shredded leaves and wilted grass during February and March. Decomposition of shredded leaves and wilted grass reduces the hydraulic conductivity (Neris et al., 2013). In addition, considerable increase in hydraulic conductivity at the end of April can also be attributed to substantial increase in vegetation density during April (van Noordwijk et al., 1991). Unlike to previous three months, hydraulic conductivity is observed to rise by 31 - 66 % with 0.142 – 0.571 m^2/m^2 increase in vegetation density at the end of April, May and June. This may be due to the absence of decomposition of wilted grass during April, May and June. In addition, any change in hydraulic

conductivity is not found within 2 m longitudinal distance from center. This may be due to less shoot growth rate.

Hydraulic conductivity at longitudinal distance greater than 1.4 m is observed to increase with shoot growth at the end of July, August and September. However, the rate of increase is relatively low during these months. The increase in hydraulic conductivity with shoot growth is found to be 19 % - 49 % at grids within 2 m longitudinal distance from center. Whereas, such increase is found to be 16 % - 76 % in the grids at longitudinal distance greater than 2 m. Greater shoot growth rate at grids away from center may be reason for relatively high hydraulic conductivity. Unlike the trend up to September, any change in hydraulic conductivity is not found over major region during October and November. This can be attributed to very low shoot growth rate during October. In addition, mix grass in 63 % of the surface area was partially wilted at the end of November. Any growth of grass was not observed during November. Therefore, change in hydraulic conductivity was not found during November. Partial wilting was identified from the shrinkage of grass.

Unlike the previous two months, substantial increase in hydraulic conductivity at grids near to the tree trunks can be observed during December. This may be due to wilting of grass in entire area. Grass wilting implies the shrinkage of roots and increase in the gap between roots and soil surrounding the root. Therefore, hydraulic conductivity was considerably increased over entire region during December. This increase in various annuli is found to be 33 - 39 %.

Previous researchers show that 33 - 296 % increase in hydraulic conductivity could be possible due to presence of vegetation. This increase in hydraulic conducted was attributed to the preferential flow at the interface between root and surrounding soil (van Noordwijk et al., 1991;

Nieber and Sidle, 2010; Ghestem et al., 2011). In addition, Jiménez et al., 2006 and Neris et al., 2013 also show that infiltration slows down (up to 50 %) due to decomposition of leaves and roots. However, spatial heterogeneity of hydraulic conductivity during entire life period of deciduous species was not studied previously. Shoot longevity of mix grass and its effect on surface hydraulic conductivity were revealed in present study.

9.4 Summary and Conclusions

Present study investigated the spatial and temporal heterogeneity of surface hydraulic conductivity in green space vegetated with deciduous species (i.e., Poaceae and Bauhinia purpurea). Field monitoring was conducted during the entire life period (i.e., around one year) of the selected species. Considerable spatial heterogeneity of vegetation density occurs during first six months (from January to June). Thereafter, vegetation density remains 1 m^2/m^2 until the plants wilt. Grass growth would not be uniform in the green space. Vegetation density at higher radial distance from the stem of the tree would be 33 % – 296 % greater than that near the tree stem. This was attributed to shade of the tree and growth competition between tree roots and grass roots. When shredded leaves and wilted grass are present during regrowth of grass, hydraulic conductivity increases by only 51 % due to 0.57 m^2/m^2 rise in vegetation density (i.e., during February and March). Whereas, hydraulic conductivity increase would be up to 66 % - 296 % during the absence of shredded leaves and wilted grass (at the end of April). Relatively less increase in hydraulic conductivity could be attributed to decomposition of leaves. Hydraulic conductivity remains unchanged when shoot growth is very less and grass is partially wilted during October and November. However, hydraulic conductivity increases by 33 - 39 % when the grass was completely wilted (i.e., at the

end of December). This was due to shrinkage of grass roots, which increases the gap between root and surrounding soil. The obtained spatial and temporal heterogeneity contours of hydraulic conductivity can be used to numerically model the runoff and ground water recharge accurately.

CHAPTER 10 CONCLUSIONS, LIMITATIONS AND FUTURE SCOPE OF THE STUDY

10.1 Conclusions

This research was initiated to explore the soil-plant atmosphere interaction in green infrastructure. The combined effects of plant and soil parameters in understanding the crack formation, suction and hydraulic conductivity were investigated. Following are the important conclusions observed from the systematic laboratory, field and numerical studies.

1. CIF in soil vegetated with crop species is higher than that of bare soil. CIF increases with shoot growth, up to a threshold length (400 mm), where lateral branch growth start forming. There was no observable increase in CIF, with further shoot growth. CIF increases with LAI up to a certain threshold value (0.56), after which the CIF remains unchanged. Two correlations were proposed for shoot parameters (SL, LAI) with the CIF for the selected species.

2. Unlike crop species (i.e., cowpea), grass species helped reducing the maximum CIF of the bare soil by 20 %. A threshold vegetation density growth of 40 % restricts further increase in CIF for the native mixed species and progressively intercepts the radiant energy falling upon the soil.

3. Soil-root composite induces 1 % to 20 % higher suction than bare soil when transpiration was absent. Depth of SIZ for uniform root distribution function (R_{df}) and non-linear R_{df} is 10 % and 11 % higher than that of linearly decreasing R_{df}. Depth of EDZ for uniformly decreasing R_{df} and non-linear R_{df} is 1.08 to 3 times higher than that of linearly decreasing R_{df}. Influence of LAI on depth of SIZ is minimal. Depth of EDZ decreases with increase in LAI.

4. Lab colour space is suitable for the differentiation of mix grass cover under tree shade (MUT), mix grass cover under self-shade (MUS) and mix grass cover without shade (MWS). Range of L values for MUT, MUS and MWS lie within 20 - 91, 92 - 162 and 162 – 233. a and b ranges

were found to be 0 – 134 and 154 - 255 for three categories of mix grass. Ranges of MUT, MUS and MWS proportions are 0.2 % - 3.0 %, 0 % - 53 % and 12 % - 49 %.

5. Trend of variation of stomatal conductance is consistent with that of suction from anaerobiosis point (near to 0 kPa) to volumetric field capacity (6±1 kPa). Thereafter, stomatal conductance decreases with increase in suction and reaches 0 mol m^{-2} s^{-1} at 2431 kPa. Change in normalized surface area of mix grass would be relatively low (within ±15 %) with increase in suction up to 138 kPa beyond which it varies drastically (by 31 % - 68 %) with increase in suction from 138 kPa to 3642 kPa. Two new relationships i.e., SCCC and SACC were proposed.

6. Mean gray value decreases with increase in surface water content. Decrement in mean gray value was more significant (i.e., 14 – 27 %) in saturation and desaturation zones of SWRC as compared to that in the residual zone (i.e., 3 - 9 %) with 3 – 4 % increase in surface water content. Correlation between mean gray value and surface water content was established for the red soil.

7. Hydraulic conductivity varies spatially during entire life period (one year) of mix grass. Hydraulic conductivity increases by 33 - 296 %, due to rise in vegetation density. Decomposition of shredded leaves and wilted grass reduce the hydraulic conductivity by 48 %. Hydraulic conductivity increases by 33 - 39 % due to wilting of grass.

10.2 Major contributions of this research

1. The correlations between plant parameters and crack intensity factor were obtained. These can be adopted to analyze the integrity of landfill cover system, nutrient leaching and infiltration through green space.

2. Unlike previous studies, actual parameters of canopy and root parameters were considered to numerically investigate suction. The scientific community can consider the variations in the parameters highlighted in this study.
3. A non-intrusive and economical colour analysis technique to differentiate and quantify the mix grass under tree shade, mix grass under self-shade and mix grass without shade was developed.
4. Two new correlations (i.e., stomatal conductance characteristic curve and surface area characteristic curve) were proposed. These can be incorporated into VADOSE/W and HYDRUS to analyze the evapotranspiration induced suction accurately.
5. A non-intrusive and economical colour analysis technique to interpret soil surface water content was successfully demonstrated in this study.
6. Spatial and temporal heterogeneity of plant growth and hydraulic conductivity during life period of mix grass was found. The obtained variations can be adopted to estimate runoff and ground water recharge accurately.

10.3 Limitations and future scope of this research

1. Further studies are required on different species to explore the threshold value of SL, LAI and vegetation density for other plant species. Shoot parameters such as shoot architecture, LAI (with LAI>1) needs to be incorporated in analyzing its effect on cracking for different species.

2. Advanced 3-dimensional soil-root composite system can improve modeling LAI and root distribution on suction induced in soil-root composite. Future studies are required to understand the effect of soil root composite water retention curves (SRCWRCs) variation corresponding to change in R_{df} and LAI on suction induced in soil root composite.

3. Temporal heterogeneity of proportions of MUT, MUS and MWS in green infrastructures can be observed for an entire day light period (i.e., at various points of time during the day). Probabilistic approach can be used to assess the requirement of number of suction sensors according to the obtained temporal variation of MUT, MUS and MWS.

4. Further studies are required to explore the diurnal variation of stomatal conductance and surface area of mix grass during continuous drying period. In addition, influence of soil and vegetation types on SCCC and SACC needs to be investigated.

5. The colour analysis technique and the obtained relation can be programmed with the UAV to quantify the surface water content. Such programming helps to monitor surface water content of large as well as densely urbanized areas at a low cost. Further studies are required to establish the correlation between surface water content and colour in terms of other types of soils.

6. It must be noted that plants would regrow in the selected urban space. The decomposition of wilted grass may alter the regrowth dynamics of mix grass. Further studies are required to explore the effect of plant regrowth on spatial heterogeneity of vegetation density and surface hydraulic conductivity.

REFERENCES

- A.S.T.M., D2487-10., 2010. Standard Practice for Classification of Soils for Engineering Purposes (Unified Soil Classification System). Annual Book of ASTM Standards, West Conshohocken, PA.
- A.S.T.M., D4318-93, 1993. Standard Test Methods for Liquid Limit, Plastic Limit and Plasticity Index of Soils. Annual Book of ASTM Standards, West Conshohocken, PA.
- A.S.T.M., D4914/D4914M-16, 2016. Standard Test Methods for Density of Soil and Rock in Place by the Sand Replacement Method in a Test Pit, Annual Book of ASTM Standards, West Conshohocken, PA.
- A.S.T.M., D698-07, 2007. Standard Test Methods for Laboratory Compaction Characteristics of Soil Using Standard Effort. Annual Book of ASTM Standards, West Conshohocken, PA.
- A.S.T.M., D854-06, 2007. Standard test method for specific gravity of soil solids by water pycnometer. Annual Book of ASTM Standards, West Conshohocken, PA.
- Abhijit, D., Malaya, C. and Sreedeep, S., 2013. A study on tensiometer measurements in salt laden soil used for irrigation scheduling. Geotech. Geol. Eng. 31(4), 1349-1357.
- Ackerly, D., 2004. Functional strategies of chaparral shrubs in relation to seasonal water deficit and disturbance. Ecol. Monogr. 74(1), 25-44.
- Ackerson, R.C., 1980. Stomatal response of cotton to water stress and abscisic acid as affected by water stress history. Plant Physiol. 65(3), 455-459.
- Agyeman, V.K., Swaine, M.D. and Thompson, J., 1999. Responses of tropical forest tree seedlings to irradiance and the derivation of a light response index. J. Ecol. 87(5), pp.815-827.

- Al-Azzawi, A., 2006. Light and optics: principles and practices, CRC Press, 18-20.
- Albright, W.H., Benson, C.H., Gee, G.W., Abichou, T., McDonald, E.V., Tyler, S.W. and Rock, S.A., 2006. Field performance of a compacted clay landfill final cover at a humid site. J. Geotech. Geoenviron. 132(11), 1393-1403.
- Allen, M.F., 1986. Use of mycorrhizae for land rehabilitation, MIRCEN J. Appl. Microb., 2(1), 161-176.
- Andersland, O.B. and Al-Moussawi, H.M., 1987. Crack formation in soil landfill covers due to thermal contraction. Waste Manage. Res. 5(1), 445-452.
- Andreasen, C., Rudemo, M. and Sevestre, S., 1997. Assessment of weed density at an early stage by use of image processing, Weed Res., 37(1), 5-18.
- Anjum, S.A., Xie, X.Y., Wang, L.C., Saleem, M.F., Man, C. and Lei, W., 2011. Morphological, physiological and biochemical responses of plants to drought stress. Afr. J. Agr. Res. 6(9), 2026-2032.
- Arifin, H.S. and Nakagoshi, N., 2011. Landscape ecology and urban biodiversity in tropical Indonesian cities. Landsc. Ecol. Eng. 7(1), 33-43.
- Arnold, J.G., Potter, K.N., King, K.W. and Allen, P.M., 2005. Estimation of soil cracking and the effect on surface runoff in a Texas Black land Prairie watershed. Hydrol. Process. 19(3): 589-603.
- Aroca, R., Porcel, R. and Ruiz-Lozano, J.M. 2011, "Regulation of root water uptake under abiotic stress conditions", J. Exp. Bot. 63(1), 43-57.
- Aroca, R., Tognoni, F., Irigoyen, J.J., Sánchez-Díaz, M. and Pardossi, A. 2001, "Different root low temperature response of two maize genotypes differing in chilling sensitivity", Plant. Physiol. Bioch. 39(12), 1067-1073.

- Avilés-Nova, F., Espinoza-Ortega, A., Castelán-Ortega, O.A. and Arriaga-Jordán, C.M., 2008. Sheep performance under intensive continuous grazing of native grasslands of Paspalum notatum and Axonopus compressus in the subtropical region of the Highlands of Central Mexico. Trop. Anim. Health. Pro. 40(7), 509-515.
- Baer, J.U., Kent, T.F. and Anderson, S.H., 2009. Image analysis and fractal geometry to characterize soil desiccation cracks. Geoderma, 154(1), 153-163.
- Baker, N. and Steemers, K., 2014. Daylight design of buildings: a handbook for architects and engineers, Routledge, 60-63.
- Barbu, B., McManis, K., and Nataraj, M., "Study of silts moisture susceptibility using the tube suction test," In Transportation Research Board 2004 Annual Meeting, CD-ROM Publication, Transportation Research Board, National Research Council, Washington DC.
- Bartlett, M.K., Scoffoni, C. and Sack, L., 2012. The determinants of leaf turgor loss point and prediction of drought tolerance of species and biomes: a global meta-analysis. Ecol. Lett. 15(5), 393-405.
- Beadle, C.L., Neilson, R.E., Talbot, H. and Jarvis, P.G., 1985. Stomatal conductance and photosynthesis in a mature Scots pine forest. I. Diurnal, seasonal and spatial variation in shoots. J. Appl. Ecol. 22(2), 557-571.
- Beckett, C.T.S., Glenn, D., Bradley, K., Guzzomi, A.L., Merritt, D. and Fourie, A.B., 2017. Compaction conditions greatly affect growth during early plant establishment. Ecol. Eng. 106, 471-481.
- Bernard, R., Soares, J.V. and Vidal-Madjar, D., 1986. Differential bare field drainage properties from airborne microwave observations, Water Resour. Res., 22(6), 869-875.

- Berretta, C., Poë, S. and Stovin, V., 2014. Moisture content behaviour in extensive green roofs during dry periods: The influence of vegetation and substrate characteristics. J. Hydrol. 511, 374-386.
- Bhatt, R., Arora, S. and Chew, C.C., 2016. Improving irrigation water productivity using tensiometers. J. Soil. Water Conserv. 15(2), pp.120-124.
- Blight, G.E., 2003. The vadose zone soil-water balance and transpiration rates of vegetation. Geotechnique, 53(1), pp.55-64.
- Boardman, N.K., 1977. Comparative photosynthesis of sun and shade plants," Ann.l rev. Plant. Physio. 28(1), 355-377.
- Boisvenue, C. and Running, S.W., 2006. Impacts of climate change on natural forest productivity–evidence since the middle of the 20th century. Glob. Change. Biol. 12(5), 862-882.
- Bordoloi, S., Hussain, R., Garg, A., Sreedeep, S. and Zhou, W.H., 2017. Infiltration characteristics of natural fiber reinforced soil. Transportation Geotechnics, 12, 37-44.
- Bordoloi, S., Yamsani, S.K., Garg, A., Sreedeep, S. and Borah, S., 2015. Study on the efficacy of harmful weed species Eicchornia crassipes for soil reinforcement. Ecol. Eng. 85, 218-222.
- Bouldin, J.L., Farris, J.L., Moore, M.T. and Cooper, C.M., 2004. Vegetative and structural characteristics of agricultural drainages in the Mississippi Delta landscapes. Environ. Pollut. 132(3), 403-411.
- Bouma, J., Dekker, L.W. and Haans, J.C.F.M., 1979. Drainability of some Dutch clay soils: a case study of soil survey interpretation. Geoderma, 22(3), 193-203.

- Bréda, N., Cochard, H., Dreyer, E. and Granier, A., 1993. Field comparison of transpiration, stomatal conductance and vulnerability to cavitation of Quercus petraea and Quercus robur under water stress. In Annales des Sciences Forestières, 50 (6), 571-582. EDP Sciences.
- Buchanan-Wollaston, V., Page, T., Harrison, E., Breeze, E., Lim, P.O., Nam, H.G., Lin, J.F., Wu, S.H., Swidzinski, J., Ishizaki, K. and Leaver, C.J., 2005. Comparative transcriptome analysis reveals significant differences in gene expression and signalling pathways between developmental and dark/starvation-induced senescence in Arabidopsis. Plant J., 42(4), 567-585.
- Burridge, J., Jochua, C.N., Bucksch, A. and Lynch, J.P., 2016. Legume shovelomics: high—throughput phenotyping of common bean (Phaseolus vulgaris L.) and cowpea (Vigna unguiculata subsp, unguiculata) root architecture in the field. Field Crop. Res. 192, 21-32.
- Büyüksalih, G. and Jacobsen, K., 2006. Comparison of DEM generation by very high resolution optical satellites. In 26th EARSeL Symposium on New Developments and Challenges in Remote Sensing, Warsaw, Poland.
- Bytnerowicz, A. and Fenn, M.E., 1996. Nitrogen deposition in California forests: a review. Envir. Pollut. 92(2), 127-146.
- Bytnerowicz, A., Alonso, R. and Arbaugh, M. eds., 2003. Ozone Air Pollution in the Sierra Nevada-Distribution and Effects on Forests, Elsevier. 2, 334-336,
- Cai, Z.Q., Poorter, L., Cao, K.F. and Bongers, F., 2007. Seedling growth strategies in Bauhinia species: comparing lianas and trees. Ann. Bot-London. 100(4), 831-838.

- Camillo, P.J. and Schmugge, T.J., 1984. Correlating rainfall with remotely sensed microwave radiation using physically based models, IEEE transactions on geoscience and remote sensing, 4, 415-423.
- Campos, Y., Sossa, H. and Pajares, G., 2016. Spatio-temporal analysis for obstacle detection in agricultural videos, Appl. Soft Comput. 45, 86-97.
- Carsel, R.F. and Parrish, R.S., 1988. Developing joint probability distributions of soil water retention characteristics. *Water resources research*, *24*(5), pp.755-769.
- Casper, B.B. and Jackson, R.B., 1997. "Plant competition underground," Annu. Rev. Ecol. Syst., 28(1), 545-570.
- Chaduvula, U., Viswanadham, B.V.S. and Kodikara, J., 2017. A study on desiccation cracking behavior of polyester fiber-reinforced expansive clay. Appl. Clay Sci. 142, 163-172.
- Chanzy, A. and Bruckler, L., 1993. Significance of soil surface moisture with respect to daily bare soil evaporation, Water Resour. Res., 29(4), 1113-1125.
- Chartzoulakis, K., Patakas, A., Kofidis, G., Bosabalidis, A. and Nastou, A., 2002. Water stress affects leaf anatomy, gas exchange, water relations and growth of two avocado cultivars. Sci. Hortic. Amsterdam. 95(1-2), 39-50.
- Chen, F. and Avissar, R., 1994. Impact of land-surface moisture variability on local shallow convective cumulus and precipitation in large-scale models," J. Appl. Meteorol., 33(12), 1382-1401.
- Cheplick, G.P., 2004. Recovery from drought stress in Lolium perenne (Poaceae): are fungal endophytes detrimental?. Am. J. Bot. 91(12), 1960-1968.

- Chertkov, V.Y. and Ravina, I., 1999. Tortuosity of crack networks in swelling clay soils. Soil. Sci. Soc. Am. J. 63(6), 1523-1530.
- Choudhury, B.J. and Monteith, J.L., 1988. A four-layer model for the heat budget of homogeneous land surfaces," Q. J. Roy. Meteor. Soc., 114(480), 373-398.
- Clark, R.N., 1999. Spectroscopy of rocks and minerals, and principles of spectroscopy," Manual of remote sensing, 3(3-58), 2-2.
- Coles, N., Trudgill, S., 1985. The movement of nitrogen fertilizer from the soil surface to drainage waters by preferential flow in weakly structured soils Slapton South Devon UK. Agriculture, Ecosystems & Environment 13: 241–259.
- Congalton, R.G., 1991 "A review of assessing the accuracy of classifications of remotely sensed data," Remote Sens. Environ., 37(1), 35-46.
- Cook, Wayne D., and Maxwell P. Chong. 1985. Colour stability and visual perception of dimethacrylate based dental composite resins," Biomaterials, 6(4), 257-264.
- Corte, A. and Higashi, A., 1960. Experimental Research on Desiccation Cracks, Soil Research report 66: U. S. Army Snow Ice and Permifrost Research Establishment, Willmette, Illinous.
- Costa, S., Kodikara, J. and Shannon, B., 2013. Salient factors controlling desiccation cracking of clay in laboratory experiments Géotechnique 63(1): 18.
- Czarnes, S., Dexter, A.R. and Bartoli, F., 2000. Wetting and drying cycles in the maize rhizosphere under controlled conditions. Mechanics of the root-adhering soil. Plant. Soil, 221(2), 253-271,

- Damesin, C. and Rambal, S., 1995. Field study of leaf photosynthetic performance by a Mediterranean deciduous oak tree (Quercus pubescens) during a severe summer drought. New Phytol. 131(2), 159-167.
- Dasog, G.S., Acton, D.F., Mermut, A.R. and JONG, E.D., 1988. Shrink-swell potential and cracking in clay soils of Saskatchewan. Can. J. Soil. Sci. 68(2), 251-260.
- De Silva, M.S., Nachabe, M.H., Šimůnek, J. and Carnahan, R., 2008. Simulating root water uptake from a heterogeneous vegetative cover. J. Irrig. Drain. E-ASCE. 134(2), 167-174.
- Deardorff, J., A., 1977. A parameterization of ground-surface moisture content for use in atmospheric prediction models, J. Appl. Meteorol. 16(11), 1182-1185.
- Deb, S.K., Shukla, M.K., Šimůnek, J. and Mexal, J.G., 2013. Evaluation of spatial and temporal root water uptake patterns of a flood-irrigated pecan tree using the HYDRUS (2D/3D) model. J. Irrig. Drain. E-ASCE. 139(8), 599-611.
- Devices, Delta-T., 2006. SM200 soil moisture sensor. User manual. Delta-T Devices Ltd, Cambridge.
- Devices, Delta-T., 2013. ML3 Theta Probe, User manual. Delta-T Devices Ltd, Cambridge.
- Devitt, D.A., Bowman, D.C. and Schulte, P.J. (1993). Response of Cynodon dactylon to prolonged water deficits under saline conditions. Plant soil, 148(2), 239-251.
- Eaton, B.C. and Giles, T.R. 2009, "Assessing the effect of vegetation-related bank strength on channel morphology and stability in gravel-bed streams using numerical models", Earth Surf. Proc. Land. 34(5), 712-724.
- El Abedine, A.Z. and Robinson, G.H., 1971. A study on cracking in some vertisols of the Sudan. Geoderma 5(3), 229-241.

- Elmi, A.A. and West, C.P., 1995. Endophyte infection effects on stomatal conductance, osmotic adjustment and drought recovery of tall fescue. New. Phytol. 131(1), 61-67.
- Engman, Edwin T., and Narinder Chauhan. 1995. Status of microwave soil moisture measurements with remote sensing, Remote Sens. Environ., 51(1), 189-198.
- Eusebius, N.P., Papalia, L., Suphioglu, C., McLellan, S.C., Varney, M., Rolland, J.M. and O'Hehir, R.E., 2002. Oligoclonal analysis of the atopic T cell response to the group 1 allergen of Cynodon dactylon (bermuda grass) pollen: pre-and post-allergen-specific immunotherapy. Int. Arch. Allergy. Imm. 127(3), 234-244.
- Famiglietti, J.S., Rudnicki, J.W. and Rodell, M., 1998. Variability in surface moisture content along a hillslope transect: Rattlesnake Hill, Texas, J. Hydrol., Vol. 210(1-4), 259-281.
- Feddes, R.A., 1982. Simulation of field water use and crop yield, Pudoc. 194-209.
- Feddes, R.A., Kowalik, P.J. and Zaradny, H., 1978, "Simulation of field water use and crop yield", Centre for Agricultural Publishing and Documentation, Bogor, Indonesia
- Feng, S., Leung, A.K., Ng, C.W.W. and Liu, H.W., 2017. Theoretical analysis of coupled effects of microbe and root architecture on methane oxidation in vegetated landfill covers, Sci. Total. Environ. 599, 1954.
- Feng, S., Ng, C.W.W., Leung, A.K. and Liu, H.W., 2017. Numerical modelling of methane oxidation efficiency and coupled water-gas-heat reactive transfer in a sloping landfill cover. Waste Manage. 68, 355-368.
- Ferreira, T. and Rasband, W., 2012. ImageJ user guide. ImageJ/Fiji, 1.

- Fitzpatrick, J. and Kirkman, H., 1995. Effects of prolonged shading stress on growth and survival of seagrass Posidonia australis in Jervis Bay, New South Wales, Australia. Mar. Ecol. Prog. Ser. 127, 279-289.
- Fox, W.E., 1964. Cracking characteristics and field capacity in a swelling soil. Soil Sci 98(413), 37-49.
- Fredlund, D.G. and Xing, A., 1994. Equations for the soil-water characteristic curve. Can. Geotech. J. 31(4), 521-532.
- Fredlund, D.G., Morgenstern, N.R. and Widger, R.A., 1978. The shear strength of unsaturated soils. Can. Geotech. J. 15(3), 313-321.
- Gallage, C.P.K. and Uchimura, T., 2010. Effects of dry density and grain size distribution on soil-water characteristic curves of sandy soils. Soils. Found. 50(1), 161-172.
- Garg, A. and Ng, C.W.W., 2015. Investigation of soil density effect on suction induced due to root water uptake by Schefflera heptaphylla. J. Plant. Nutr. Soil Sc. 178(4), 586-591.
- Garg, A., Bordoloi, S., Mondal, S., Ni, J.J. and Sreedeep, S., 2018. Investigation of mechanical factor of soil reinforced with four types of fibers: An integrated experimental and extreme learning machine approach. J. Nat. Fibers. 1-15.
- Garg, A., Coo, J.L. and Ng, C.W.W., 2015c. Field study on influence of root characteristics on soil suction distribution in slopes vegetated with Cynodon dactylon and Schefflera heptaphylla. Earth Surf. Proc. Land., 40(12), 1631-1643.
- Garg, A., Hazra, B., Zhu, H. and Wen, Y., 2019. A simplified probabilistic analysis of water content and wilting in soil vegetated with non-crop species. Catena, 175, 123-131.

- Garg, A., Leung, A.K. and Ng, C.W.W., 2015b. Comparisons of soil suction induced by evapotranspiration and transpiration of S. heptaphylla. Can. Geotech. J. 52(12), 2149-2155.
- Garg, A., Leung, A.K., Ng, C.W.W., 2015a. Transpiration reduction and root distribution functions for a non-crop species Schefflera heptaphylla. Catena 135, 78–82.
- Garg, A., Li, J., Berretta, C., and Garg, A. 2017a. A new computational approach for estimation of wilting point for green infrastructure. Measurement, 111, 351-358.
- Garg, A., Vijayaraghavan, V., Zhang, J., and Lam, J. S. L., 2017b. Robust model design for evaluation of power characteristics of the cleaner energy system. Renew. Energ. 112, 302-313.
- Garg, A., Vijayaraghavan, V., Zhang, J., Li, S., and Liang, X., 2017c. "Design of robust battery capacity model for electric vehicle by incorporation of uncertainties", Int. J. Energ. Res., *41*(10), pp.1436-1451.
- Gasmo, J., Hritzuk, K.J., Rahardjo, H. and Leong, E.C., 1999. "Instrumentation of an unsaturated residual soil slope," Geotech. Test. J., 22(2), 134-143.
- Ghestem, M., Sidle, R.C. and Stokes, A., 2011. The influence of plant root systems on subsurface flow: implications for slope stability. Bioscience, 61(11), pp.869-879.
- Ghosh, T., Bhandari, G. and Hazra, S., 2003. Application of a 'bio-engineering'technique to protect Ghoramara Island (Bay of Bengal) from severe erosion. Journ. Coast. Conserv. 9(2), 171-178.
- Gish, T.J. and Jury, W.A., 1983. Effect of plant roots and root channels on solute transport. Transactions of the ASAE, 26(2), 440-0444.

- Gomes, M.D.M.D.A., Lagôa, A.M.M.A., Medina, C.L., Machado, E.C. and Machado, M.A., 2004. Interactions between leaf water potential, stomatal conductance and abscisic acid content of orange trees submitted to drought stress. Braz. J. Plant Physiol. 16(3), 155-161.
- Gómez-Robledo, L., López-Ruiz, N., Melgosa, M., Palma, A.J., Capitán-Vallvey, L.F. and Sánchez-Marañón, M., 2013. Using the mobile phone as Munsell soil-colour sensor: An experiment under controlled illumination conditions," Comput. Electron. Agr., Vol. 99, 200-208.
- Gonzalez-Ollauri, A. and Mickovski, S.B., 2015. Hydrological effect of vegetation against shallow landslides: a technical approach. Proceedings of the XVI ECSMGE Geotechnical Engineering for Infrastructure and Development, 1753-1758.
- Goodchild, M.S., Kuhn, K.D. and Jenkins, M.D., 2014. Soil moisture responses to vapour pressure deficit in polytunnel-grown tomato under soil moisture triggered irrigation control. Delta-T Devices Ltd, Cambridge.
- Gross, K., Homlicher, A., Weinreich, A. and Wagner, E., 1996. Effect of shade on stomatal conductance, net photosynthesis, photochemical efficiency and growth of oak saplings. In Annales des sciences forestières. EDP Sciences. 53(2-3), 279-290.
- Guyer, D.E., Miles, G.E., Schreiber, M.M., Mitchell, O.R. and Vanderbilt, V.C., 1986, "Machine vision and image processing for plant identification," T ASAE, 29(6), 1500-1507.
- Habib, A., Shin, S.W., Kim, K., Kim, C., Bang, K.I., Kim, E.M. and Lee, D.C., 2007. Comprehensive analysis of sensor modeling alternatives for high resolution imaging satellites," Photogramm. Eng. Rem. S., 73(11), 1241-1251.

- Hallik, L., Niinemets, Ü. and Wright, I.J., 2009. Are species shade and drought tolerance reflected in leaf-level structural and functional differentiation in Northern Hemisphere temperate woody flora?. New. Phytol. 184(1), 257-274.
- Hemmati, S., Gatmiri, B., Cui, Y.J. and Vincent, M., 2012. Thermo-hydro-mechanical modelling of soil settlements induced by soil-vegetation-atmosphere interactions. Eng. Geol. 139, 1-16.
- Herbel, C.H., Ares, F.N. and Wright, R.A., 1972. Drought effects on a semidesert grassland range. Ecology, 53(6), 1084-1093.
- Hillel, D., Krentos, V.D. and Stylianou, Y. 1972, Procedure and test of an internal drainage method for measuring soil hydraulic characteristics in situ, Soil Sci. 114(5), 395-400.
- Hino, M., Odaka, Y., Nadaoka, K. and Sato, A., 1988. Effect of initial soil moisture content on the vertical infiltration process—A guide to the problem of runoff-ratio and loss, J. Hydrol., 102(1-4), 267-284.
- Huang, S., Peng, X., Huang, Q. and Zhang, W., 2010. Soil aggregation and organic carbon fractions affected by long-term fertilization in a red soil of subtropical China. Geoderma, 154(3-4), 364-369.
- Huat, B.B., Ali, F.H. and Low, T.H., 2006. Water infiltration characteristics of unsaturated soil slope and its effect on suction and stability. Geotech. Geol. Eng. 24(5), 1293-1306.
- Jackson, T.J., 1993. III. Measuring surface soil moisture using passive microwave remote sensing," Hydrol. Process., 7(2), 139-152.
- Jarvis, P.G. and Mansfield, T.A. eds., 1981. Stomatal physiology. Cambridge University Press. 8, 140-145.

- Javaux, M., Schröder, T., Vanderborght, J. and Vereecken, H., 2008. Use of a three-dimensional detailed modeling approach for predicting root water uptake. Vadose. Zone. J. 7(3), 1079-1088.
- Jayanthi, P.N.V., Kuntikana, G. and Singh, D.N., 2017. Stabilization of Fine-Grained Soils Against Desiccation Cracking Using Sustainable Materials. Adv. Civ. Eng. 6(1), 36-67.
- Jeong, S., Park, S.H. and Kim, C.H., 2013, February. Simulation of morphology changes in drying leaves. In Computer Graphics Forum . Blackwell Publishing Ltd. 32(1), 204-215.
- Jim, C.Y. and Liu, H.T., 2001, Species diversity of three major urban forest types in Guangzhou City, China. Forest Ecol. Manag. 146(1), 2001, 99-114.
- Jimenez, C.C., Tejedor, M., Morillas, G. and Neris, J., 2006. Infiltration rate in andisols: effect of changes in vegetation cover (Tenerife, Spain). J. Soil Water. Conserv. 61(3), 153-158.
- Johannes, A., Picon, A., Alvarez-Gila, A., Echazarra, J., Rodriguez-Vaamonde, S., Navajas, A.D. and Ortiz-Barredo, A., 2017. Automatic plant disease diagnosis using mobile capture devices, applied on a wheat use case, Comput. Electron. Agri., 138, 200-209.
- Johnston, J.R. and Hill, H.O., 1944. A study of the shrinking and swelling properties of rendzina soils. Soil. Sci. Soc. Am. J. 9(C), 24-29.
- Joseph, G., 2005. Fundamentals of remote sensing, Universities Press., p. 53.
- Kahn, B.A. and Stoffella, P.J., 1991. Nodule distribution among root morphological components of field-grown cowpeas. Journal of the American Society for Horticultural Science, 116(4), 655-658.

- Kang, B.T., Grimme, H. and Lawson, T.L., 1985. Alleu cropping sequentially cropped maize and cowpea with Leucaena on a sandy soil in Southern Nigeria. Plant. Soil, 85(2), 267-277.
- Keane, J., 2014. Pico-solar Electric Systems: The Earthscan Expert Guide to the Technology and Emerging Market. Routledge, p. 19.
- Kokutse, N.K., Temgoua, A.G.T. and Kavazović, Z., 2016. Slope stability and vegetation: Conceptual and numerical investigation of mechanical effects. Ecol. Eng. 86, 146-153.
- Koyama, K. and Takemoto, S., 2014. Morning reduction of photosynthetic capacity before midday depression. Sci. Rep-UK. 4, 4389.
- Kumar, S.V., Dirmeyer, P.A., Peters-Lidard, C.D., Bindlish, R. and Bolten, J., 2018. Information theoretic evaluation of satellite soil moisture retrievals," Remote Sens. Environ. 204, 392-400.
- Kuo, H.L., 1965. On formation and intensification of tropical cyclones through latent heat release by cumulus convection," J. Atmos. Sci., 22(1), 40-63.
- Lambe, T. W., and Whitman, R. V., 2008. Soil mechanics SI version, John Wiley & Sons, 517-520.
- Lau, I.C., Ong, C.C., Laukamp, C., de Caritat, P. and Thomas, M., 2017. The acquisition and processing of voluminous spectral reflectance measurements of soils and powders for national datasets, In Geoscience and Remote Sensing Symposium (IGARSS), IEEE International, 4482-4484.
- Lee, E.W., Hau, B.C. and Corlett, R.T. 2005. Natural regeneration in exotic tree plantations in Hong Kong, China, Forest Ecol. Manag. 212(1), 358-366.

- Lee, I.C., Hong, S.W., Whang, S.S., Lim, P.O., Nam, H.G. and Koo, J.C., 2011. Age-dependent action of an ABA-inducible receptor kinase, RPK1, as a positive regulator of senescence in Arabidopsis leaves. Plant. Cell Physiol. 52(4), 651-662.
- Lehmann, J., Peter, I., Steglich, C., Gebauer, G., Huwe, B. and Zech, W., 1998. Below-ground interactions in dryland agroforestry. Forest Ecol. Manag. 111(2-3), 157-169.
- Leishman, M.R. and Westoby, M., 1994. The role of seed size in seedling establishment in dry soil conditions--experimental evidence from semi-arid species. J. Ecol. 249-258.
- Leung, A.K. and Ng, C.W.W., 2013 "Analyses of groundwater flow and plant evapotranspiration in a vegetated soil slope," Can. Geotech. J., 50(12), 1204-1218.
- Leung, A.K. and Ng, C.W.W., 2016. Field investigation of deformation characteristics and stress mobilisation of a soil slope," Landslides, 13(2), 229-240.
- Leung, A.K., Coo, J.L., Ng, C.W.W. and Chen, R. 2016. New transient method for determining soil hydraulic conductivity function", Can. Geotech. J., 53(8), 1332-1345.
- Leung, A.K., Garg, A. and Ng, C.W.W., 2015b. Effects of plant roots on soil-water retention and induced suction in vegetated soil. Eng. Geol., 193, 183-197.
- Leung, A.K., Garg, A., Coo, J.L., Ng, C.W.W. and Hau, B.C.H., 2015a. Effects of the roots of Cynodon dactylon and Schefflera heptaphylla on water infiltration rate and soil hydraulic conductivity. Hydrol. Process. 29(15), 3342-3354.
- Li, J.H. and Zhang, L.M., 2010. Geometric parameters and REV of a crack network in soil. Comput. Geotech. 37(4), 466-475.
- Li, J.H. and Zhang, L.M., 2011. Study of desiccation crack initiation and development at ground surface. Eng. Geol. 123(4), 347-358.

- Li, J.H., Li, L., Chen, R. and Li, D.Q., 2016. Cracking and vertical preferential flow through landfill clay liners. Eng. Geol., 206, 33-41.
- Liang, T., Bengough, A.G., Knappett, J.A., MuirWood, D., Loades, K.W., Hallett, P.D., Boldrin, D., Leung, A.K. and Meijer, G.J., 2017. Scaling of the reinforcement of soil slopes by living plants in a geotechnical centrifuge. Ecol. Eng. 109, 207-227.
- Lin, D.G., Huang, B.S. and Lin, S.H., 2010, 3-D numerical investigations into the shear strength of the soil–root system of Makino bamboo and its effect on slope stability, Ecol. Eng. Vol. 36(8), 992-1006.
- Lin, T.T., Lai, T.M., and Fon, D.S., 1994. Gray-scale and Colour Machine Vision Systems for Seeding Detection, Proceedings of the 5th International Conference on Computers in Agriculture, 105-110.
- Linderman, R.G. 1988. Mycorrhizal interactions with the rhizosphere microflora: the mycorrhizosphere effect, Phytopathology, 78(3), 366-371.
- Liu, H.W., Feng, S. and Ng, C.W. 2016. Analytical analysis of hydraulic effect of vegetation on shallow slope stability with different root architectures, Comput. Geotech. 80, 115-120.
- Lo Gullo, M.A., Nardini, A., Trifilò, P. and Salleo, S., 2005. Diurnal and seasonal variations in leaf hydraulic conductance in evergreen and deciduous trees. Tree Physiol. 25(4), 505-512.
- Loades, K.W., Bengough, A.G., Bransby, M.F. and Hallett, P.D., 2010. Planting density influence on fibrous root reinforcement of soils. Ecol. Eng. 36(3), 276-284.

- Logsdon, S., Allmaras, R.R., Wu, L., Swan, J.B. and Randall, G.W., 1990. Macroporosity and its relation to saturated hydraulic conductivity under different tillage practices. Soil. Sci. Soc. Am. J. 54(4), 1096-1101.
- Maas, E.V. and Poss, J.A., 1989. Salt sensitivity of cowpea at various growth stages. Irrig. Sci. 10(4), 313-320.
- Macai-Pasqualino, E.J., Costes, N.C. and Parker, J.K., 1993. Digital image techniques for volume change measurements in triaxial tests. In Digital Image Processing: Techniques and Applications in Civil EngineeringAmerican Society of Civil EngineersNational Science Foundation Engineering Foundation.
- McCord, T.B. and Gaffey, M.J., 1974. Asteroids: Surface composition from reflection spectroscopy. Science, 186(4161), 352-355.
- McCord, T.B. and Johnson, T.V., 1970. Lunar spectral reflectivity (0.30 to 2.50 microns) and implications for remote mineralogical analysis. Science. 169(3948), 855-858.
- McGechan, M.B., 1990. A review of losses arising during conservation of grass forage: Part 2, storage losses. J. Agric. Eng. Res. 45, pp.1-30.
- Meerow, S. and Newell, J.P., 2017. Spatial planning for multifunctional green infrastructure: Growing resilience in Detroit. Landscape. Urban. Plan. 159, 62-75.
- Meyer, G.E. and Neto, J.C., 2008. Verification of colour vegetation indices for automated crop imaging applications," Comput. Electron. Agr., 63(2), 282-293.
- Mi, H., 1995. Kinematic wave formulation for flow through macroporous soil. Ph.D. Thesis, Department of Civil and Environmental Engineering, Wayne State University, Detroit, MI.

- Miller, C.J., Mi, H. and Yesiller, N., 1998. Experimental analysis of desiccation crack propagation in clay liners. J. Am. Water. Resour. As. 34(3), 677-686.
- Min, T.K. and Huy, P.T., 2008. Digital Image Analysis (DIA) for Estimating the Degree of Saturation of The Soil-Water Characteristic Curves (SWCC), J. Korean Geotech. Soc., 24(3), 53-63.
- Mitchell, A.R. and Van Genuchten, M.T., 1992. Shrinkage of bare and cultivated soil. Soil. Sci. Soc. Am. J. 56(4), 1036-1042.
- Mitchell, A.R., Ellsworth, T.R. and Meek, B.D., 1995. Effect of root systems on preferential flow in swelling soil. Commun. Soil. Sci. Plan. 26(15-16), 2655-2666.
- Miyazawa, S.I., Livingston, N.J. and Turpin, D.H., 2005. Stomatal development in new leaves is related to the stomatal conductance of mature leaves in poplar (Populus trichocarpa× P. deltoides). J. Exp. Bot. 57(2), 373-380.
- Monteith, J. L., 1965. Evaporation and environment. In Symp. Soc. Exp. Biol.19(205-23), 4.
- Mooney, H.A., Field, C., Yanes, C.V. and Chu, C., 1983. Environmental controls on stomatal conductance in a shrub of the humid tropics. P. Natl. Acad. Sci. Usa, 80(5), 1295-1297.
- Morgan, R.P. and Rickson, R.J., 2003. Slope stabilization and erosion control: a bioengineering approach. Taylor & Francis.
- Munemasa, S., Hauser, F., Park, J., Waadt, R., Brandt, B. and Schroeder, J.I., 2015. Mechanisms of abscisic acid-mediated control of stomatal aperture. Curr. Opin. in plant boil. 28, 154-162.

- Neris, J., Tejedor, M., Rodríguez, M., Fuentes, J. and Jiménez, C., 2013. Effect of forest floor characteristics on water repellency, infiltration, runoff and soil loss in Andisols of Tenerife (Canary Islands, Spain). Catena, 108, 50-57.
- Ng, C.W., Liu, J., Chen, R. and Xu, J. 2015b. "Physical and numerical modeling of an inclined three-layer (silt/gravelly sand/clay) capillary barrier cover system under extreme rainfall", Waste Manage. 38, 210-221.
- Ng, C.W.W. and Leung, A.K., 2011. Measurements of drying and wetting permeability functions using a new stress-controllable soil column, J. Geotech. Geoenviron. 138(1), 58-68.
- Ng, C.W.W., Feng, S. and Liu, H.W. 2015a. A fully coupled model for water–gas–heat reactive transport with methane oxidation in landfill cover, Sci. Total. Environ. 508, 307-319.
- Ng, C.W.W., Leung, A.K. and Woon, K.X., 2014. Effects of soil density on grass-induced suction distributions in compacted soil subjected to rainfall. Can. Geotech. J. 51, 311–321.
- Ng, C.W.W., Leung, A.K., 2011. Measurements of drying and wetting permeability functions using a new stress-controllable soil column. J. Geotech. Geoenviron. 138 (1), 58–68.
- Ng, C.W.W., Liu, H.W. and Feng, S., 2015c. Analytical solutions for calculating pore-water pressure in an infinite unsaturated slope with different root architectures, Can. Geotech. J. 52 (12), 1981-1992.
- Ng, C.W.W., Ni, J.J., Leung, A.K. and Wang, Z.J., 2016. A new and simple water retention model for root-permeated soils. Géotech. Lett., 6(1), 106-111.

- Ng, C.W.W., Wong, H.N., Tse, Y.M., Pappin, J.W., Sun, H.W., Millis, S.W. and Leung, A.K. 2011. A field study of stress-dependent soil–water characteristic curves and permeability of a saprolitic slope in Hong Kong", Geotechnique, 61 (6), 511-521.
- Ni, J.J., Bordoloi, S., Shao, W., Garg, A., Xu, G. and Sarmah, A.K., 2020. Two-year evaluation of hydraulic properties of biochar-amended vegetated soil for application in landfill cover system. Science of the Total Environment, 712, p.136486.
- Nieber, J.L. and Sidle, R.C., 2010. How do disconnected macropores in sloping soils facilitate preferential flow?. Hydrol. Process. 24(12), pp.1582-1594.
- Niinemets, Ü. and Valladares, F., 2006. Tolerance to shade, drought, and waterlogging of temperate Northern Hemisphere trees and shrubs. Ecol. Monogr. 76(4), 521-547.
- Ollobarren, P., Capra, A., Gelsomino, A. and La Spada, C., 2016. Effects of ephemeral gully erosion on soil degradation in a cultivated area in Sicily (Italy). CATENA 145, 334-345.
- Omasa, K., Hosoi, F. and Konishi, A., 2006. 3D lidar imaging for detecting and understanding plant responses and canopy structure. J. Exp. Bot. 58(4), 881-898.
- Panda, B., Paul, S.C. and Tan, M.J., 2017. Anisotropic mechanical performance of 3D printed fiber reinforced sustainable construction material, Mater. Lett. 209, 146-149.
- Panda, B., Paul, S.C., Hui, L.J., Tay, Y.W.D. and Tan, M.J., 2017. Additive manufacturing of geopolymer for sustainable built environment. J. Clean. Prod. 167, 281-288.
- Pardossi, A., Vernieri, P. and Tognoni, F., 1992. Involvement of abscisic acid in regulating water status in Phaseolus vulgaris L. during chilling, Plant Physiol. 100(3), 1243-1250.
- Parke, E.L., Linderman, R.G. and Black, C.H. 1983. The role of ectomycorrhizas in drought tolerance of Douglas-fir seedlings, New Phytologist, 95(1), 83-95.

- Pei, Z.M., Murata, Y., Benning, G., Thomine, S., Klüsener, B., Allen, G.J., Grill, E. and Schroeder, J.I., 2000. Calcium channels activated by hydrogen peroxide mediate abscisic acid signalling in guard cells. Nature, 406(6797), 731.
- Penman, H. L., 1948. Natural evaporation from open water, bare soil and grass. In Proceedings of the Royal Society of London A: Mathematical, Physical and Engineering Sciences. The Royal Society. 193(1032), 120-145.
- Pérez, J.M.M. and Pascau, J., 2013. Image processing with ImageJ," Packt Publishing Ltd. 15-32.
- Peters, S.B., Siemens, G. and Take, W.A., 2011. "Characterization of transparent soil for unsaturated applications," Geotech. Test. J., 34(5), 445-456.
- Philipp, I. and Rath, T., 2002. Improving plant discrimination in image processing by use of different colour space transformations, Comput. Electron. Agr., 35(1), 1-15.
- Pirasteh-Anosheh, H., Ranjbar, G., Pakniyat, H. and Emam, Y., 2016. Physiological mechanisms of salt stress tolerance in plants: An overview. Plant-environment interaction: Responses and approaches to mitigate stress, 141-160.
- Pitanga, H.N., Gourc, J.P. and Vilar, O.M., 2011. Enhanced measurement of geosynthetic interface shear strength using a modified inclined plane device. Geotech. Test. J., 34(6), 643-652.
- Poë, S., Stovin, V. and Berretta, C., 2015. Parameters influencing the regeneration of a green roof's retention capacity via evapotranspiration," J. Hydrol., 523, 356-367.
- Pollen-Bankhead, N. and Simon, A., 2010. Hydrologic and hydraulic effects of riparian root networks on streambank stability: Is mechanical root-reinforcement the whole story?. Geomorphology, 116(3-4), 353-362.

- Prasad, R., 1988. A linear root water uptake model, J. Hydrol. 99 (3-4), 297-306.
- Punmia, B. C., and Jain, A. K., 2005. Soil mechanics and foundations, Firewall Media, 144-146.
- Puppala, A.J., Katha, B. and Hoyos, L.R., 2004. Volumetric shrinkage strain measurements in expansive soils using digital imaging technology. Geotech. Test. J., 27(6), 547-556.
- Quan, M. and Liang, J., 2017. The influences of four types of soil on the growth, physiological and biochemical characteristics of Lycoris aurea (L'Her.) Herb. Sci. Rep-Uk, 7, 43284.
- Raes, D. and Deproost, P., 2003. Model to assess water movement from a shallow water table to the root zone. Agr. Water. Manage. 62(2), 79-91.
- Rambal, S., 1993. The differential role of mechanisms for drought resistance in a Mediterranean evergreen shrub: a simulation approach. Plant, Cell. Environ. 16(1), 35-44.
- Rasband, W.S., ImageJ, U.S. and National Institutes of Health, 2011. Bethesda, Maryland, USA, 1997–2014.
- Rayhani, M.H.T., Yanful, E.K. and Fakher, A., 2008. Physical modeling of desiccation cracking in plastic soils. Eng. Geol. 97(1), 25-31.
- Reddy, V. and Jagadish, K.S., 1993. The static compaction of soils. Géotechnique, 43(2), 337-41.
- Reginato, R.J. and Van Bavel, C.H.M., 1964. Soil Water Measurement with Gamma Attenuation 1, Soil Sci. Soc. Am. J., 28(6), 721-724.
- Reubens, B., Moeremans, C., Poesen, J., Nyssen, J., Tewoldeberhan, S., Franzel, S., Deckers, J., Orwa, C. and Muys, B., 2011. Tree species selection for land rehabilitation in

Ethiopia: from fragmented knowledge to an integrated multi-criteria decision approach," Agroforestry Syst., 82(3), 303-330.

- Reynolds, S.G., 1970. The gravimetric method of soil moisture determination Part IA study of equipment, and methodological problems" J. Hydrol., 11(3), 258-273.
- Richards, B.G. 1965. Measurement of free energy of soil moisture by the psychrometric technique, using thermistors, Buttersworth & Company, Australia.
- Ringrose-Voase, A.J. and Sanidad, W.B., 1996. A method for measuring the development of surface cracks in soils: application to crack development after lowland rice. Geoderma 71(3), 245-261.
- Roth, K., Schulin, R., Flühler, H. and Attinger, W., 1990. Calibration of time domain reflectometry for water content measurement using a composite dielectric approach, Water Resour. Res., 26(10), 2267-2273.
- Russ, J. C., and Russ, J. C., 2007. Introduction to image processing and analysis," CRC press, 4-13.
- Schymanski, S.J., Or, D. and Zwieniecki, M., 2013. Stomatal control and leaf thermal and hydraulic capacitances under rapid environmental fluctuations. PloS one, 8(1), e54231.
- Scoffoni, C., Chatelet, D.S., Pasquet-kok, J., Rawls, M., Donoghue, M.J., Edwards, E.J. and Sack, L., 2016. Hydraulic basis for the evolution of photosynthetic productivity. Nature plants, 2, p.16072.
- Scoffoni, C., Rawls, M., McKown, A., Cochard, H. and Sack, L., 2011. Decline of leaf hydraulic conductance with dehydration: relationship to leaf size and venation architecture. Plant Physiol. 156(2), 832-843.

- Sharp, R.E. and Davies, W.J., 1985. Root growth and water uptake by maize plants in drying soil. J. Exp. Bot. 36(9), 1441-1456.
- Sills, L.A.K., Mumford, K.G. and Siemens, G.A., 2017. Quantification of Fluid Saturations in Transparent Porous Media, Vadose Zone J., 16(2).
- Šimunek, J., Van Genuchten, M.T. and Šejna, M., 2012, "HYDRUS: Model use, calibration, and validation", Transactions of the ASABE, 55(4), 1263-1274.
- Singh, B.B., Ajeigbe, H.A., Tarawali, S.A., Fernandez-Rivera, S. and Abubakar, M., 2003. Improving the production and utilization of cowpea as food and fodder. Field Crop. Res. 84(1), 169-177.
- Singh, K., Pandey, V.C. and Singh, R.P., 2013. Cynodon dactylon: an efficient perennial grass to revegetate sodic lands. Ecol. Eng. 54, 32-38.
- Singh, S., 2009, Weather variability and summer rice yield in wet monsoon environment of upper Brahmaputra valley, VAYU MANDAL, 46.
- Smith, B., Prentice, I.C. and Sykes, M.T., 2001. Representation of vegetation dynamics in the modelling of terrestrial ecosystems: comparing two contrasting approaches within European climate space. Global Ecol. Biogeogr. 10(6), 621-637.
- Smith, T. and Guild, J., 1993. The CIE colourimetric standards and their use, TrOS..Vol. 33(3), p. 73.
- Snow, D.T., 1969. Anisotropie permeability of fractured media. Water. Resour. Res. 5(6), 1273-1289.
- Solanki, C.S., 2015. Solar photovoltaics: fundamentals, technologies and applications. PHI Learning Pvt. Ltd., p. 330.

- Solleti, S.K., Bakshi, S., Purkayastha, J., Panda, S.K. and Sahoo, L., 2008. Transgenic cowpea (Vigna unguiculata) seeds expressing a bean α-amylase inhibitor 1 confer resistance to storage pests, bruchid beetles. Plant. Cell. Rep. 27(12), 1841-1850.
- Somma, F., Hopmans, J.W. and Clausnitzer, V., 1998. Transient three-dimensional modeling of soil water and solute transport with simultaneous root growth, root water and nutrient uptake. Plant. Soil. 202(2), 281-293.
- Song, L., Li, J.H., Zhou, T. and Fredlund, D.G., 2017. Experimental study on unsaturated hydraulic properties of vegetated soil. Ecol. Eng. 103, 207-216.
- Stevens, D.B., 1995. Vadose Zone Hydrology. CRC press
- Stovin, V., Poë, S. and Berretta, C., 2013. A modelling study of long term green roof retention performance. J. Environ. Manage. 131, 206-215.
- Strothmann, W., Ruckelshausen, A., Hertzberg, J., Scholz, C. and Langsenkamp, F., 2017. Plant classification with In-Field-Labeling for crop/weed discrimination using spectral features and 3D surface features from a multi-wavelength laser line profile system," Comput. Electron. Agr. 134, 79-93.
- Sun, D. and Liddle, M.J., 1993. A survey of trampling effects on vegetation and soil in eight tropical and subtropical sites. Environ. Manage. 17(4), 497-510.
- Swartz, G.L., 1966. Water entry into a black earth under flooding. Queensl. J. Agric. Anim. Sci 23, 407-422.
- Take, W.A., Beddoe, R.A., Davoodi-Bilesavar, R. and Phillips, R. 2015, "Effect of antecedent groundwater conditions on the triggering of static liquefaction landslides", Landslides, 12(3), 469-479.

- Tang, C., Shi, B., Gao, W., Chen, F. and Cai, Y., 2007. Strength and mechanical behavior of short polypropylene fiber reinforced and cement stabilized clayey soil. Geotext. Geomembranes. 25(3), 194-202.
- Tang, C.S., Shi, B., Cui, Y.J., Liu, C. and Gu, K., 2012. Desiccation cracking behavior of polypropylene fiber–reinforced clayey soil. Can. Geotech. J. 49(9), 1088-1101.
- Tardieu, F. and Simonneau, T., 1998. Variability among species of stomatal control under fluctuating soil water status and evaporative demand: modelling isohydric and anisohydric behaviours. J. Exp. Bot. 419-432.
- Thomas, B., Murphy, D.J. and Murray, B.G., 2016. Encyclopedia of applied plant sciences. Academic Press. 31-34.
- Thomas, G.W. and Phillips, R.E., 1979. Consequences of water movement in macropores. J. Environ. Qual. 8(2), 149-152.
- Tilley, R.J., 2010. Colour and the optical properties of materials: an exploration of the relationship between light, the optical properties of materials and colour. John Wiley & Sons, 419-487.
- Tipple, B.J. and Pagani, M., 2007. The early origins of terrestrial C4 photosynthesis. Annu. Rev. Earth Planet. Sci., 35, 435-461.
- Tobin, R.L. and Kulmatiski, A., 2018. Plant identity and shallow soil moisture are primary drivers of stomatal conductance in the savannas of Kruger National Park. PloS one, 13(1), p.e 0191396.
- Torres, M.A., Armenteros, E.D.L., Fernández, R.O. and Fernández, P.G., 2004. Digital image analysis for the estimation of cracked areas and the soil shrinkage characteristic

curve in clay soils amended with composted sewage sludge. Span J. Agric. Res. 2(3), 473-479.

- Tratch, D. 1996, Moisture uptake within the root zone, M.Sc. Thesis, Department of Civil Engineering, University of Saskatchewan, Saskatoon, Saskatchewan, Canada.
- UMS GMBH MÜNCHEN, 2009. T5, T5x pressure transducer tensiometer: User manual.
- Vaio, M., Speranza, P., Valls, J.F., Guerra, M. and Mazzella, C., 2005. Localization of the 5S and 45S rDNA sites and cpDNA sequence analysis in species of the Quadrifaria group of Paspalum (Poaceae, Paniceae), Ann. Bot. 96(2), 191-200.
- Van de Vyvere, L. and Desenfans, O., 2016. MISTRALE: Soil moisture mapping service based on a UAV-embedded GNSS-Reflectometry sensor," In EGU General Assembly Conference Abstracts., 18, p. 5905.
- van der Schalie, R., de Jeu, R., Parinussa, R., Rodríguez-Fernández, N., Kerr, Y., Al-Yaari, A., Wigneron, J.P. and Drusch, M., 2018. The Effect of Three Different Data Fusion Approaches on the Quality of Soil Moisture Retrievals from Multiple Passive Microwave Sensors," Remote Sens.-Basel., 10(1), p.107.
- Van Genuchten, M.T., 1980. A closed-form equation for predicting the hydraulic conductivity of unsaturated soils 1. Soil Sci. Soc. Am. J. 44(5), 892-898.
- Van Noordwijk, M., Heinen, M. and Hairiah, K., 1991. Old tree root channels in acid soils in the humid tropics: important for crop root penetration, water infiltration and nitrogen management. In Plant-Soil Interactions at Low pH (423-430). Springer, Dordrecht.
- Varado, N., Braud, I. and Ross, P.J., 2006. Development and assessment of an efficient vadose zone module solving the 1D Richards' equation and including root extraction by plants. J. Hydrol. 323(1-4), 258-275.

- Vardhan, H., Bordoloi, S., Garg, A. and Garg, A., 2017. Compressive strength analysis of soil reinforced with fiber extracted from water hyacinth. Eng. Computation. 34(2).
- Villeneuve, P.J., Jerrett, M., Su, J.G., Burnett, R.T., Chen, H., Wheeler, A.J. and Goldberg, M.S., 2012. A cohort study relating urban green space with mortality in Ontario, Canada. Environ. Res. 115, 51-58.
- Vrugt, J.A., Hopmans, J.W. and Šimunek, J., 2001. Calibration of a two-dimensional root water uptake model. Soil. Sci. Soc. Am. J. 65(4), 1027-1037.
- Wang, C., Zhang, Z.Y., Liu, Y. and Fan, S.M., 2017. Geometric and fractal analysis of dynamic cracking patterns subjected to wetting-drying cycles. Soil. Till. Res. 170, 1-13.
- Wang, F.E., Chen, Y.X., Tian, G.M., Kumar, S., He, Y.F., Fu, Q.L. and Lin, Q., 2004. Microbial biomass carbon, nitrogen and phosphorus in the soil profiles of different vegetation covers established for soil rehabilitation in a red soil region of southeastern China. Nutr. Cycl. Agroecosys. 68(2), 181-189.
- Warren, C.R., 2008. Soil water deficits decrease the internal conductance to CO2 transfer but atmospheric water deficits do not. J. Exp Bot. 59(2), 327-334.
- Watson, K.K., 1966, An instantaneous profile method for determining the hydraulic conductivity of unsaturated porous materials, Water Resour. Res. 2(4), 709-715.
- Waugh, W.J., Thiede, M.E., Bates, D.J., Cadwell, L.L., Gee, G.W. and Kemp, C.J., 1994. Plant cover and water balance in gravel admixtures at an arid waste-burial site. J. Environ. Qual. 23(4), 676-685.
- Werner, C., Correia, O. and Beyschlag, W., 1999. Two different strategies of Mediterranean macchia plants to avoid photoinhibitory damage by excessive radiation levels during summer drought. Acta. Oecol. 20(1), 15-23.

- Wilkinson, S. and Davies, W.J., 1997. Xylem sap pH increase: a drought signal received at the apoplastic face of the guard cell that involves the suppression of saturable abscisic acid uptake by the epidermal symplast. Plant. Physiol. 113(2), 559-573.
- Wolch, J.R., Byrne, J. and Newell, J.P., 2014. Urban green space, public health, and environmental justice: The challenge of making cities 'just green enough'," Landscape. Urban Plan., 125, 234-244.
- Wong, S.C., Cowan, I.R. and Farquhar, G.D., 1979. Stomatal conductance correlates with photosynthetic capacity. Nature, 282(5737), p. 424.
- Wu, J., Zhang, R. and Gui, S., 1999. Modeling soil water movement with water uptake by roots. Plant. soil, 215(1), 7-17.
- Yesiller, N., Miller, C.J., Inci, G. and Yaldo, K., 2000. Desiccation and cracking behavior of three compacted landfill liner soils. Eng. Geol. 57(1), 105-121.
- Yoshida, S. and Adachi, K., 2004. Numerical analysis of crack generation in saturated deformable soil under row-planted vegetation. *Geoderma*, *120*(1-2), pp.63-74.
- Yoshimoto, N., Orense, R.P., Tanabe, F., Kikkawa, N., Hyodo, M. and Nakata, Y., 2011. Measurement of degree of saturation on model ground by digital image processing, Soils. Found. 51(1),167-177.
- Yuen, K., Graham, J. and Janzen, P., 1998. Weathering-induced fissuring and hydraulic conductivity in a natural plastic clay. Can. Geotech. J. 35(6), 1101-1108.
- Zakaria, Z.A., Wen, L.Y., Rahman, N.I.A., Ayub, A.H.A., Sulaiman, M.R. and Gopalan, H.K., 2007. Antinociceptive, anti-inflammatory and antipyretic properties of the aqueous extract of Bauhinia purpurea leaves in experimental animals. Medical Principles and Practice, 16(6), 443-449.

- Zhang, R., 1997. Infiltration models for the disk infiltrometer. Soil. Sci. Soc. Am. J. 61(6), 1597-1603.
- Zhou, Y., Chen, J. And Wang, X., 2009. Research on Resistance Cracking and Enhancement Mechanism of Plant Root in Slope Protection by Vegetation [J]. J. Wuhan Uni. (Natural Science Edition), 5, p.023.
- Zhu, H. and Zhang, L.M., 2015a. Evaluating suction profile in a vegetated slope considering uncertainty in transpiration. Comput. Geotech. 63, 112-120.
- Zhu, H. and Zhang, L.M., 2015b. Field investigation of erosion resistance of common grass species for soil bioengineering in Hong Kong", Acta Geotech. 5(11), 1047-1059.
- Zreda, M., Desilets, D., Ferré, T.P.A. and Scott, R.L., 2008. Measuring soil moisture content non-invasively at intermediate spatial scale using cosmic-ray neutrons, Geophys. Res. Lett., 35(21).

LIST OF PUBLICATIONS FROM THIS RESEARCH WORK

Papers in refereed journals

- **Gadi, V.K**., Hussain, R., Bordoloi, S., Hossain, S., Singh, S.R., Garg, A., Sekharan, S., Karangat, R. and Lingaraj, S., (2019). Relating stomatal conductance and surface area with evapotranspiration induced suction in a heterogeneous grass cover. ***Journal of Hydrology***, 568, pp.867-876.
- **Gadi, V.K**., Bordoloi, S., Garg, A., Sahoo, L., Berretta, C. and Sekharan, S., (2018). Effect of shoot parameters on cracking in vegetated soil. ***Environmental Geotechnics***, 5(2), pp.123-130.
- **Gadi, V.K**., Tang, Y.R., Das, A., Monga, C., Garg, A., Berretta, C. and Sahoo, L., 2017. Spatial and temporal variation of hydraulic conductivity and vegetation growth in green infrastructures using infiltrometer and visual technique. ***Catena***, 155, pp.20-29.
- **Gadi, V.K**. Garg, A., Manogaran, I.P., Sekharan, S., and Zhu, H.H., 2018. Understanding Soil Surface Water Content Using Light Reflection Theory: A Novel Colour Analysis Technique Considering Variability in Light Intensity. ***Journal of Testing and Evaluation***, 48(5).
- **Gadi, V.**, Singh, S., Singhariya, M. and Garg, A., (2018). Modeling soil-plant-water interaction: effects of canopy and root parameters on soil suction and stability of green infrastructure. ***Engineering Computations***, 35(3), pp.1543-1566.
- **Gadi, V.K**., Manogaran, I.P., Garg, A., Berretta, C. and Sreedeep, S., 2017. A novel colour analysis technique for differentiation of mix grass cover under shade and without shade in green infrastructures. ***Advances in Civil Engineering Materials***, 6(1), pp.564-582.

- **Gadi, V.K**., Bordoloi, S., Garg, A., Kobayashi, Y. and Sahoo, L., 2016. Improving and correcting unsaturated soil hydraulic properties with plant parameters for agriculture and bioengineered slopes. ***Rhizosphere***, 1, pp.58-78.
- Bordoloi, S., Hussain, R., **Gadi, V.K**., Bora, H., Sahoo, L., Karangat, R., Garg, A. and Sreedeep, S., 2018. Monitoring soil cracking and plant parameters for a mixed grass species. ***Géotechnique Letters***, 8(1), pp.49-55.

Book chapters

- Sekharan, S., **Gadi, V.K.**, Bordoloi, S., Saha, A., Kumar, H., Hazra, B. and Garg, A., 2019. Sustainable Geotechnics: A Bio-geotechnical Perspective. In *Frontiers in Geotechnical Engineering* (pp. 313-331). Springer, Singapore.
- **Gadi, V.K.**, Hossain, S., Deka, G., Garg, A., Karangat, R., Sekharan, S. and Sahoo, L., 2018, October. Spatial Heterogeneity of Hydraulic Conductivity in Green Infrastructure Due to Presence of Wilted and Live Grass: A Field Study. In *The International Congress on Environmental Geotechnics* (pp. 393-400). Springer, Singapore.
- Garg, A., **Gadi, V.K.,** Hossain, S., Karangat, R., Sekharan, S. and Sahoo, L., 2018, October. Role of Plant Health Parameters in Understanding Spatial Heterogeneity of Hydraulic Conductivity of Vegetated Soil: A Case Study of Urban Green Infrastructure Monitoring. In *The International Congress on Environmental Geotechnics* (pp. 377-384). Springer, Singapore.